NASA CR-167857
SSS-R-81-5140

NASA-CR-167857
19820018502

ADDITIONAL EXTENSIONS TO THE NASCAP COMPUTER CODE, Volume III

M.J. Mandell
D.L. Cooke

S-CUBED

Prepared for
National Aeronautics and Space Administration
Lewis Research Center

Contract NAS3-22536

1 Report No NASA CR-167857	2 Government Accession No	3 Recipient's Catalog No
4 Title and Subtitle ADDITIONAL EXTENSIONS TO THE NASCAP COMPUTER CODE, VOLUME III		5 Report Date August 1981 6 Performing Organization Code
7 Author(s) M. J. Mandell, D. L. Cooke		8 Performing Organization Report No SSS-R-81-5140
9 Performing Organization Name and Address S-CUBED P. O. Box 1620 La Jolla, CA 92038		10 Work Unit No 11 Contract or Grant No NAS3-22536
12 Sponsoring Agency Name and Address National Aeronautics and Space Administration Lewis Research Center 21000 Brookpark Road, Cleveland, OH 44135		13 Type of Report and Period Covered Contractor Report 9/9/1980 - 12/22/1981 14 Sponsoring Agency Code 5532

15 Supplementary Notes

Project Manager, James C. Roche, NASA-Lewis Research Center, Cleveland, OH

16 Abstract

The ION computer code is designed to calculate charge exchange ion densities, electric potentials, plasma temperatures, and current densities external to a neutralized ion engine in R-Z geometry. The present version assumes the beam ion current and density to be known and specified, and the neutralizing electrons to originate from a hot-wire ring surrounding the beam orifice. The plasma is treated as being resistive, with an electron relaxation time comparable to the plasma frequency. Together with the thermal and electrical boundary conditions described below and other straightforward engine parameters, these assumptions suffice to determine the required quantities.

The ION code, written in ASCII FORTRAN for UNIVAC 1100 series computers, is designed to be run interactively, although it can also be run in batch mode. The input is free-format, and the output is mainly graphical, using the machine-independent graphics developed for the NASCAP code. The executive routine calls the code's major subroutines in user-specified order, and the code allows great latitude for restart and parameter change.

17 Key Words (Suggested by Author(s))	18 Distribution Statement
Ion Engines Electrostatic Propulsion Charge-Exchange Plasma Ion Beam Neutralization	Publicly available (no restrictions on provision to domestic or foreign requesters)

19 Security Classif (of this report)	20 Security Classif (of this page)	21 No of Pages	22 Price*
UNCLASSIFIED	UNCLASSIFIED	97	

* For sale by the National Technical Information Service, Springfield Virginia 22161

NASA-C-168 (Rev 10-75)

N82-26378#

TABLE OF CONTENTS

LIST OF ILLUSTRATIONS

LIST OF ILLUSTRATIONS (Continued)

LIST OF ILLUSTRATIONS (Continued)

LIST OF TABLES

SUMMARY

The ION computer code is designed to calculate charge exchange ion densities, electric potentials, plasma temperatures, and current densities external to a neutralized ion engine in R-Z geometry. The present version assumes the beam ion current and density to be known and specified, and the neutralizing electrons to originate from a hot-wire ring surrounding the beam orifice. The plasma is treated as being resistive, with an electron relaxation time comparable to the plasma frequency. Together with the thermal and electrical boundary conditions described below and other straightforward engine parameters, these assumptions suffice to determine the required quantities.

The ION code, written in ASCII FORTRAN for UNIVAC 1100 series computers, is designed to be run interactively, although it can also be run in batch mode. The input is free-format, and the output is mainly graphical, using the machine-independent graphics developed for the NASCAP code. The executive routine calls the code's major subroutines in user-specified order, and the code allows great latitude for restart and parameter change.

1. INTRODUCTION

The ION computer code is designed to calculate charge exchange ion densities, electric potentials, plasma temperatures, and current densities external to a neutralized ion engine in R-Z geometry. The present version assumes the beam ion current and density to be known and specified, and the neutralizing electrons to originate from a hot-wire ring surrounding the beam orifice. The plasma is treated as being resistive, with an electron relaxation time comparable to the plasma frequency. Together with the thermal and electrical boundary conditions described below and other straightforward engine parameters, these assumptions suffice to determine the required quantities.

The ION code, written in ASCII FORTRAN for UNIVAC 1100 series computers, is designed to be run interactively, although it can also be run in batch mode. The input is free-format, and the output is mainly graphical, using the machine-independent graphics developed for the NASCAP code. The executive routine calls the code's major subroutines in user-specified order, and the code allows great latitude for restart and parameter change.

In Chapter II of this report we outline the theoretical treatment employed by the ION code. Chapter III discusses the use of the code, describing the input parameters and the functions of the major subroutines. Chapter IV presents some sample results, and Chapter V contains a sample run.

2. THEORY

The major theoretical components to the ION computer code have been previously presented in the open literature. This Chapter will outline and review the code theory. For convenience, the published detailed descriptions are reproduced in Appendices A and B.

A 30 cm diameter mercury thruster with 2 A of beam current and 25 mA of charge exchange ion current can be expected to produce charge exchange ion densities at the beam edge on the order of 10^{14} m^{-3} (Appendix B and references therein). Since plasma densities in low earth orbit are on the order of 10^{10} - 10^{12} m^{-3}, the charge exchange plasma will dominate the local environment. Such a plasma will be characterized by long collision lengths and ($\sim 10^{3}$m) and short Debye lengths ($\sim 10^{-3}$m).

While this plasma is not collision dominated, the short Debye length implies that small scale fluctuating fields may create an effective collision frequency, ν_{eff}, that will be effective in randomizing electron velocities on the scale of typical problem dimensions (~1m). This suggests that except within a few Debye lengths of particle sinks and sources (or the sheaths of high voltage surfaces) we can expect the plasma to be quasineutral. Quasineutrality is a basic assumption throughout ION. Appendix A describes the theoretical and experimental evidence for a barometric law correlation between potential ϕ, density ρ, and temperature θ:

$$\phi(r) = \theta \, \ell n \, (\frac{n(r)}{n_0}) \quad .$$

Also described in Appendix A are experiments where a barometric law did not adequately explain the observations, suggesting the need for a comprehensive electron transport model. ION utilizes a barometric law assumption only as an initial approximation. In Appendix A it is

demonstrated that measured neutralizer electron temperatures and potential variations can be qualitatively explained in terms of the anomalous resistivity of the thruster generated plasma to the flow of electrons if we invoke an effective collision frequency comparable to the electron plasma frequency.

The ION code is constructed from four main theoretical models: An ion beam model, a free expansion model for neutrals, a hydrodynamic-charge exchange ion model, and a fluid model for the neutralizer electrons. Of these four, the first two are analytic and require very little computing while the second two are numerical. The neutral expansion model is described in Appendix C, the hydrodynamic charge exchange ion model in Appendix B, and the electron fluid model in Appendix A. The code operates in R-Z geometry on a discrete rectangular mesh of nodal points. At present, the ion beam is modeled as columnar with no spreading. Depletion due to charge exchange is ignored. The beam originates at $z = 0$, is centered at $r = 0$, and has either a quadratic or Gaussian profile. (See Chapter III). The neutral efflux is described analytically by a free expansion model assuming a uniform emission over the thruster throat with a Maxwellian velocity spread. The charge exchange ions are generated within the beam with zero initial velocities. The generation rate is equal to the product of the local beam flux, neutral density, and the charge exchange cross-section.

We use a hydrodynamic description for both the charge exchange ions and the neutralizer electrons. However, for each case there are differing approximations that can be made in solving the hydrodynamic equations. Therefore, purely for the purpose of discussion, the charge exchange model is referred to as hydrodynamic, and the electron model is labeled fluid.

The hydrodynamic model of the charge-exchange ions, described in Appendix B, is based upon a time stepped solution of the mass and momentum equations in finite difference form. A barometric law

relationship is assumed between density, potential and temperature. The mechanics of the finite difference formulations are given in detail in Appendix B. The major simplifying assumption in this model is that charge exchange ions are quite cold so that pressure terms may be neglected. This means that the inertial term in the momentum equation ($\vec{\nabla} \cdot \rho \vec{V} \vec{V}$) in Eq. (3) of Appendix B) forces the equations to be parabolic in nature. It is this parabolic nature that necessitates a time-stepped finite difference approach. The initial and boundary conditions for this model are discussed in Chapter III.

The electron fluid calculation follows after the charge exchange ion calculation using the ion densities as input. For the electron model, we make the assumption that the plasma offers a significant resistance to the flow of electrons (due to the effective collision frequency). It then follows that the electron drift velocities will be small compared to thermal velocities, which allows the inertial term in the momentum and energy equations to be dropped. Thus, the conservation equations for mass, momentum and energy may be solved, along with the ideal gas equation of state, in closed elliptic form. A finite element approach is used to solve directly for the steady state. This model is discussed in Appendix A.

The switching between finite difference and finite element approaches may seem cumbersome, but the conversions are quite efficient compared to the difficulties encountered otherwise. Finally, it should be mentioned that since there is currently no iteration between the ion and electron calculations, the resulting parameters will not be entirely self-consistent. This limitation does not appear to be severe in the test cases modeled so far, but a truly predictive model should be free from such limitations. This will be a subject for future work.

3. CODE USAGE

A. OVERVIEW

The ION code is invoked by the statement

```
@ XQT  absoluteelementname
```

It assigns files 9 and 21 as restart files, which may be aliased (@USE) to user permanent files, or later copied to permanent files. It also assigns and writes printed output on files (by default) 19 and 20, and uses files 11 and 12 as scratch files. Graphical output is generated by writing NASCAP-type pseudo plot calls on file 2 and interfacing to the user's graphics library with the standard NASCAP postprocessor (PLOTREAD).

After invoking the ION code, the user's first task is to enter the problem parameters (Table 3.1). Acceptable sets of input are shown in Figures 3.1. After encountering an 'END' card in the parameter input, a summary is printed (Figure 3.2).

Subsequent major subroutine calls are made at user request. These calls are listed in Table 3.2. For a new problem the first call will be to subroutine CHEX, which determines the steady state charge-exchange ion density. (This calculation usually converges in the default of 300 steps, but may take several minutes of computer time. For batch runs, a larger value of 500 steps is recommended.) Next subroutine POTENT is called to perform the calculation of temperatures and potentials. Entry points RECHEX and RESUME are available to restart a non-converged calculation of CHEX or POTENT, respectively, and entry point NEWPOT may be used instead of POTENT to perform a calculation with altered thermal boundary conditions or

TABLE 3.1. PROBLEM PARAMETERS

KEYWORD	DEFAULT	MEANING
Grid Size		
NR	25 (max)	Number of radial coordinate values.
NZ	25 (max)	Number of Z-coordinate values.
RMAX	1.	Radius of computational space. (meters)
ZMAX	1.	Length of computational space. (meters)
Ion Beam Characteristics		
CURRent	1.	Beam current. (amperes)
RADIus	1.	Beam radius on entry. (m)
ENERgy	1000.	Beam ion energy (eV).
MASS	200.59	Ion mass in amu.
PROFile	GAUS	Beam profile acceptable values are 'GAUS' and 'QUAD'.
SPREAdangle	0.	Half-angle characterizing beam spread. (Non-zero spread angle not implemented.)
Charge Exchange Ion Production (Physical)		
SIGMA	6×10^{-19}	Charge exchange production cross-section (m^2)
FLOW (variable CNEUT)	2.	Fuel flow in ampere equivalent
TEMPerature	1.	Neutral temperature (eV).

KEYWORD	DEFAULT	MEANING
Charge Exchange Ion Production (Computational)		
ECHA	10.	Characteristic accelerating voltage for charge exchange ions.
VDTR (variable VDTBYR)	0.2	Particle tracking timestep constant (dimensionless)
ETA	.05	Velocity diffusion constant (dimensionless)
RHOMin	1.E12	Minimum density to be used in calculating barometric potential. (m^{-3})
NSTEPs	300	Number of iterative timesteps in hydrodynamic solution.
Thermal and Current Boundary Conditions		
THETai	1.	Temperature of isothermal boundary surfaces. (eV)
THERbc	'ISOT'	Thermal boundary condition 'ISOT' - Isothermal everywhere. 'SINK' - Isothermal on orifice plate. 'INSU' - Insulating orifice plate.
RNEUtr	1.	Radius of ring neutralizer
NITEr	1	Number of potential-temperature iterations.
Output Destinations		
OUTPut LUNCHX LUNPOT		LUNCHX = Logical unit number for charge exhange ion densities and velocities (Default 19). LUNPOT = Logical number for current and potential printout (Default 20).
DEST	'NONE'	Plot destination
TITLE	'NASA-S-CUBED ION ENGINE CODE'	Plot title (beginning in Col. 9)

```
1.      NR 24
2.      NZ 24
3.      RMAX  15
4       ZMAX .30
5.      CURRENT .085
6.      FLOW .14
7       SIGMA 5.E-19
8.      TEMP .06
9.      RADIUS .07
10.     PROFILE QUADRATIC
11.     RNEUT .08
12.     ENERGY 3000.
13.     THETAI 2.
14.     NSTEPS 500
15.     RHOMIN 1.E10
16.     THERBC INSU
17.     END
```

Figure 3.1a. Input data representative of SERT II thruster.

```
1.      NR 25
2.      NZ 25
3.      RMAX .36
4.      ZMAX .72
5.      CURRENT 1.
6.      FLOW 1.25
7.      SIGMA 5.E-19
8.      TEMP .06
9.      RADIUS .15
10.     RNEUT .17
11.     ENERGY 1100.
12.     NSTEPS 500
13      RHOMIN 1.E10
14      THERBC SINK
15.     END
```

Figure 3.1b. Input data representative of 30 cm thruster.

```
CODE OPTION SUMMARY

   NR          NZ          RMAX        ZMAX
   25          25          1.0000      1.0000

   BEAM CURRENT            BEAM RADIUS           BEAM ENERGY
    1.000000 AMPS            1.0000 M              1000.0 EV

   MASS (AMU)              PROFILE               SPREAD ANGLE
      200.59                 GAUS                    .0 DEG.
                                ION MASS =  3.355-025 KG.
                                PEAK CURRENT =  5.968+018 M**(-2) SEC**(-1)
                                ION VELOCITY =   30883.3 M/SEC

   SIGMA                   FLOW                  TEMP
    6.0-019             2.000000 AMPS          1.000 EV

   ECHAR             VDTR              ETA              RHOMIN          NSTEPS
    10.000             .200              .050           1.00+012         300

   THERMAL BC = 'ISOT' WITH TEMPERATURE     1.00 EV.

   NEUTRALIZER RADIUS =    1.0000          2 ITERATIONS.

   PRINTED OUTPUT: LOGICAL UNITS NO. 19 AND  20.

   PLOT DESTINATION = NONE
   PLOT TITLE =        NASA - S-CUBED ION ENGINE PLASMA CODE
```

Figure 3.2a. Code Option Summary (Default values).

```
CODE OPTION SUMMARY

   NR          NZ          RMAX        ZMAX
   25          25          .3600       .7200

   BEAM CURRENT            BEAM RADIUS           BEAM ENERGY
    1.000000 AMPS            .1500 M               1100.0 EV

   MASS (AMU)              PROFILE               SPREAD ANGLE
      200.59                 GAUS                    .0 DEG.
                                ION MASS =  3.355-025 KG.
                                PEAK CURRENT =  2.652+020 M**(-2) SEC**(-1)
                                ION VELOCITY =   32390.7 M/SEC

   SIGMA                   FLOW                  TEMP
    5.0-019             1.250000 AMPS          .060 EV

   ECHAR             VDTR              ETA              RHOMIN          NSTEPS
    10.000             .200              .050           1.00+010         500

   THERMAL BC = 'SINK' WITH TEMPERATURE     1.00 EV.

   NEUTRALIZER RADIUS =     .1700          2 ITERATIONS.

   PRINTED OUTPUT: LOGICAL UNITS NO. 19 AND  20.

   PLOT DESTINATION = CALC
   PLOT TITLE =          SAMPLE INPUT DATA
```

Figure 3.2b. Code Option Summary (Values similar to Fig. 3.1b).

TABLE 3.2. MAJOR SUBROUTINES OF ION CODE

Major Subroutines

(called by main routine)

Called automatically

DEFOPT - Sets default options.

INPUT - Reads user input of problem parameters.

INPRNT - Summarizes problem parameters.

Called on user request

CHANGE [lun]-Change input values by reading from logical unit no. lun (default 5).

CHEX - Hydrodynamic calculation for charge exchange ion density and velocity. Results on logical unit no. 9.

RECHEX - Restart of CHEX calculation.

POTENT - Initialize and iteratively calculate potentials and temperatures. Results on logical unit no. 21.

NEWPOT - Same as POTENT, but skips initialization and begins calculation on new case.

RESUME - Continues iterative calculation of POTENT starting from most recent iterate.

PLOT - Generate graphical output.

neutralizer position. The CHANGE subroutine may be used to alter problem parameters, and the PLOT subroutine is called for graphical output.

B. INPUT PARAMETERS

i. Grid Size and Resolution

The ION code discretizes the ion engine plasma problem on a finite element grid of NR by NZ gridpoints. For the charge exchange ion calculation each dimension has a maximum of 25. For POTENT the size may be increased to 30 by 30. The physical size of the computational space is RMAX by ZMAX. It is suggested that ZMAX be approximately double RMAX, and RMAX approximately double the beam radius. Resolution should be sufficient to model the density falloff at the beam edge. RMAX and ZMAX may be reduced between CHEX and POTENT if desired.

ii. Ion Beam Characteristics

These variables are self-explanatory, with the exception of the beam profile. Two choices are currently available

GAUSsian:

$$J(r) = J_0 \, e^{-3(r/R)^2}$$

QUADratic:

$$J(r) = J_0 \quad 1 - (r/R)^2 \quad [r < R]$$

where R is the specified beam radius. The GAUSsian profile is smoother and gives more reliable convergence, particularly in the CHEX calculation. The QUADratic profile is likely to give poor results when charge exchange ion production is low.

iii. Charge Exchange Ion Production (Physical)

The rate of charge exchange ion production is proportional to

(a) the cross-section SIGMa,

(b) the excess of fuel FLOW over beam CURRent;

(c) the inverse square root of the neutral TEMPerature. Typical value for the neutral TEMPerature is 300°C = .06 eV.

iv. Charge Exchange Ion Production (Computational)

These parameters govern the operation of the CHEX calculation and, with the exception of NSTEPS, are not recommended for change. The "characteristic energy" ECHA, should be roughly the barometric potential difference between the beam and the charge exchange cloud:

$$ECHA \approx e\, \ell n\, (\rho_{beam}/\rho_{ch.ex.}) .$$

Together with VDTR, this determines the hydrodynamic timestep. The velocity diffusion, ETA, is used to promote convergence, and can usually be reduced if the timestep is shortened. RHOMIN should approximate the minimum density expected in the problem. NSTEPS is the number of steps to be run to achieve steady state. (See discussion of CHEX routine below).

v. Thermal and Current Boundary Conditions

These provide the temperature used in the CHEX calculation, as well as the thermal boundary condition and neutralizer position for the POTENT calculation. These parameters may be changed prior to

executing POTENT or NEWPOT. NITER is the number of iterations performed on calling POTENT, NEWPOT, or RESUME.

vi. Output Destinations

The printed output from CHEX and POTENT is rather lengthy. For CHEX, the densities and velocities are printed for all node points, and for POTENT the densities, currents and potentials. Normally, these are sent to scratch files, from which they may be edited. To have them actually printed, input the card

OUTPUT 6 6

DEST specifies the site-dependent plot destination on automatic execution of NASCAP PLOTREAD., and TITLE allows user specification of a plot title, which may be changed during the course of the run.

C. SUBROUTINE CHEX (RECHEX)

The charge exchange ion density calculation is the most time consuming part of the ION code, taking 1-1.5 seconds per step at S-CUBED. It outputs immediately the neutral efflux and the resulting charge exchange current. Every fifty steps it prints the charge exchange ion density near the beam origin, which gives some indication of convergence. The true test of convergence, however is the 'TOTAL DNDT' printed by the POTENT routine. If this CHEX calculation is properly converged, this number should be within 10 percent of the charge exchange current. Otherwise, RECHEX should be used to continue the calculation.

CHEX writes its internal information on logical unit No. 9, and prints output on LUNCHX. The printed output lists velocity at each node point. The densities printed correspond to positions

halfway toward the next R and Z values. Plots of the charge exhange ion densities and currents are available after processing by the initialization stage of POTENT.

D. SUBROUTINE POTENT (NEWPOT, RESUME)

This routine calculates the potentials needed to drive the electrons from the neutralizer through the resistive plasma, and the temperature profile from the resultant plasma heating. The potential boundary condition is that the mean potential is zero. The thermal boundary conditions are isothermal at RMAX and ZMAX, and either isothermal or insulating at the orifice plate. Alternatively, the plasma may be considered isothermal, in which case no heat flow calculations are performed.

After initialization, this routine performs alternate ICCG (Incomplete Cholesky Conjugate Gradient) calculations for the potential and temperature fields. For each ICCG calculation, convergence is indicated by the numerator (RDOTR) being several orders of magnitude smaller than the denominator (RDOTR1). For the overall calculation convergence requires each denominator being several orders of magnitude smaller than its initial value. Convergence takes the most iterations (~ 5) for the INSUlating boundary condition. The most apparent symptom of incomplete convergence is the appearance of a convection cell around the beam edge in the current plots. The RESUme command may be used to perform further iterations on an unconverged calculation. To perform an additional POTEnt calculation with altered thermal boundary condition or neutralizer radius, the NEWPot command may be used.

E. SUBROUTINE PLOT

This is the user requested subroutine that controls the graphical output by ION. It has been designed as an interactive, device independent, menu type package but it can also be used in a

batch mode of operation. Aside from the required control commands or cards, all of the required data is taken from the temporary file 21. If that file's data had been saved from a previous run, the user could preassign 21., copy the old data to it, @XQT ION, and call PLOT immediately to produce or reproduce plots from previous runs. The user should be warned however, that if more than one problem is run per execution of ION, file 21. will contain only the most recent data and the results of the earlier run will have been lost. The output of PLOT is coded and stored in file 2. This file should be kept and used as input to NASCAP*PLOTREAD which will actually perform the plotting. File 2. is not overwritten if multiple runs are made in a single execution of ION. Successive calls to subroutine PLOT are automatically assigned sequence numbers, and the user may change titles with the CHANGE subroutine.

Upon calling PLOT, the interactive user will see the primary menu shown in Figure 3.3a, and will be prompted for the plot desired. The appropriate response is the integer associated with the desired plot. Following the transmittal of plot request, the menu will reappear and another plot may be chosen. This process may be repeated indefinitely and is terminated by a blank record. If plot 99 is chosen, the user is presented the menu shown in Figure 3.3b. These are all cross-sectional plots so after responding with the appropriate integer, the user is prompted for the desired Z direction nodal index (1,2,3, etc). If the user responds with a negative integer the plot will be a constant r cross-section. This process may be repeated indefinitely and is terminated by a blank record which will return the user to the primary menu.

```
          1     POTENTIAL CONTOURS
          2     ION DENSITY CONTOURS
          3     ION DENSITY (LOG)
          4     ION CURRENT VECTORS
          5     ION CURRENT (LOG)
          6     TOTAL CURRENT VECTORS
          7     TOTAL CURRENT (LOG)
          8     TOTAL CURRENT*RADIUS
          9     ELECTRON CURRENT VECTORS
          10    ELECTRON CURRENT (LOG)
          11    ELECTRON TEMPERATURE
          99    RADIUS PLOT
          12    CHARGE EXCHANGE ION DENSITY CONTOURS
          13    CHARGE EXCHANGE ION CURRENT CONTOURS
 WHICH  PLOT >99
```

Figure 3.3a.

```
   CHOSE CROSS-SECTIONAL PLOTS
         1     POTENTIALS
         2     ION DENSITY
         3     ELECTRON TEMPERATURE
 WHICH  PLOT >
```

Figure 3.3b.

Figure 3.3. Subroutine PLOT menus.

4. TEST CASES

In this Chapter we present four test cases for parameters representing the SERT II thruster, and two calculations for a 30 cm diameter thruster. These calculations were performed prior to collecting and refining the code to its present form, so we omit any detailed output. Also, the plots presented were made using the DISSPLA plot package and differ somewhat from the NASCAP-like plots produced by the final version of the code. Nonetheless, we believe these results represent well the type of calculation performed by the ION code.

A. SERT II CALCULATIONS

The SERT II thruster was modeled for the ION code as having a 7 cm radius ion beam. The beam had consisted of 0.085 amperes of 3 keV Hg ions. The beam profile was assumed to be

$$J(r,z) = J_0 (1 - (r/.07)^2)$$

An additional 0.055 ampere equivalent flow of 0.06 eV neutrals resulted in 0.9 mA of charge exchange ions, which expanded in barometric potentials characterized by a 2 eV electron temperature. The thermal boundary conditions at RMAX = 0.20 and ZMAX = 0.40 were set to 2 eV, while the orifice plate could be either insulating or a 2 eV heat sink. The neutralizer radius was either 8 cm or 10 cm. The results for maximum potential and temperature are shown in Table 4.1. It is apparent that the orifice plate boundary condition has substantial effect, and also, that moving the neutralizer closer to the beam has some effect in reducing joule heating of the plasma.

TABLE 4.1. SERT II RESULTS

Neutralizer Position	Thermal Boundary Condition 2 eV	Insulating Thermal Boundary
0.08	θ_{max} = 2.3 eV ϕ_{max} = 13.8 V	θ_{max} = 4.1 eV ϕ_{max} = 24.2 V
0.10	θ_{max} = 2.4 eV ϕ_{max} = 14.7 V	θ_{max} = 4.5 eV ϕ_{max} = 24.2 V

The plasma density for this model is shown in Figure 4.1. The density varies from over 10^{15} m^{-3} at the beam center to ~10^{12} m^{-3} at the upper right of the plot. The sharp drop at the beam edge is apparent. It is also clear from the figure that near the orifice plate the beam plasma density and charge exchange plasma density are comparable.

Figures 4.2-4.5 show the results of these runs for potential, electron temperature, and total current. In all cases, it appears that the hottest temperatures occur near the neutralizer. The resemblance between the potential contours and logarithmic density contours indicate the extent to which the barometric law is valid. The total current plots indicate beam neutralization within about one thruster diameter of the orifice; downstream current patterns result from incomplete convergence. There is some indication of a shorter neutralization length for the 2 eV orifice plate than for the insulating orifice plate.

B. 30 CM THRUSTER CALCULATIONS

Two further calculations were run comparing insulating and heat sink boundary conditions for a 30 cm diameter thruster. The thruster emitted one ampere of 1100 eV Hg ions, and produced 20 mA of charge exchange ions. Thus the current densities and plasma densities are both appreciably higher than for the SERT II cases. The ambient electron temperature was set to 1 eV, and the neutralizer radius to 17 cm.

The beam profile used was a Gaussian:

$$J(r) = J_0 \exp\left[-3(r/r_{95})^2\right]$$

where the nominal beam radius, r_{95}, contains 95 percent of the beam current. The resulting charge exchange ion density (Figure 4.6b) and total density (Figure 4.6a) is much smoother than in the SERT II case, where a quadratic beam profile was assumed.

Despite the lower electron temperature boundary conditions, the results (Figures 4.7-4.8) show temperatures and potentials similar to, or even greater than, the comparable SERT II cases. For the insulating case, we see the temperature maximum at the beam center rather than near the neutralizer. Otherwise, the qualitative conclusions are similar to those of the previous cases.

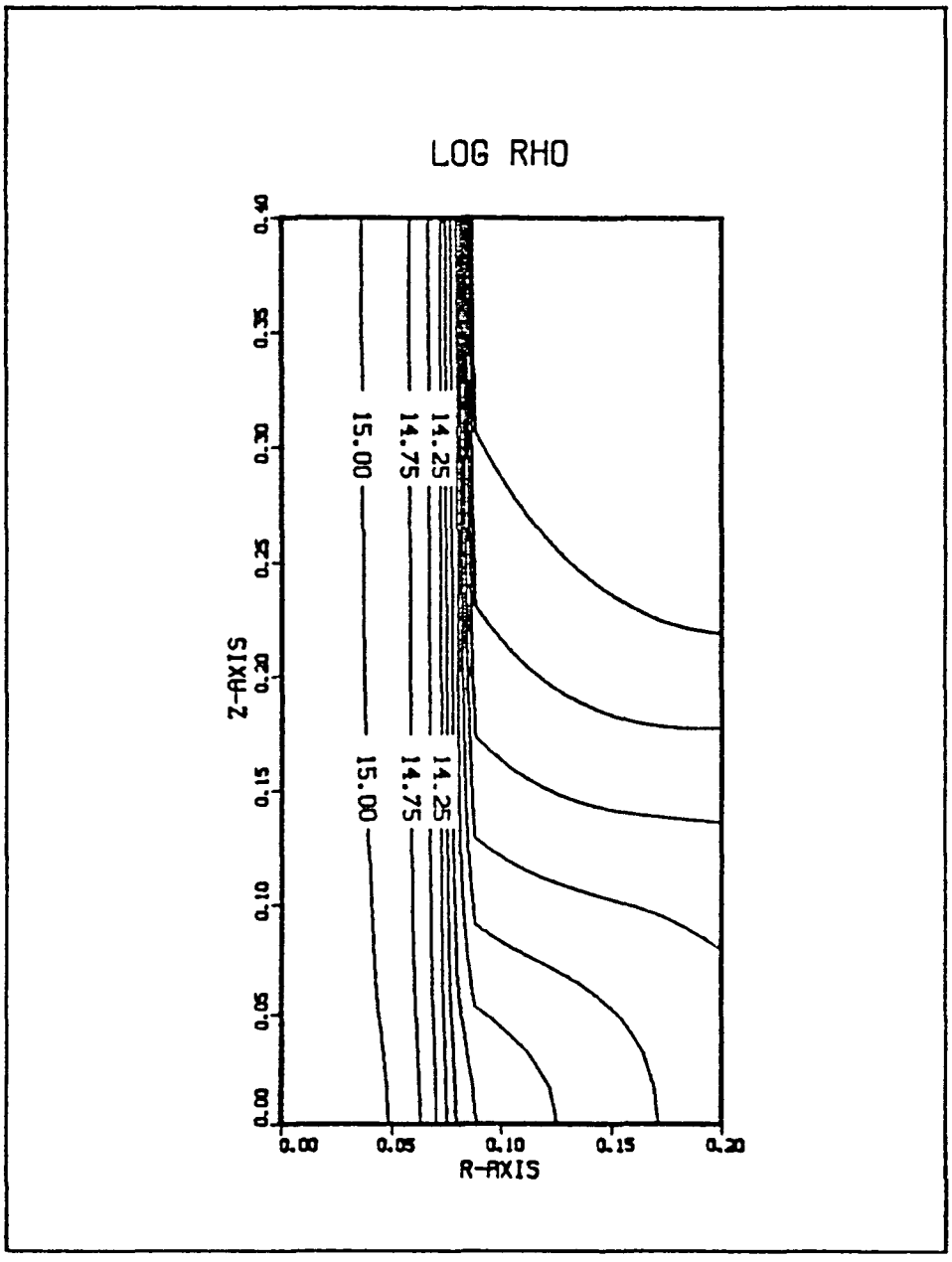

Figure 4.1. Logarithmic plasma density (beam plus charge exchange ions) for SERT II thruster cases. (Contour labels are common logarithm of density in m^{-3}.)

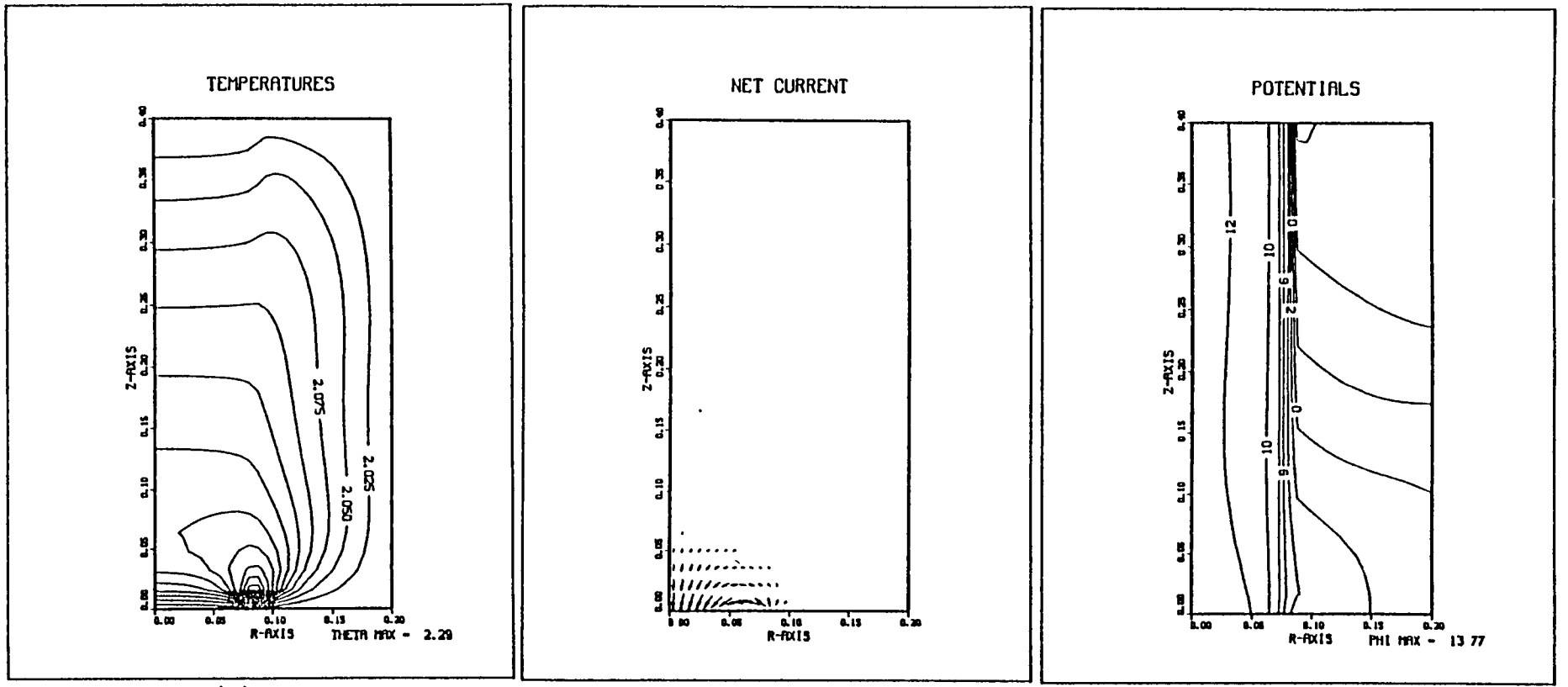

(a) (b) (c)

Figure 4.2. Temperature (a), current density (b), and potentials (c), for SERT II case: 2 eV orifice plate; 8 cm neutralizer radius.

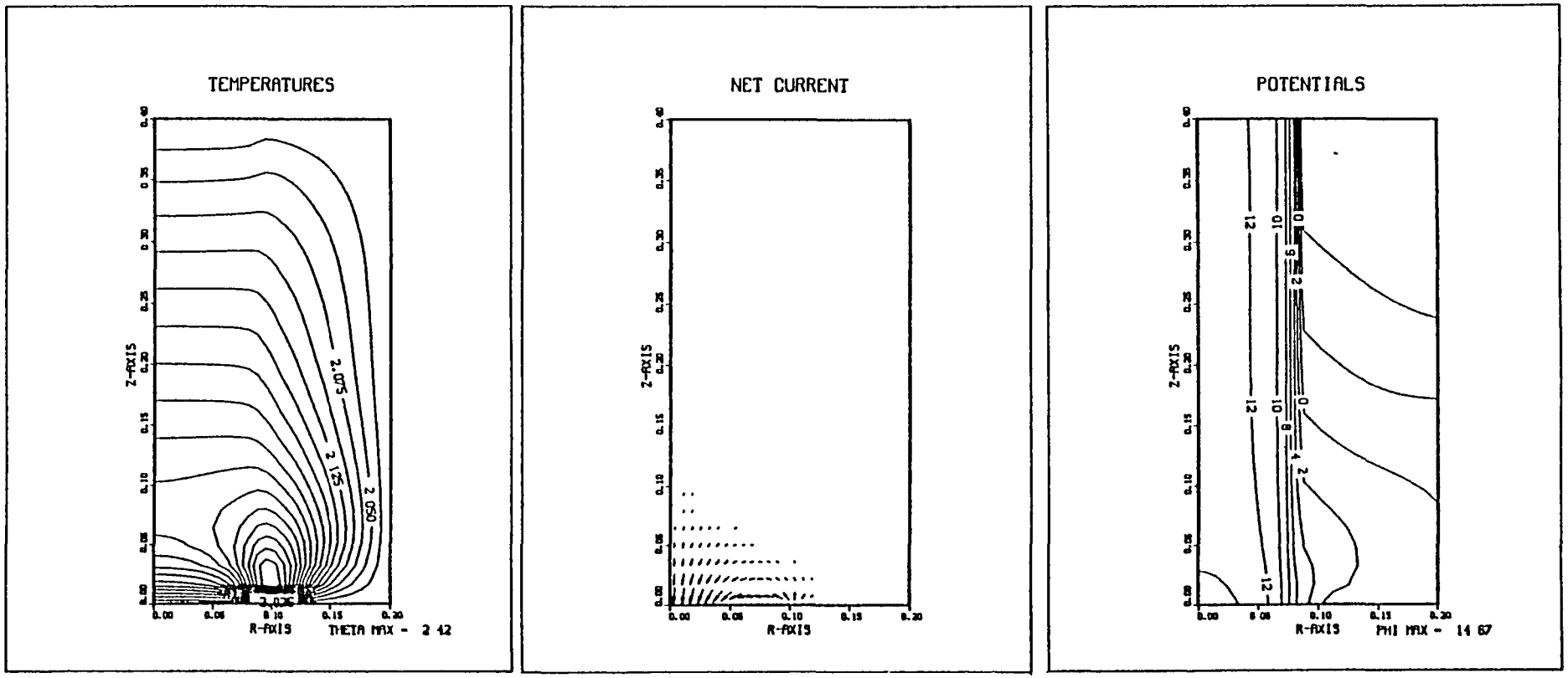

(a) (b) (c)

Figure 4.3. Temperature (a), current density (b), and potentials (c), for SERT II case: 2 eV orifice plate; 10 cm neutralizer radius.

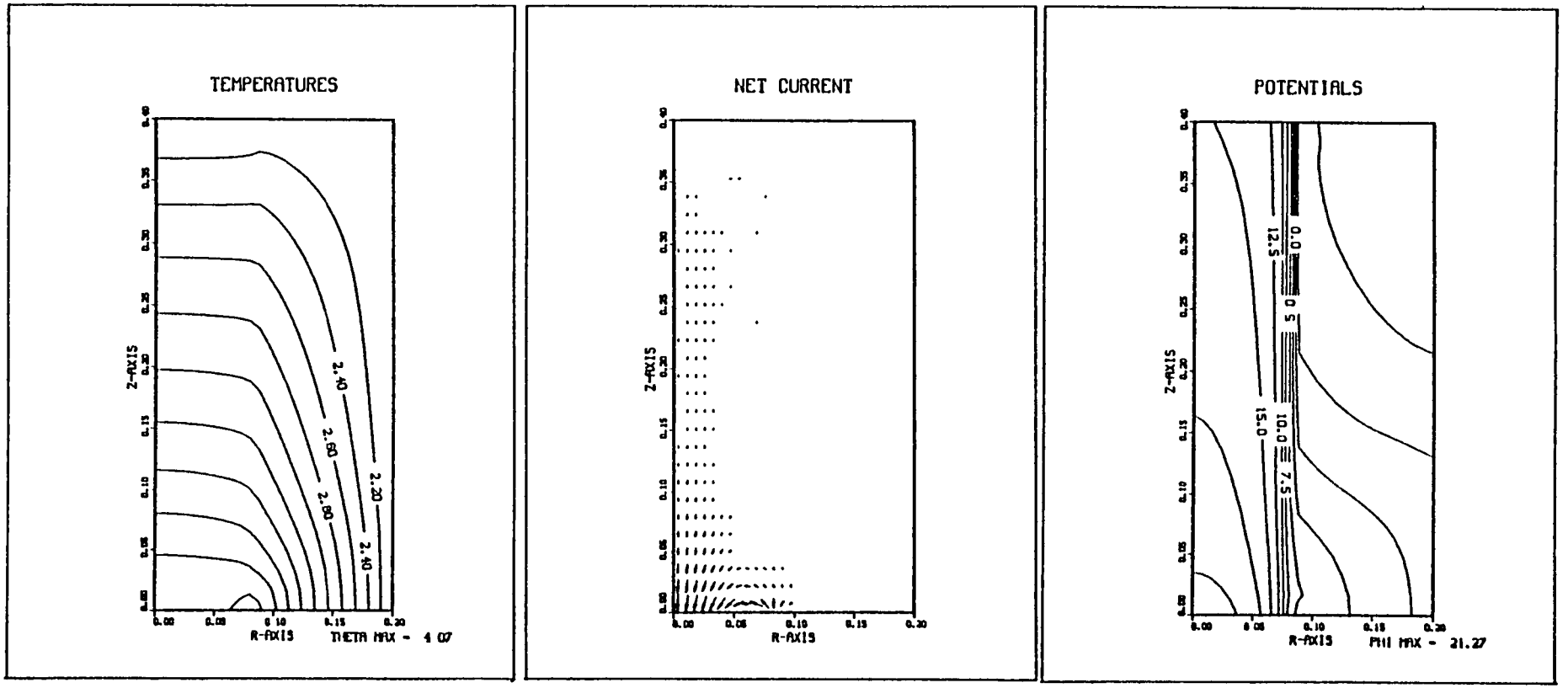

(a) (b) (c)

Figure 4.4. Temperature (a), current density (b), and potentials (c), for SERT II case: insulating orifice plate; 8 cm neutralizer radius.

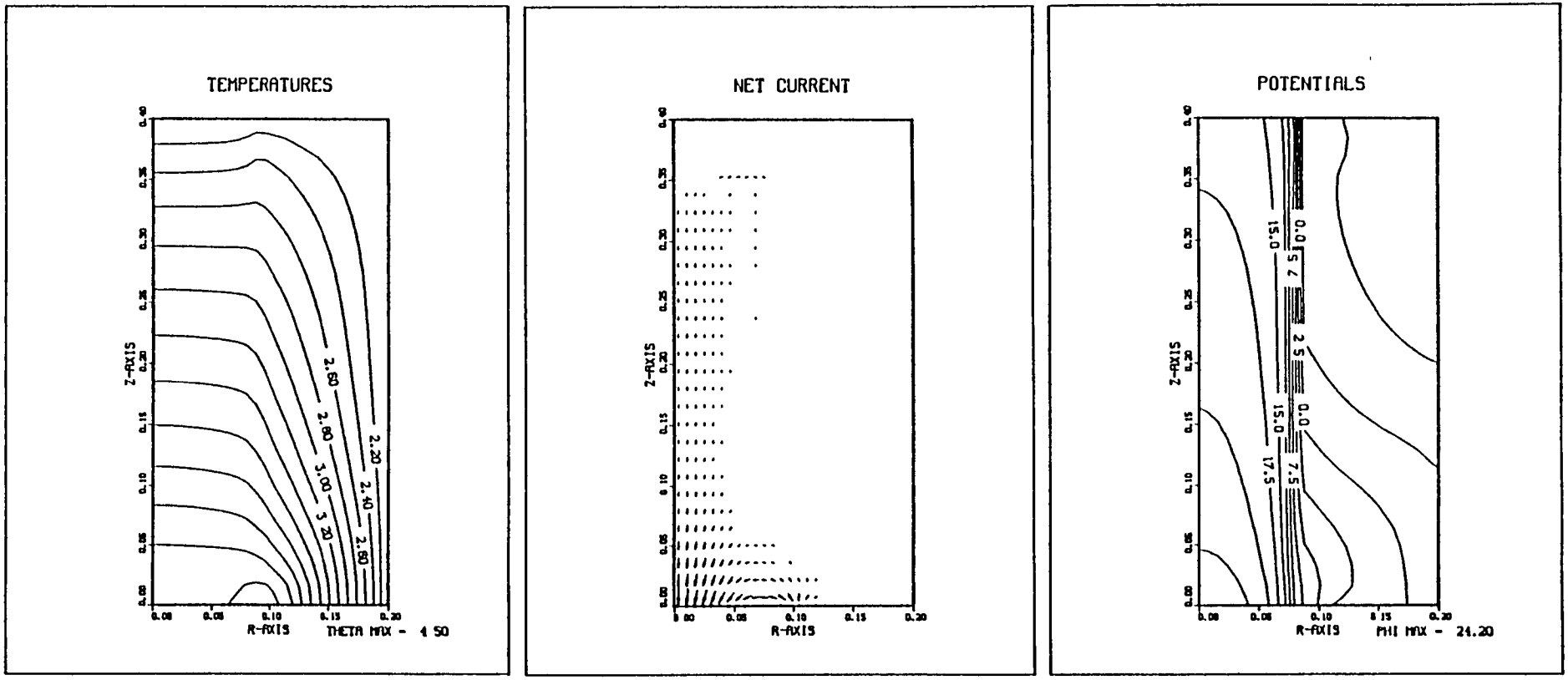

(a) (b) (c)

Figure 4.5. Temperature (a), current density (b), and potentials (c), for SERT II case: insulating orifice plate; 10 cm neutralizer radius.

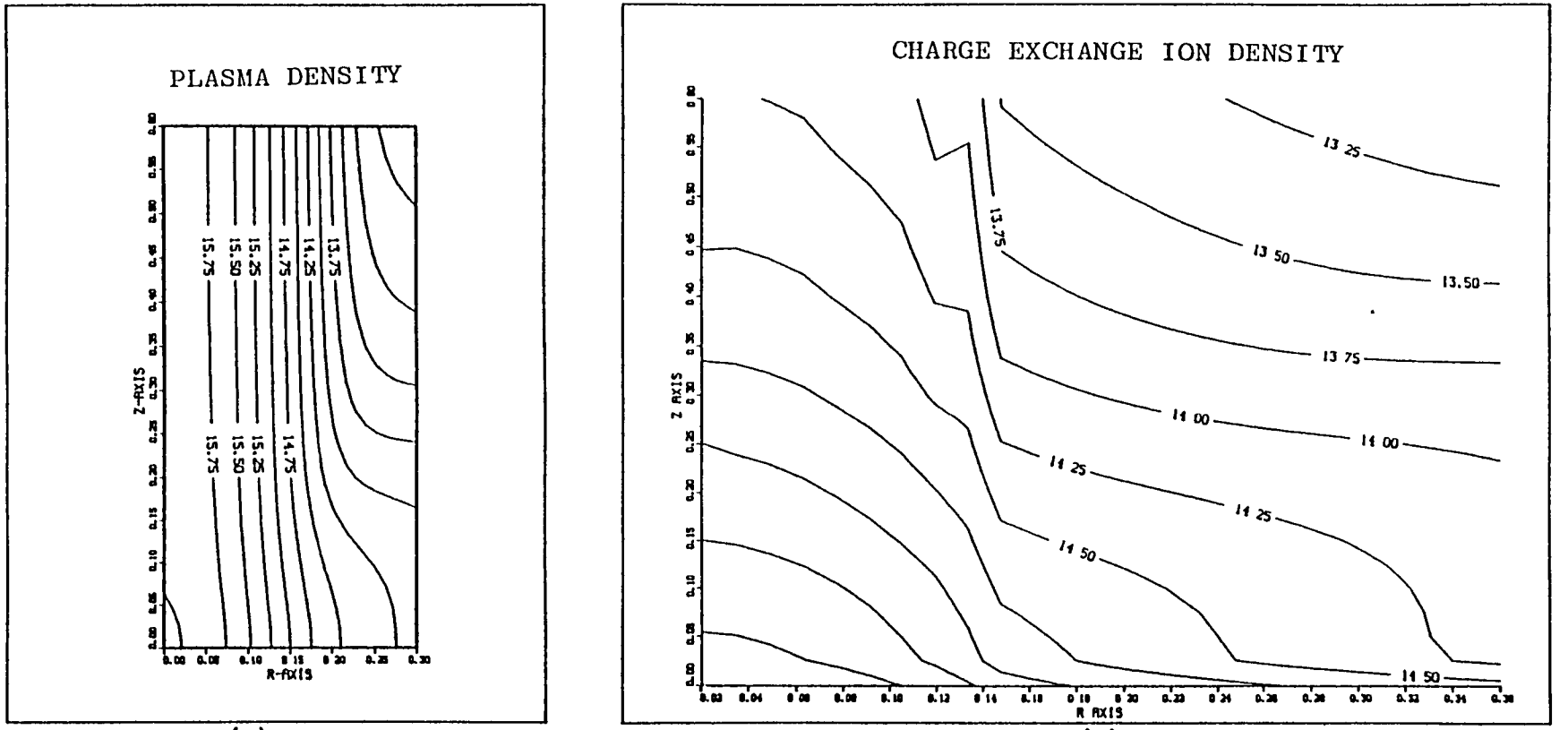

(a) (b)

Figure 4.6. Logarithmic contours of plasma density (a) and charge exchange ion density (b). (Contour labels are common logarithm of density in m^{-3}.)

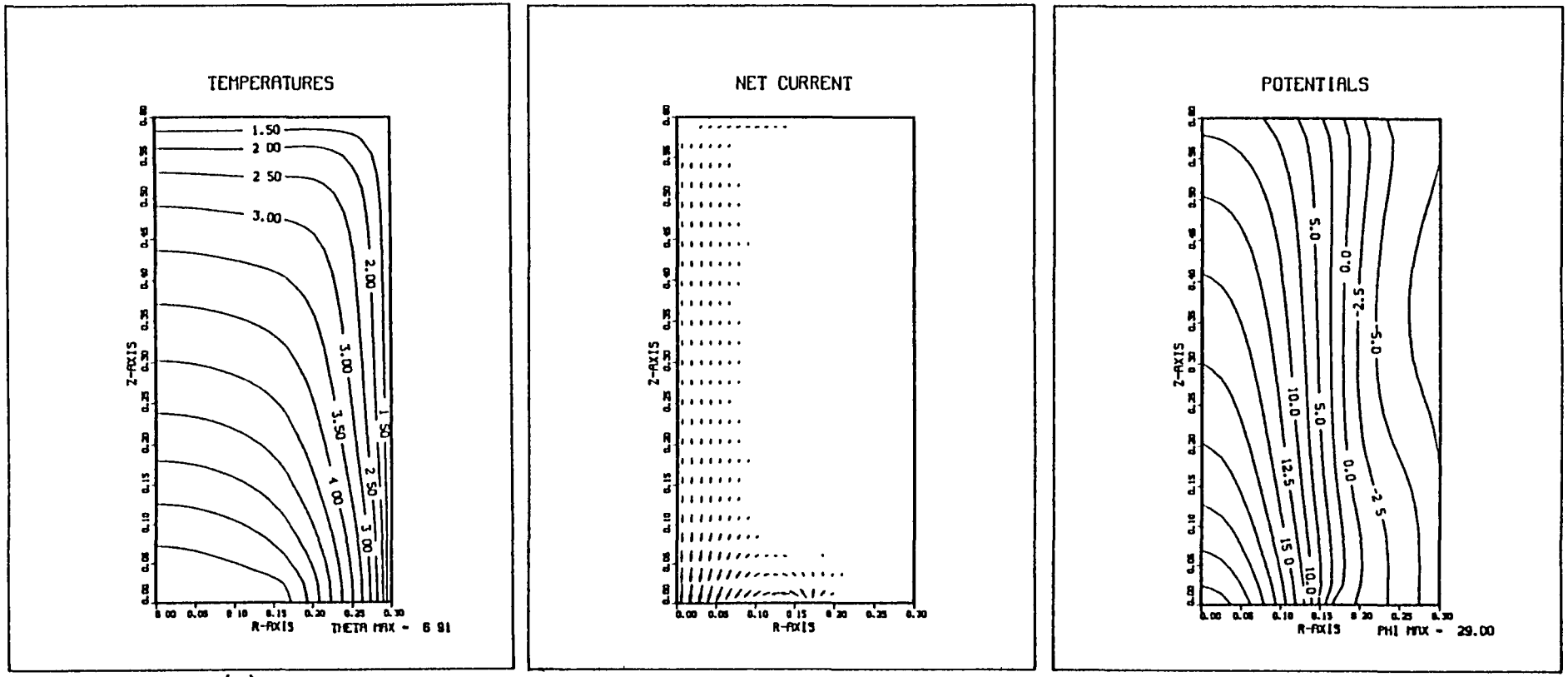

(a) (b) (c)

Figure 4.7. Temperature (a), current density (b), and potentials (c), for 30 cm thruster with insulating orifice plate.

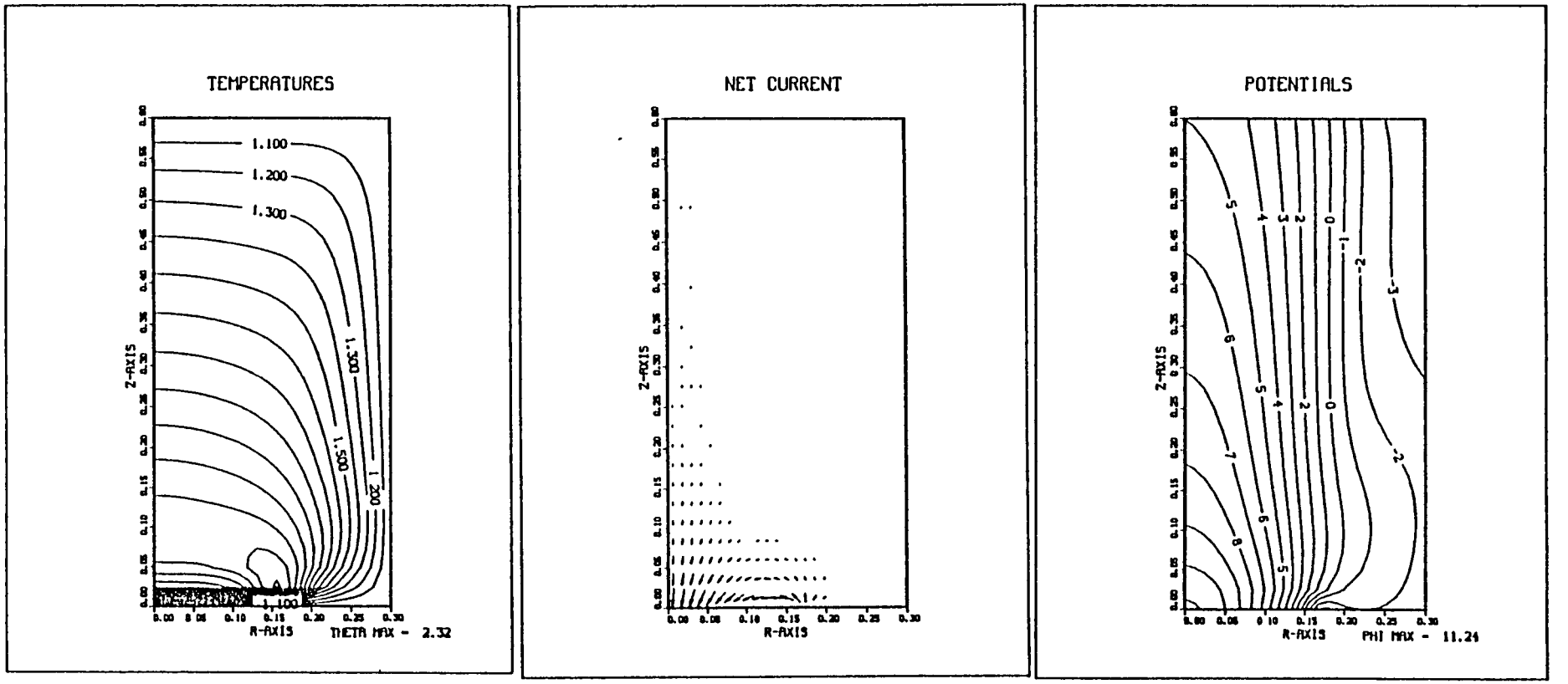

(a) (b) (c)

Figure 4.8. Temperature (a), current density (b), and potentials (c), for 30 cm thruster with 1 eV orifice plate.

5. SAMPLE RUN

In this Chapter we present a sample run of the ION CODE. The run was performed in batch mode on S-CUBED's UNIVAC 1100/81, using ASCII FORTRAN Level 9R1 with full optimization, and the plots were done on the Gould electrostatic plotter. The run conditions represent variants on the SERT II thruster.

Figure 5.1 shows the runstream for the sample run. The initial portion of the runstream involves breakpointing to a print file, printing a header and printing the runstream. After invoking the ION code [@XQT BIGION.BIGION] the initial input is @ADDed from data element BIGION.SERT. The remaining input is explicitly shown. At the end of the runstream, restart files 9 and 21 are copied from the temporary files created by ION into permanent files. (Alternatively, ION could have run directly on permanent files by

```
@ASG,PU    SAVE9.
@ASG,PU    SAVE 21.
@USE        9,SAVE9
@USE       21,SAVE21.)
```

Figure 5.2 shows the first page of output from the ION code. ION issues a welcome message and requests input. The input cards (resulting from the @ADD statement) are echoed. Then a complete option summary is printed. Next the charge exchange ion calculation (CHEX) is invoked. The neutral efflux and total charge exhange current are printed. As this hydrodynamic calculation is rather lengthy, a message is printed every fifty steps. On invoking POTENT, we notice that the 'TOTAL DNDT' does not match the charge exchange production, indicating incomplete convergence in CHEX. The four ICCG messages constitute two iterations of potential and temperature calculations. (The GETCH warning may be ignored if the subsequent fraction indicates convergence.) Convergence is achieved when, in the final pair of ICCG's the numerators are small compared with the denominators, and (more important) the denominators are small compared with their initial values.

Figure 5.3 shows the next section of output. The PLOT subroutine was requested, and we were presented with a plot menu. We requested plot 1 (potentials). The plot menu repeats (not shown) after each plot. We continued by requesting plots 3, 12, and 13, terminating with a blank card. The plots, together with title frame, are shown in Figures 5.4-5.8.

The printout continues in Figure 5.9. We prepare to restart the CHEX calculation by changing the number of steps to 50. While about it, we route the plots to the electrostatic plotter (S-CUBED feature). RECHEX is called to continue the hydrodynamic charge exchange calculation, and DNDT, as calculated by POTENT, is significantly better. We then request again the same plots (Figures 5.10-5.14; plot menus omitted.)

In Figure 5.15 we repeat RECHEX and POTENT, now having rather good convergence. The third sequence of plots appears in Figures 5.16-5.20. In Figure 5.21 we RESUME the potential calculation where we left off in 5.15. This time we plot potentials, temperatures, and currents (Figures 5.22-5.25). The convection cell around the beam edge (Figure 5.25) is indicative of incomplete convergence.

In Figure 5.26 we change the thermal boundary condition to ISOThermal. NEWPOT is invoked for a potential calculation using the same ion densities as previously. We plot potentials and currents (Figures 5.27-5.29). In Figure 5.30 we repeat the calculations for a 1 eV orifice plate. Here we see good convergence in four iterations. Plots of potential, temperature and current are requested (Figures 5.31-5.34). Finally (Figure 5.35) an END card exits us from the ION code, we execute the DISSPLA plot interface routine, and complete the run.

```
 1:@RUN MJM,111[illegible]
 2:@DELETE,C BIGIONTEST.
 3:@ASG,UP BIGIONTEST.
 4:@FREE BIGIONTEST.
 5:@ASG,A BIGIONTEST.
 6:@BRKPT PRINT$/BIGIONTEST
 7:@BIG-NAME,P
 8:ION CODE RUN
 9:BOX 24
10.@MOD,N .8,8 .M,88,4,4
11:@ED,R RUNSTART.BIGION
12:LNP*
13:@XQT BIGION.BIGION
14:@ADD BIGION.SERT
15:CHEX
16:POTENT
17:PLOT
18:1
19:3
20:12
21:13
22:
23:CHANGE
24:NSTEPS 50
25:DEST ELECTROSTATIC
26:END
27:RECHEX
28:POTENT
29:PLOT
30:1
31:3
32:12
33:13
34:
35:RECHEX
36:POTENT
37:PLOT
38:1
39:3
40:12
41:13
42:
43:RESUME
44:PLOT
45.1
46:11
47*8
48:
49:CHANGE
50:THERBC ISOT
51.END
52.NEWPOT
53*PLOT
54.1
55:8
56:
57:CHANGE
58:THERBC SINK
59:NITER 4
60:END
61:NEWPOT
62:PLOT
63:1
64:11
65.8
66:
67.END
68.@PMD,EL
69:@ASG,PU SAVE9.
70.@ASG,PU SAVE21.
71:@COPY 9.,SAVE9.
72:@COPY 21.,SAVE21.
73:@BIG-NAME,P
74:ION CODE RUN
75:END
76:BOX 24
77:@BRKPT PRINT$
78:@FREE*.
79:@SYM,U BIGIONTEST.
80:@FIN
EOF·80
NO CORRECTIONS APPLIED.

@XQT BIGION.BIGION
```

Figure 5.1. Runstream for sample run, as printed by lines 11-12 of runstream, followed by @XQT command invoking ION code.

```
   WELCOME TO ION COMPUTER CODE
   DATE=081181       TIME=113357

<PLEASE ENTER OR ADD INPUT PARAMETERS>

NR 24
NZ 24
RMAX .15
ZMAX .30
CURRENT .085
FLOW .14
SIGMA 5.E-19
TEMP .06
RADIUS .07
RNEUT .085
ENERGY 3000.
NSTEPS 300
RHOMIN 1.E10
THERBC INSU
END

CODE OPTION SUMMARY

   NR          NZ          RMAX        ZMAX
   24          24           .1500       .3000

   BEAM CURRENT            BEAM RADIUS          BEAM ENERGY
     .085000 AMPS             .0700 M             3000.0 EV

   MASS (AMU)              PROFILE              SPREAD ANGLE
      200.59                 GAUS                    .0 DEG.
                                ION MASS =  3.355-025 KG.
                                PEAK CURRENT =  1.035+020 M**(-2) SEC**(-1)
                                ION VELOCITY =   53491.5 M/SEC

   SIGMA                   FLOW                 TEMP
    5.0-019             .140000 AMPS           .060 EV

   ECHAR            VDTR            ETA             RHOMIN          NSTEPS
    10.000           .200             .050          1.00+010         300

   THERMAL BC = 'INSU' WITH TEMPERATURE    1.00 EV.

   NEUTRALIZER RADIUS =    .0850          2 ITERATIONS.

   PRINTED OUTPUT: LOGICAL UNITS NO. 19 AND  20.

   PLOT DESTINATION = NONE
   PLOT TITLE =       NASA - S-CUBED ION ENGINE PLASMA CODE

***TIME LEFT =  1792 SECONDS***

******CHEX
NEUTRAL EFFLUX =   .0550 EQUIVALENT AMPS.
 TOTAL GENERATION RATE =  .000773 AMPS
CHEX -   50 STEPS COMPLETED.  RHO(   .005,   .007) =   2.906+014
CHEX -  100 STEPS COMPLETED.  RHO(   .005,   .007) =   4.438+014
CHEX -  150 STEPS COMPLETED.  RHO(   .005,   .007) =   4.825+014
CHEX -  200 STEPS COMPLETED.  RHO(   .005,   .007) =   4.784+014
CHEX -  250 STEPS COMPLETED.  RHO(   .005,   .007) =   4.665+014
CHEX -  300 STEPS COMPLETED.  RHO(   .005,   .007) =   4.565+014

***TIME LEFT =  1391 SECONDS***

******POTENT

  CURRENT ENTERING FROM LEFT =   8.54-002
  CURRENT EXITING AT RIGHT   =   8.54-002
  CURRENT EXITING AT RMAX    =   5.84-004
  TOTAL DNDT                 =  -5.84-004
EMITTER AT NODE    14.
GETRHS -- CURZO,ELJ =  8.54-002  2.46+001
***WARNING*** GETCH --- CH( 5477) = -1.00+000

    ICCG --- RDOTR/RDOTR1 =   2.32-005/  7.76-001     NITER= 31

    ICCG --- RDOTR/RDOTR1 =   3.18-014/  1.35-001     NITER= 25
***WARNING*** GETCH --- CH( 5477) = -1.00+000

    ICCG --- RDOTR/RDOTR1 =   2.16-003/  6.74-001     NITER= 31

    ICCG --- RDOTR/RDOTR1 =   7.92-015/  9.92-003     NITER= 24
```

Figure 5.2. Output resulting from lines 13-16 of runstream.

```
******PLOT


          1      POTENTIAL CONTOURS
          2      ION DENSITY CONTOURS
          3      ION DENSITY (LOG)
          4      ION CURRENT VECTORS
          5      ION CURRENT (LOG)
          6      TOTAL CURRENT VECTORS
          7      TOTAL CURRENT (LOG)
          8      TOTAL CURRENT*RADIUS
          9      ELECTRON CURRENT VECTORS
          10     ELECTRON CURRENT (LOG)
          11     ELECTRON TEMPERATURE
          99     RADIUS PLOT
          12     CHARGE EXCHANGE ION DENSITY CONTOURS
          13     CHARGE EXCHANGE ION CURRENT CONTOURS
WHICH  PLOT ##
```

Figure 5.3. Plot menu (line 17 of runstream).

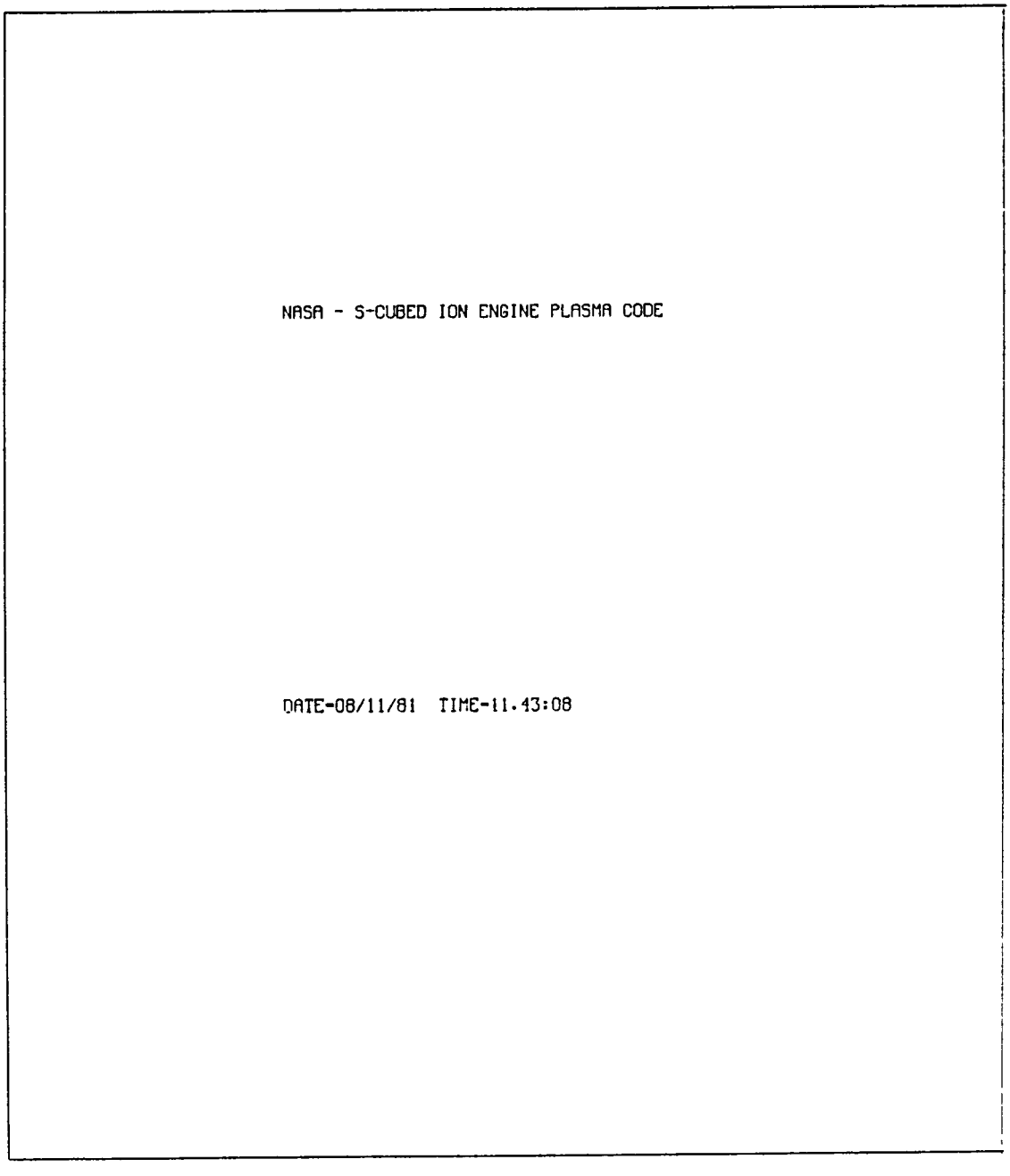

Figure 5.4. Plot title page.

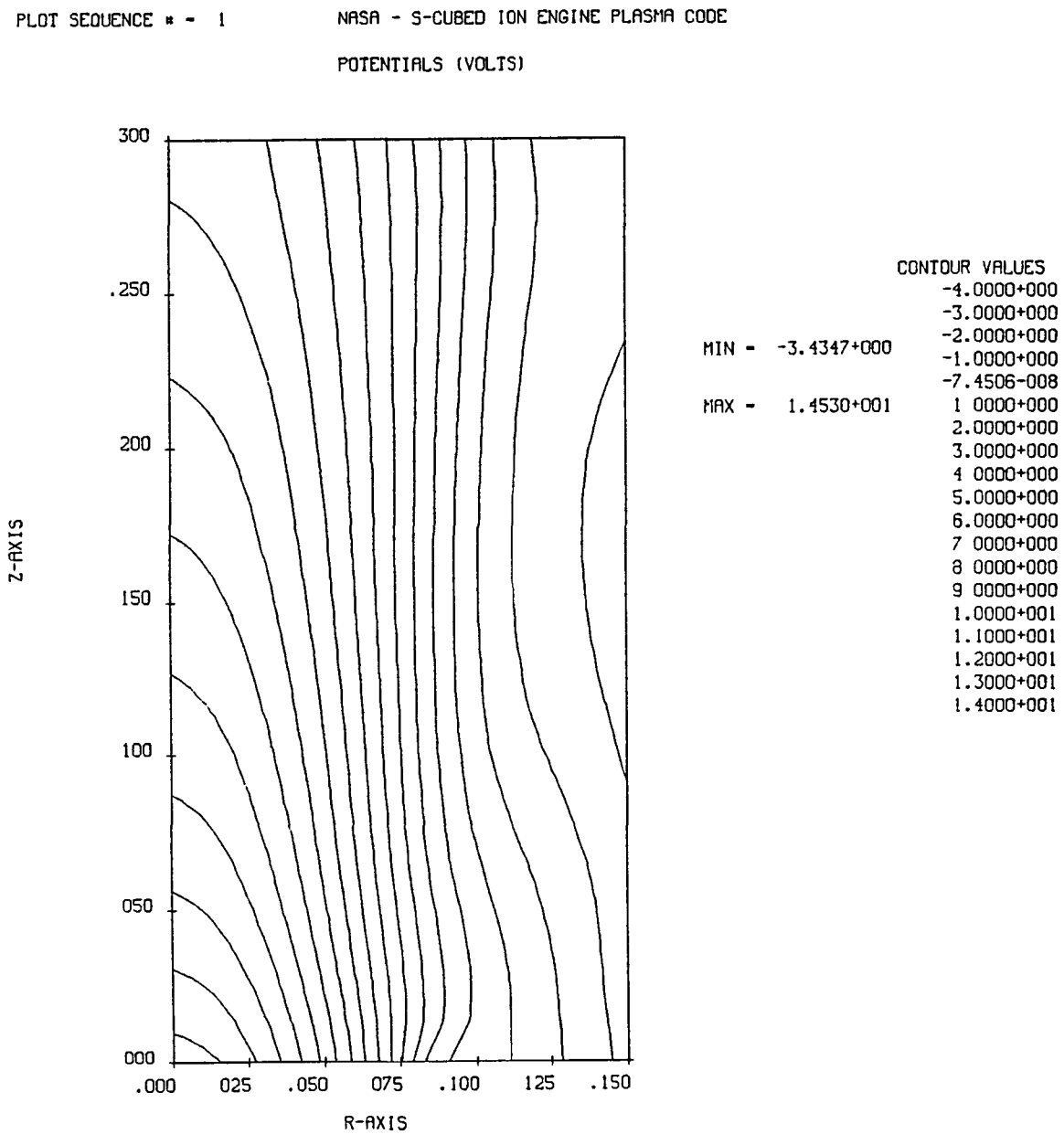

Figure 5.5. Potential contour plot requested in line 18 of runstream.

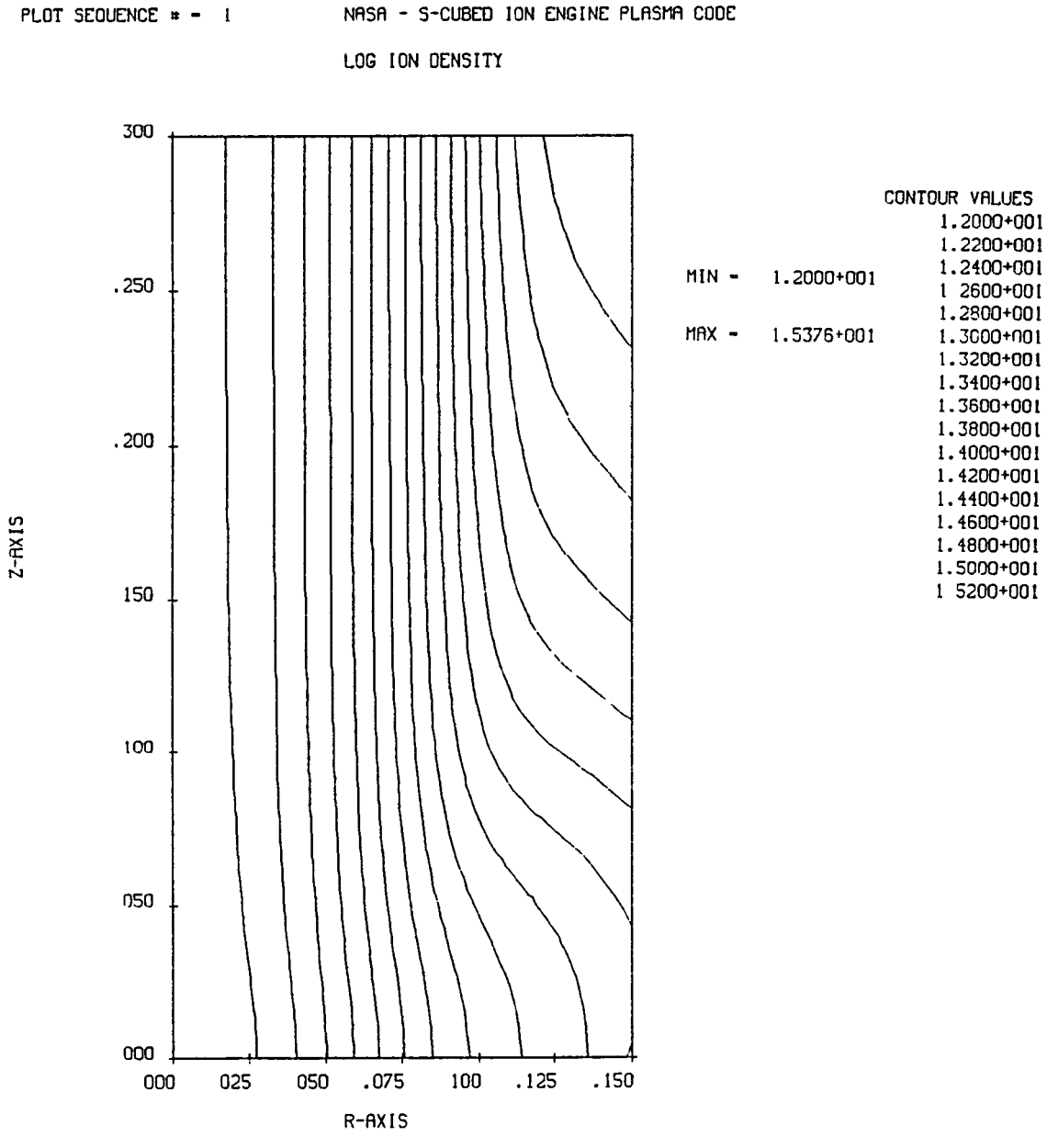

Figure 5.6. Logarithmic ion density contour plot requested in line 19 of runstream.

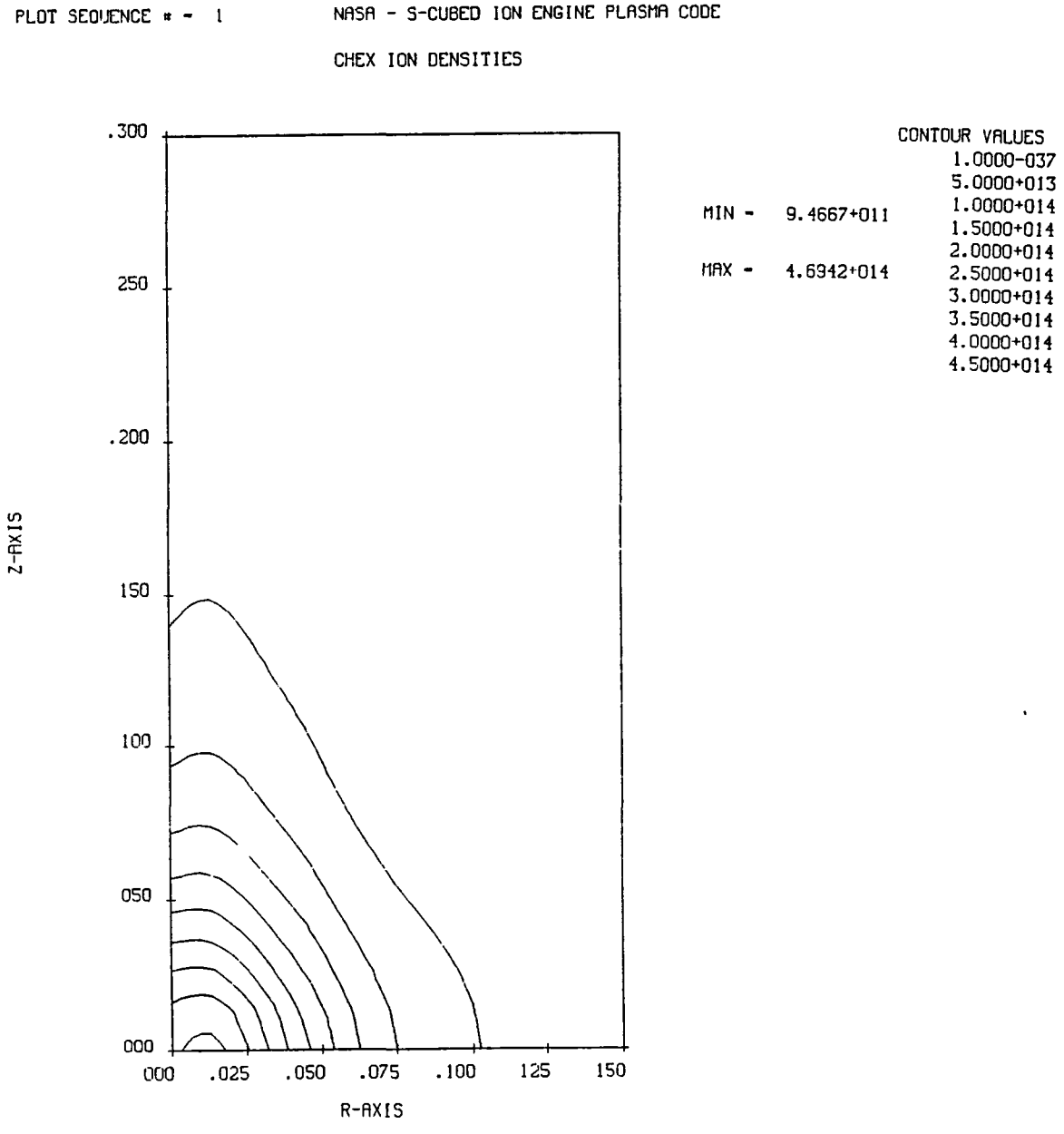

Figure 5.7. Charge exchange ion density contour plot requested in line 20 of runstream.

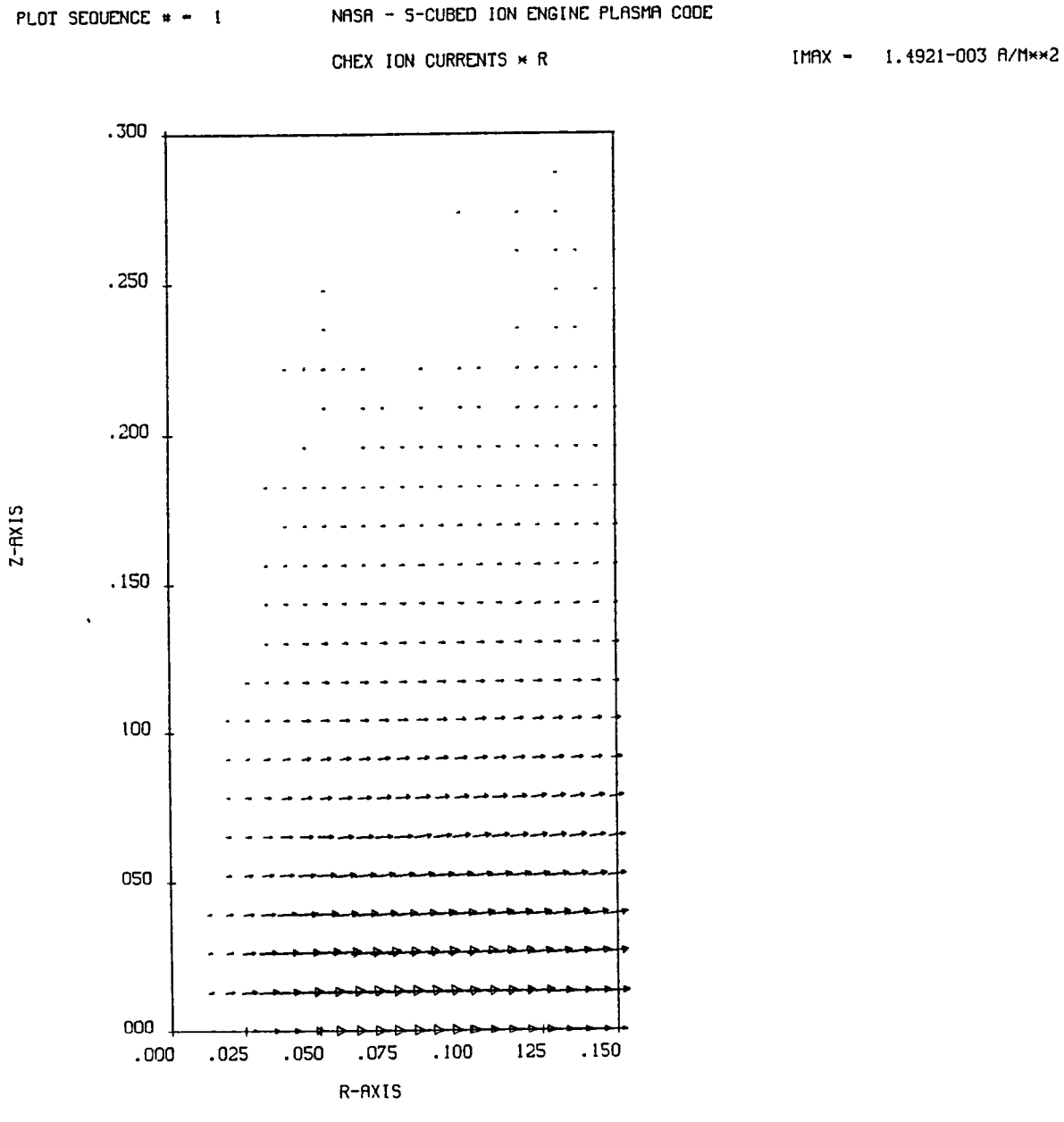

Figure 5.8. Charge exchange current vector plot requested in line 21 of runstream.

```
***TIME LEFT =  1340 SECONDS***

******CHANGE
NSTEPS 50
DEST ELECTROSTATIC
***FBREAK*** GROUP NO.  2 IN THIS CARD IMAGE - TOO LONG
DEST ELECTROSTATIC
END

CODE OPTION SUMMARY

   NR          NZ          RMAX        ZMAX
   24          24           .1500       .3000

   BEAM CURRENT            BEAM RADIUS          BEAM ENERGY
     .085000 AMPS            .0700 M              3000.0 EV

   MASS (AMU)              PROFILE              SPREAD ANGLE
      200.59                 GAUS                  .0 DEG.
                                ION MASS =  3.355-025 KG.
                                PEAK CURRENT =  1.035+020 M**(-2) SEC**(-1)
                                ION VELOCITY =   53491.5 M/SEC

   SIGMA                   FLOW                 TEMP
    5.0-019             .140000 AMPS           .060 EV

   ECHAR          VDTR            ETA             RHOMIN          NSTEPS
    10.000         .200            .050          1.00+010           50

   THERMAL BC = 'INSU' WITH TEMPERATURE     1.00 EV.

   NEUTRALIZER RADIUS =     .0850          2 ITERATIONS.

   PRINTED OUTPUT. LOGICAL UNITS NO. 19 AND  20.

   PLOT DESTINATION = ELEC
   PLOT TITLE =       NASA - S-CUBED ION ENGINE PLASMA CODE

***TIME LEFT =  1340 SECONDS***

******RECHEX
NEUTRAL EFFLUX =    .0550 EQUIVALENT AMPS.
 TOTAL GENERATION RATE =  .000773 AMPS
CHEX -    50 STEPS COMPLETED.  RHO(    .005,    .007) =   4.498+014

***TIME LEFT =  1275 SECONDS***

******POTENT

  CURRENT ENTERING FROM LEFT =   8.54-002
  CURRENT EXITING AT RIGHT   =   8.54-002
  CURRENT EXITING AT RMAX    =   6.92-004
  TOTAL DNDT                 =  -6.93-004
EMITTER AT NODE    14.
GETRHS -- CURZO,ELJ =  8.54-002  2.46+001
***WARNING*** GETCH --- CH( 5477) = -1.00+000

    ICCG --- RDOTR/RDOTR1 =   2.30-002/  7.75-001      NITER= 31

    ICCG --- RDOTR/RDOTR1 =   1.34-013/  1.41-001      NITER= 24
***WARNING*** GETCH --- CH( 5477) = -1.00+000




    ICCG --- RDOTR/RDOTR1 =   2.16-006/  7.14-001      NITER= 31

    ICCG --- RDOTR/RDOTR1 =   7.73-015/  9.73-003      NITER= 23

***TIME LEFT =  1233 SECONDS***

******PLOT
```

Figure 5.9. Output resulting from lines 23-29 of runstream.

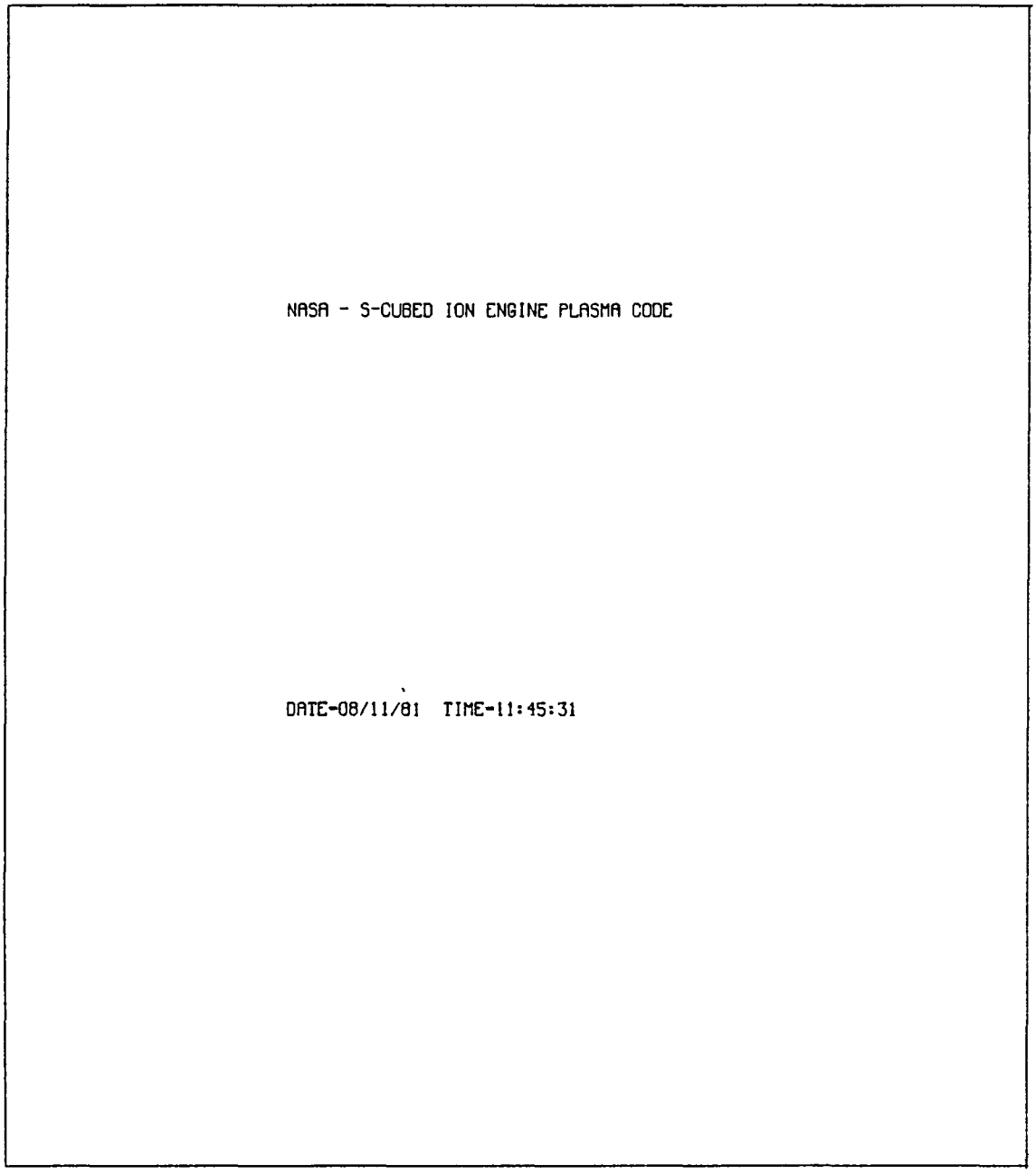

Figure 5.10. Plot title page (line 29 of runstream).

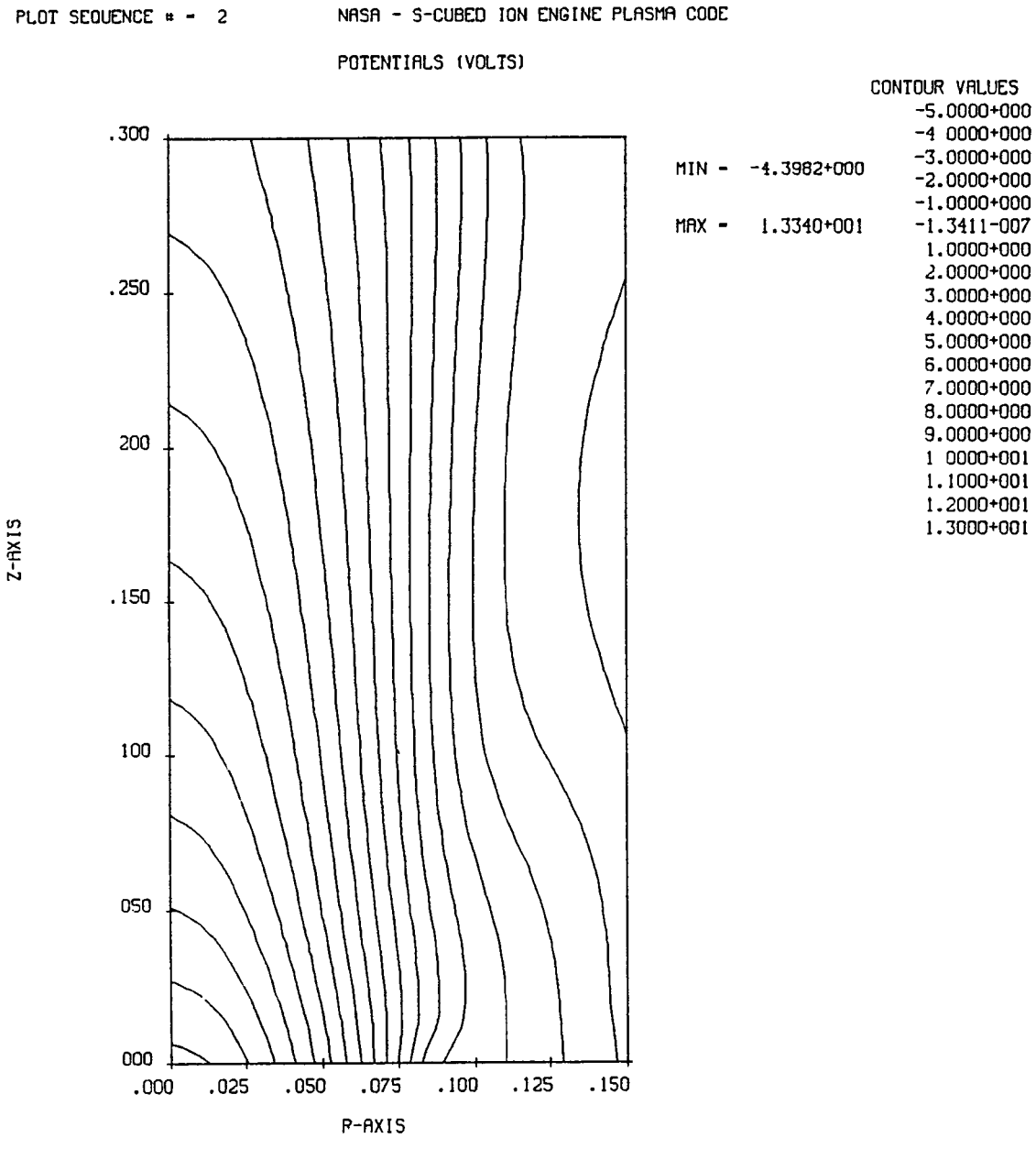

Figure 5.11. Potential contour plot (line 30).

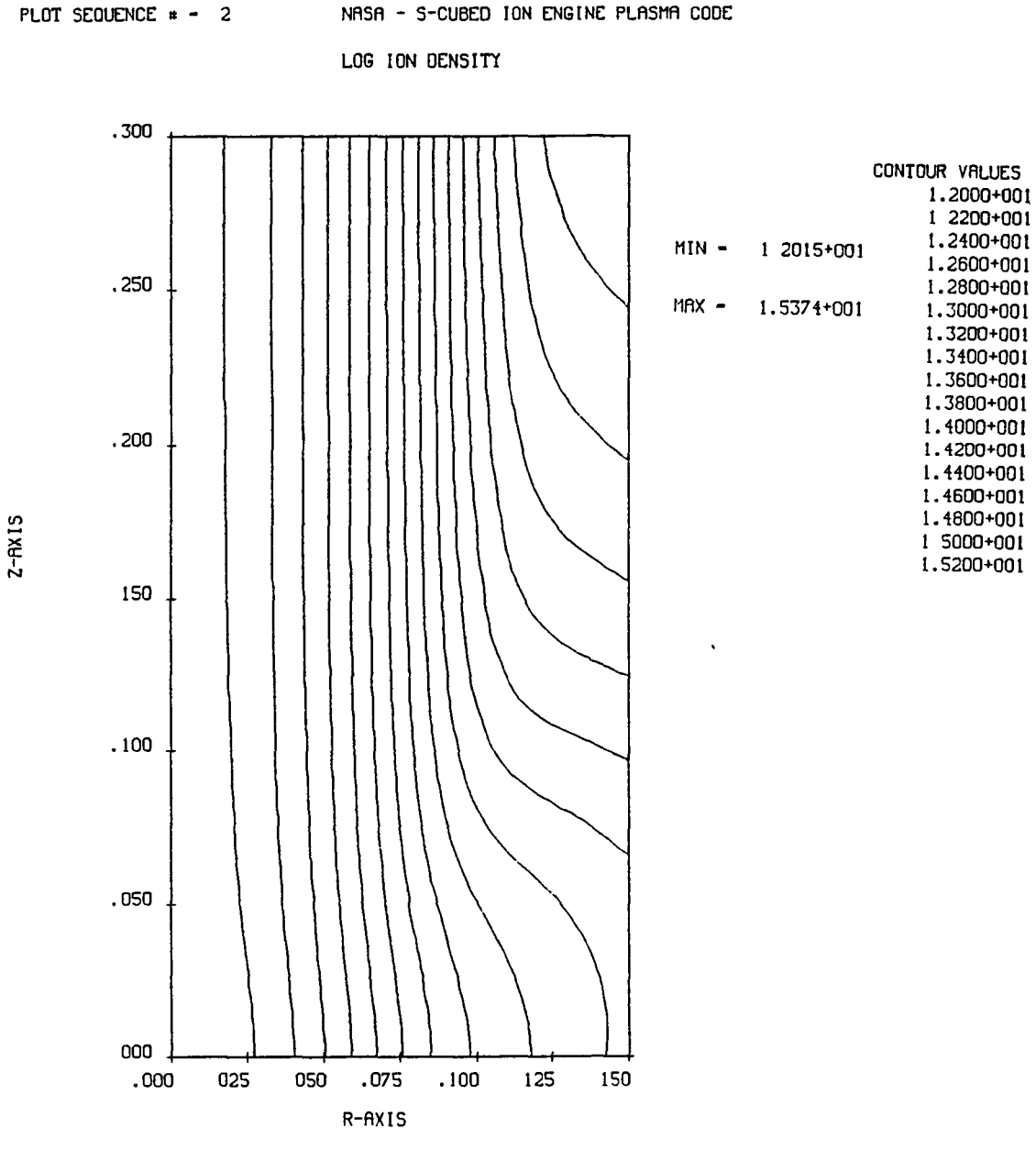

Figure 5.12. Ion density logarithmic contour plot (line 31).

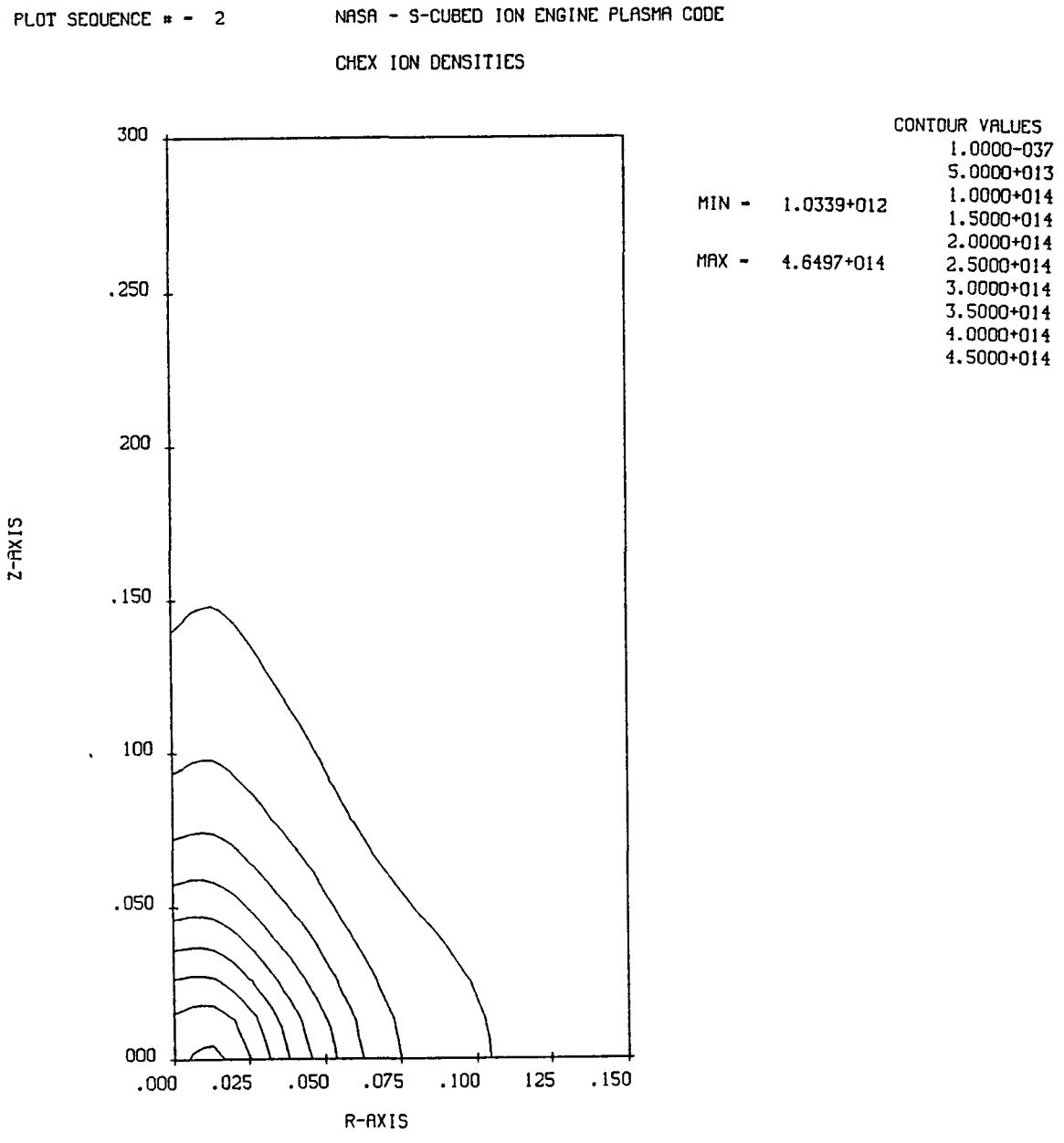

Figure 5.13. Charge exchange ion density contours (line 32).

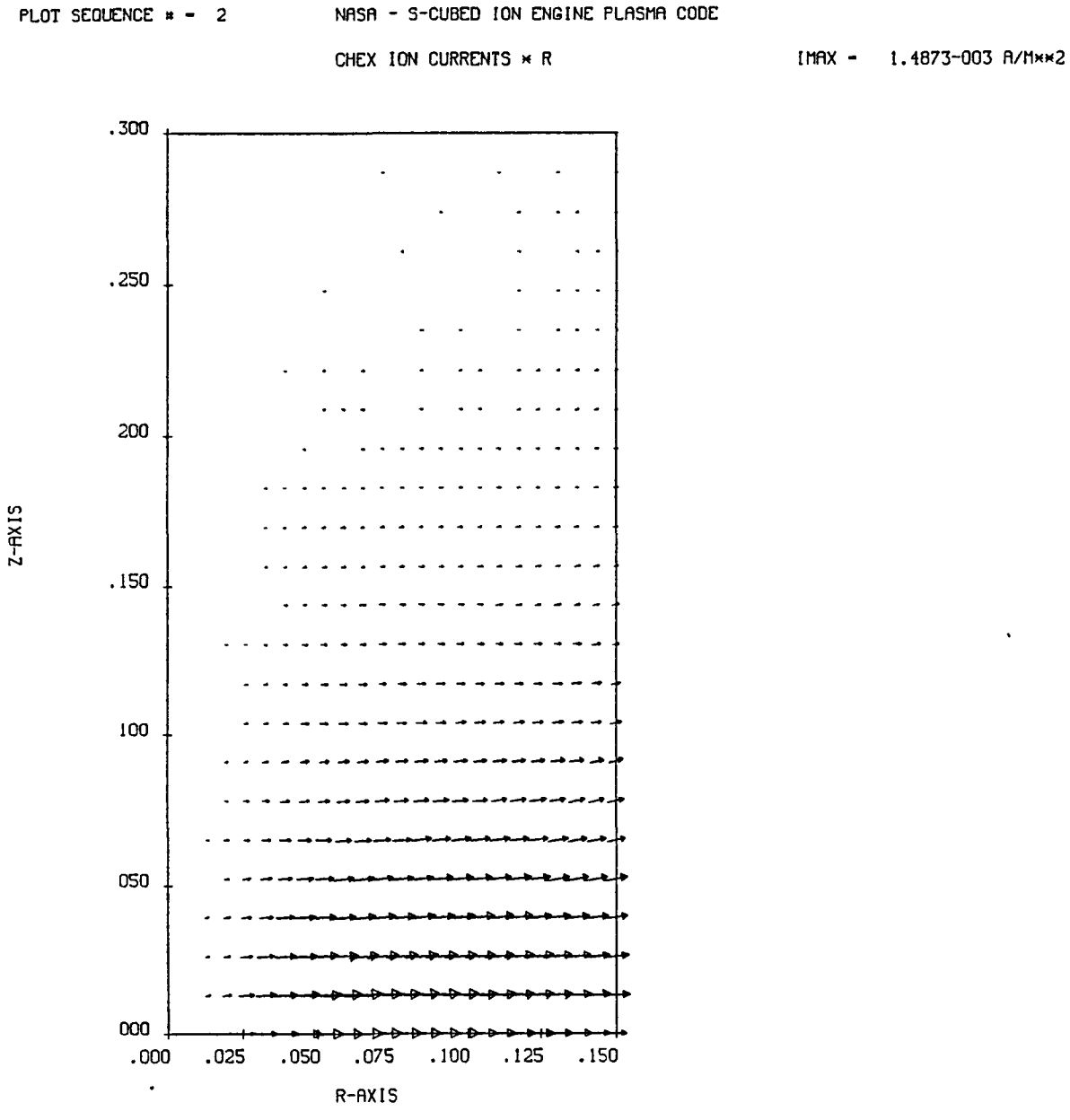

Figure 5.14. Charge exchange ion current vector plot (line 33).

```
***TIME LEFT =  1231 SECONDS***

******RECHEX
NEUTRAL EFFLUX =    .0550 EQUIVALENT AMPS.
 TOTAL GENERATION RATE =  .000773 AMPS
CHEX -   50 STEPS COMPLETED.  RHO(   .005,   .007) =   4.453+014

***TIME LEFT =  1160 SECONDS***

******POTENT

  CURRENT ENTERING FROM LEFT =   8.54-002
  CURRENT EXITING AT RIGHT   =   8.54-002
  CURRENT EXITING AT RMAX    =   7.43-004
  TOTAL DNDT                 =  -7.43-004
EMITTER AT NODE     14.
GETRHS -- CURZO,ELJ =  8.54-002  2.46+001
***WARNING*** GETCH --- CH( 5477) = -1.00+000

    ICCG --- RDOTR/RDOTR1 =   1.44-004/  7.77-001      NITER= 31

    ICCG --- RDOTR/RDOTR1 =   1.14-013/  1.33-001      NITER= 24
***WARNING*** GETCH --- CH( 5477) = -1.00+000

    ICCG --- RDOTR/RDOTR1 =   1.08-004/  6.21-001      NITER= 31

    ICCG --- RDOTR/RDOTR1 =   4.53-015/  8.36-003      NITER= 24

***TIME LEFT =  1118 SECONDS***

******PLOT
```

Figure 5.15. Output resulting from lines 35-37 of runstream.

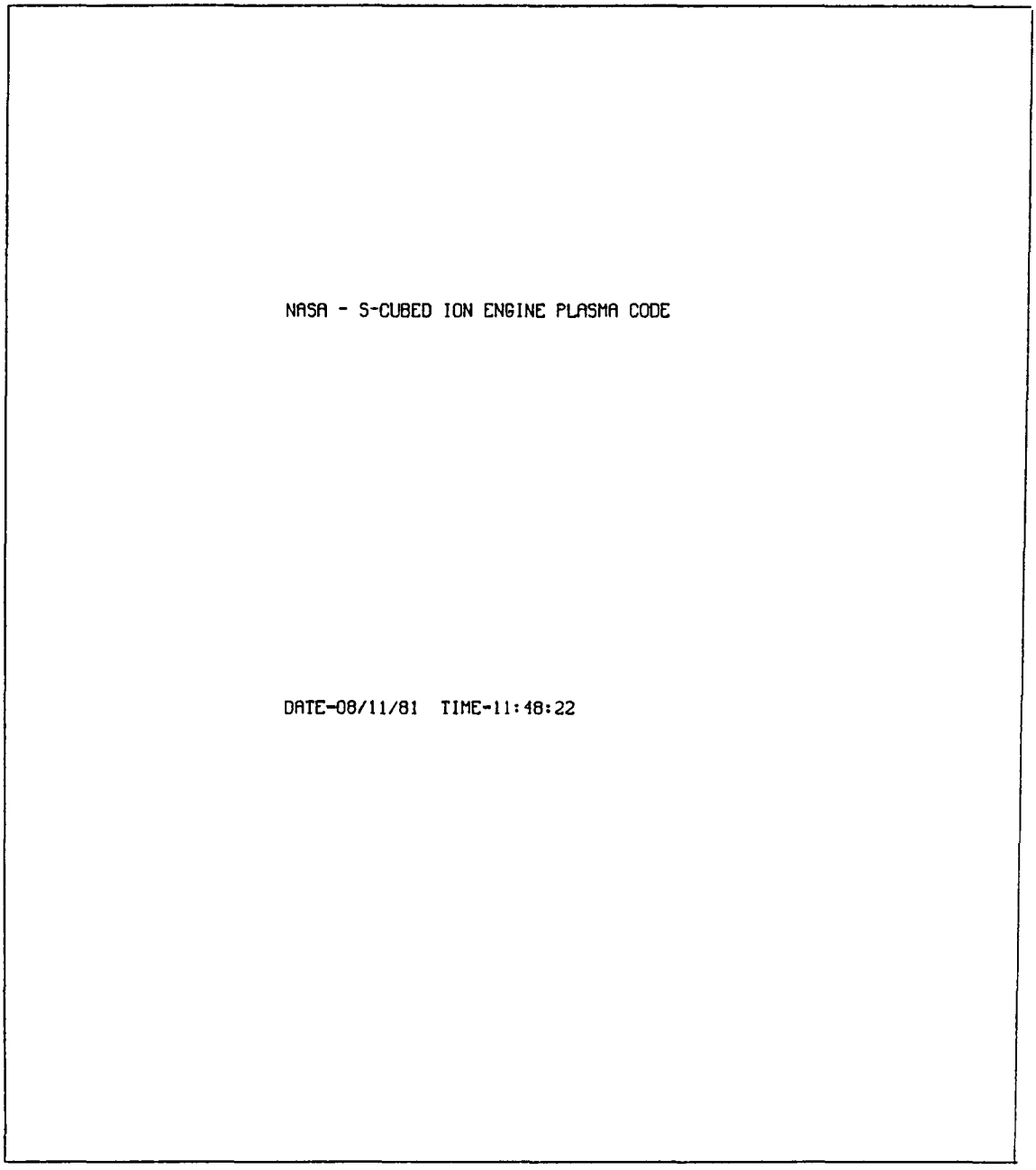

Figure 5.16. Plot title page (line 37 of runstream).

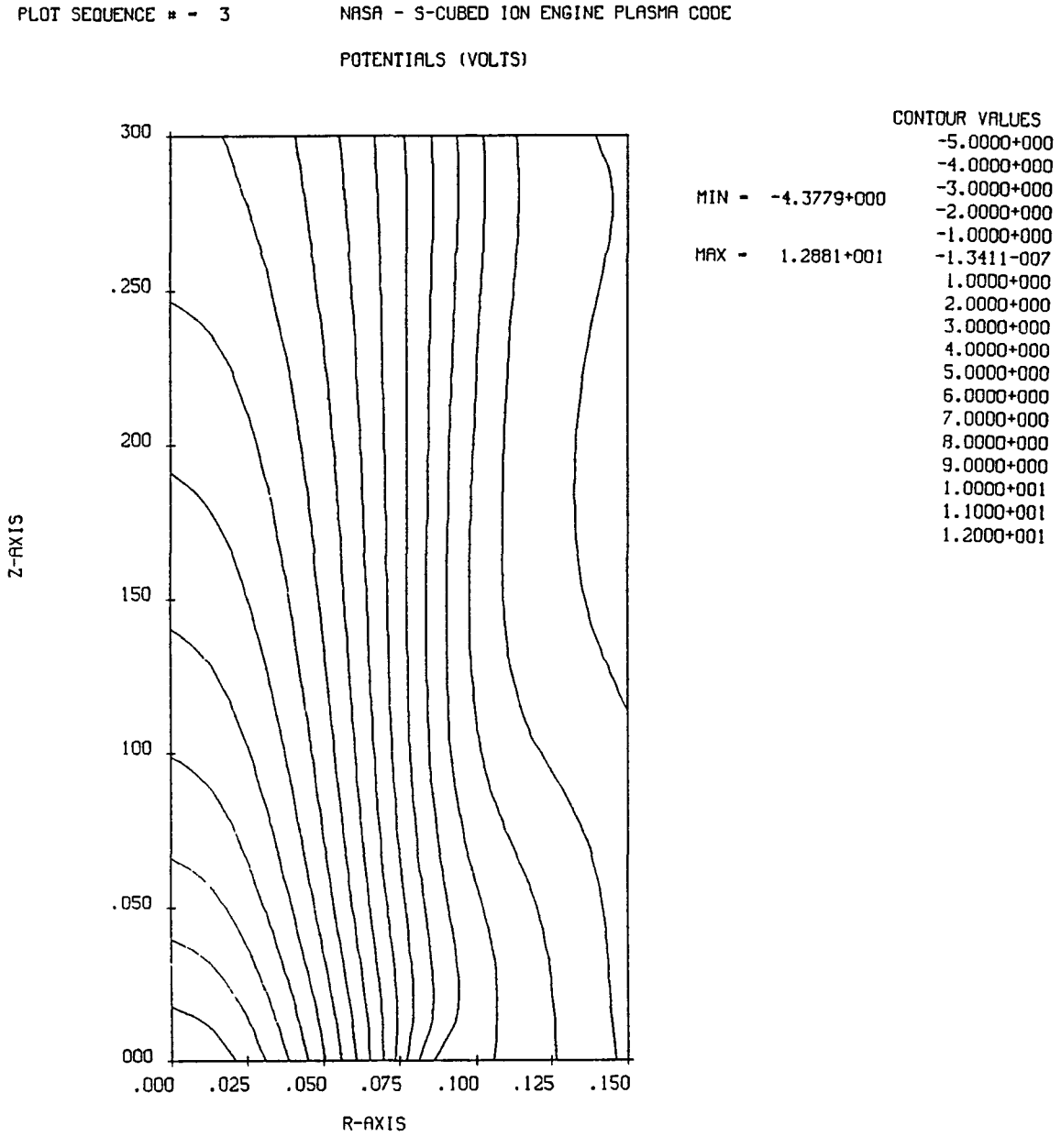

Figure 5.17. Potential contour plot (line 38).

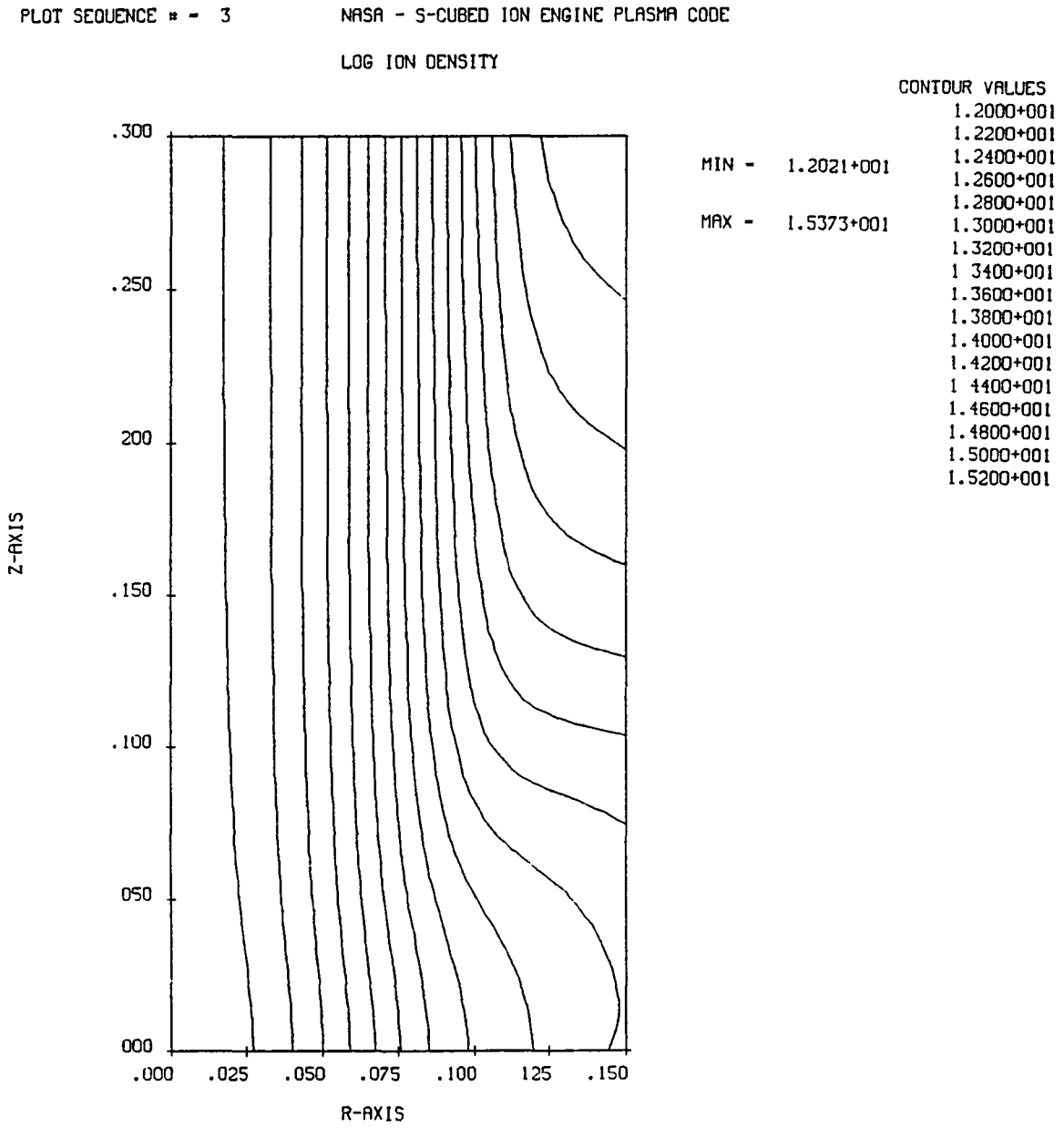

Figure 5.18. Ion density logarithmic contours (line 39).

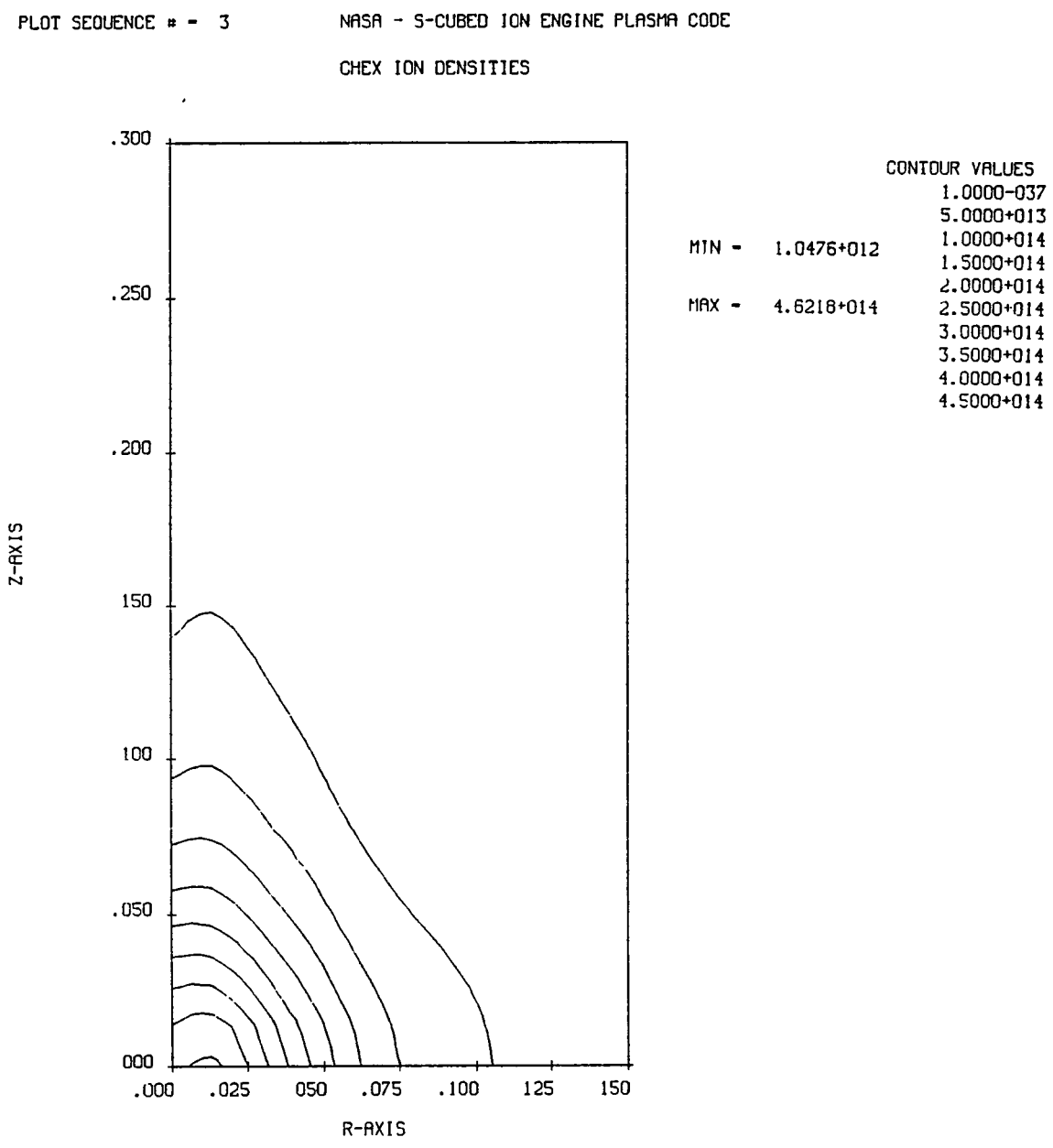

Figure 5.19. Charge exchange ion density contours (line 40).

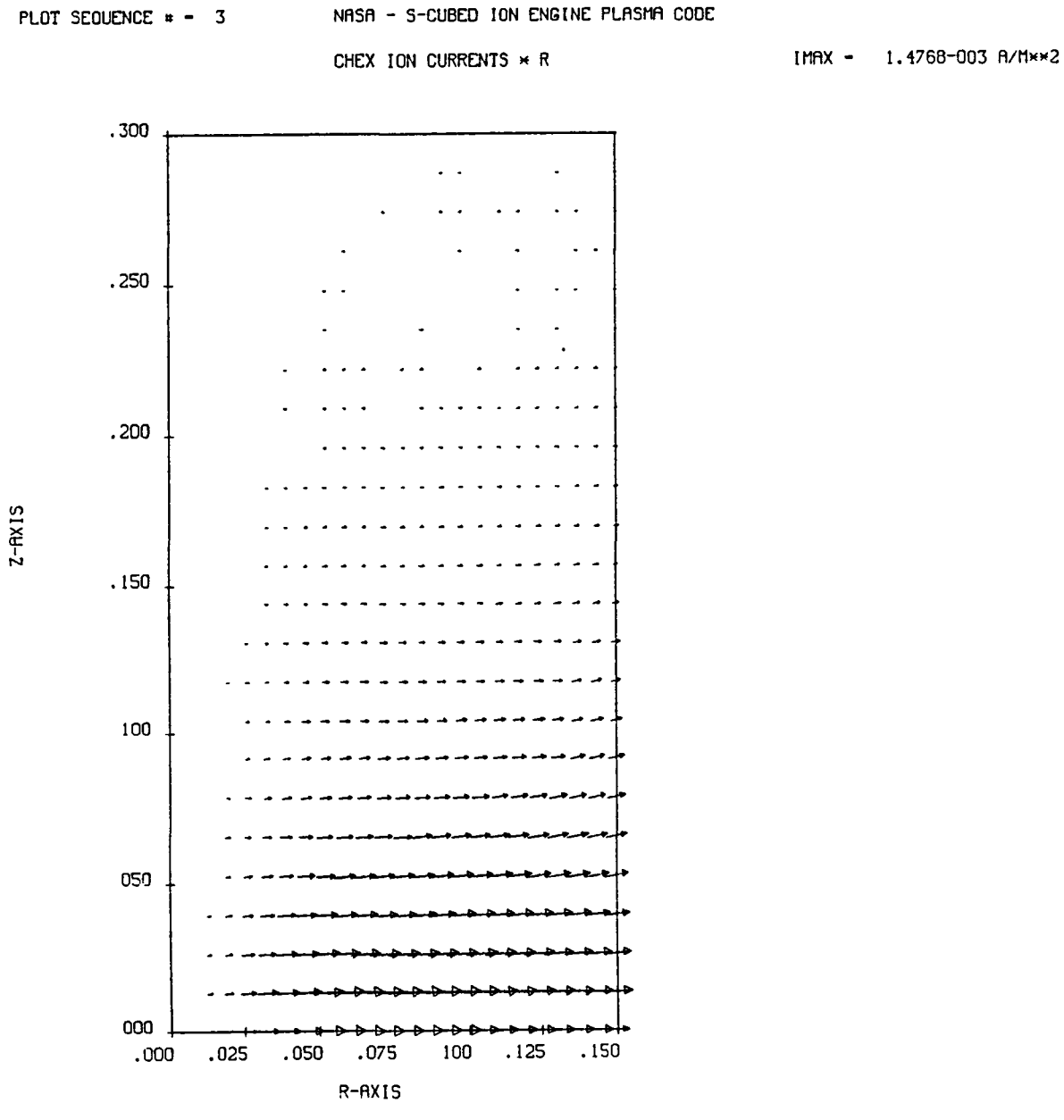

Figure 5.20. Charge exchange current vectors (line 41; cf. Figures 5.8, 5.14).

```
***TIME LEFT =  1116 SECONDS***

******RESUME
EMITTER AT NODE     14.
GETRHS -- CURZO,ELJ =  8.54-002  2.46+001
***WARNING*** GETCH --- CH( 5477) = -1.00+000
    ICCG --- RDOTR/RDOTR1 =   1.18-006/  2.92-002     NITER= 31
    ICCG --- RDOTR/RDOTR1 =   1.12-016/  7.97-004     NITER= 24
***WARNING*** GETCH --- CH( 5477) = -1.00+000
    ICCG --- RDOTR/RDOTR1 =   3.14-009/  8.49-004     NITER= 31
    ICCG --- RDOTR/RDOTR1 =   1.47-017/  5.47-005     NITER= 24
***TIME LEFT =  1080 SECONDS***

******PLOT
```

Figure 5.21. Output resulting from lines 43-44 of runstream.

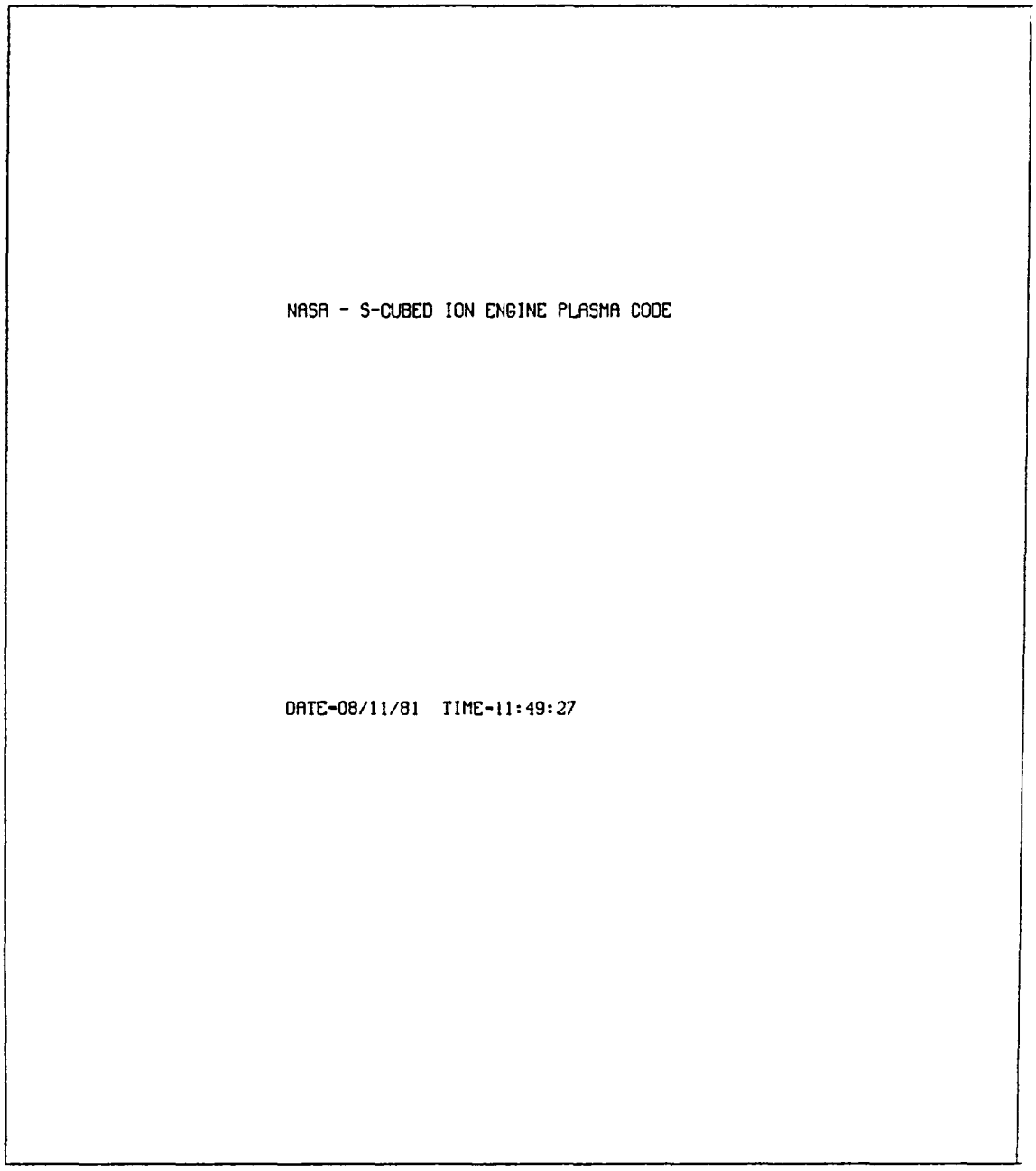

Figure 5.22. Plot title page (line 44).

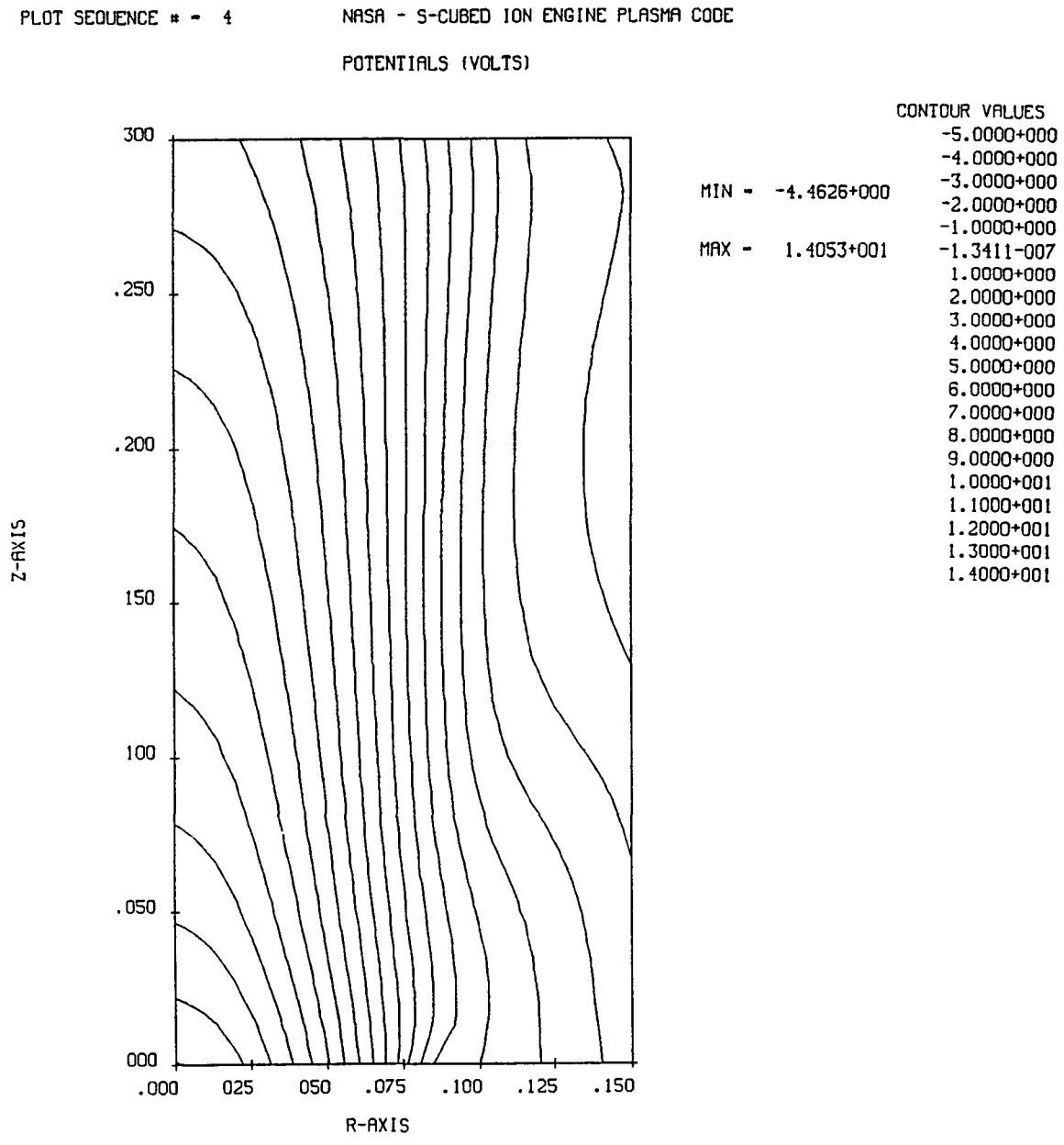

Figure 5.23. Potential contour plots (line 45).

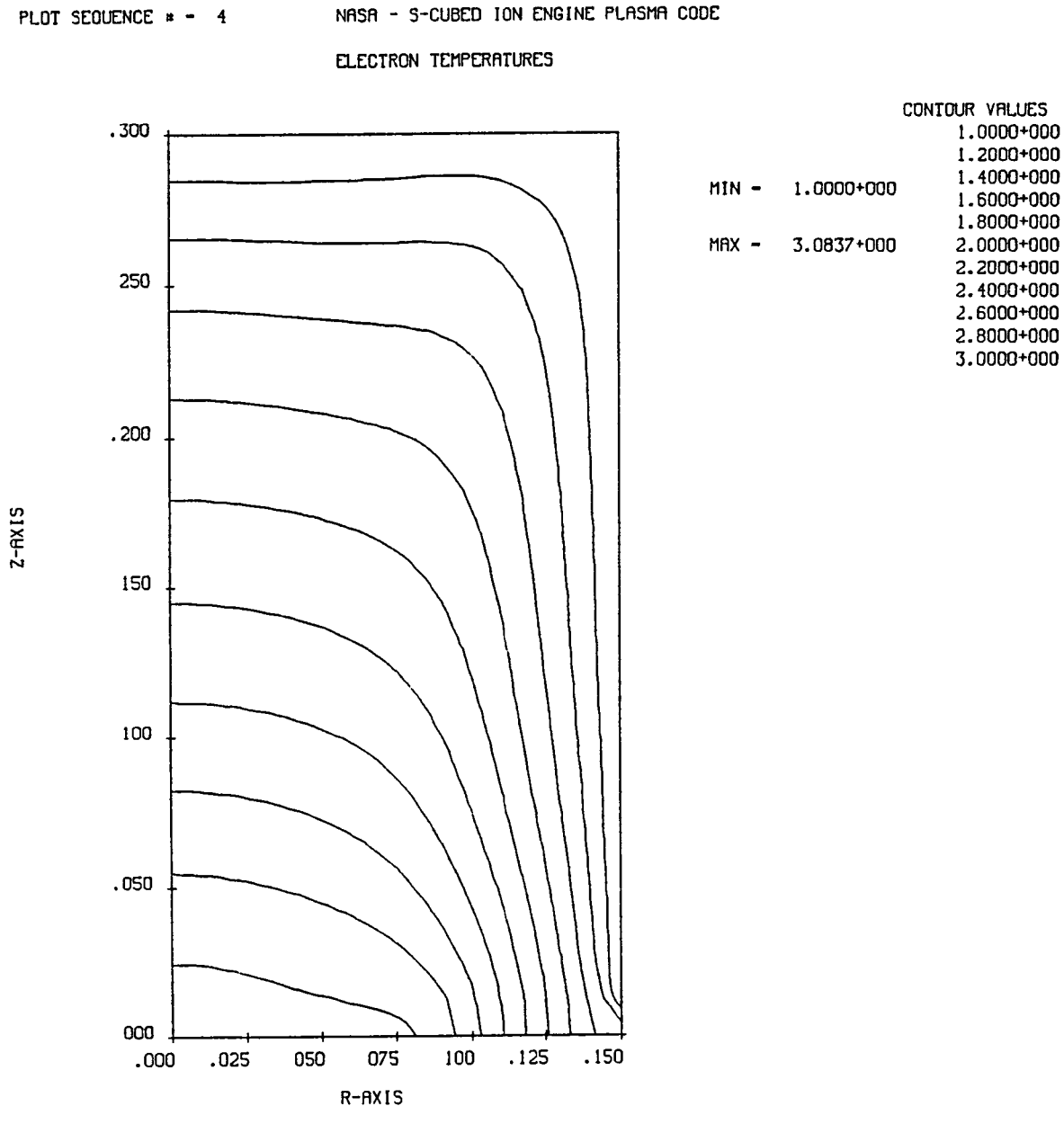

Figure 5.24. Electron temperature contours (line 46).

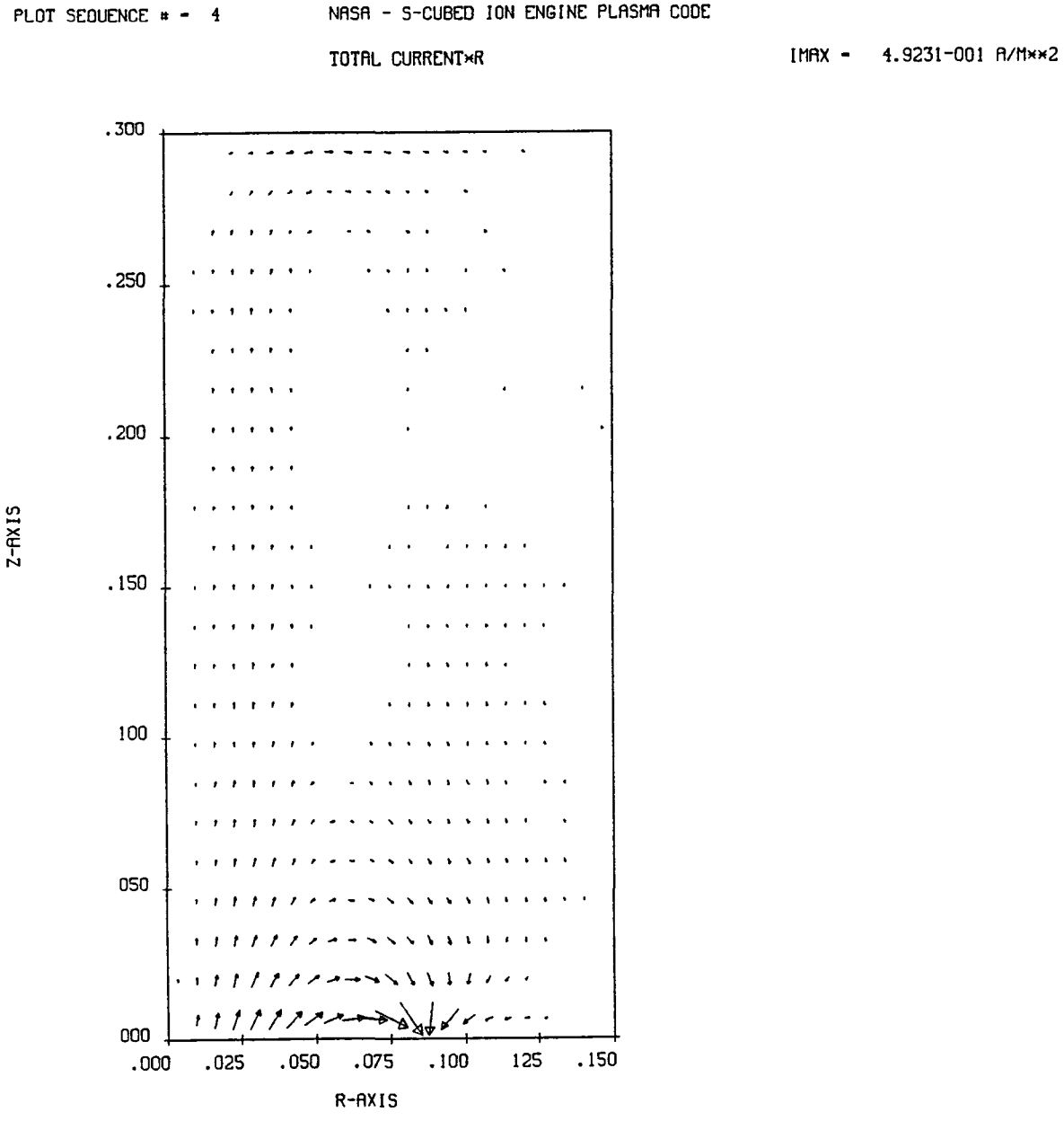

Figure 5.25. Current vectors (line 47).

```
***TIME LEFT =  1078 SECONDS***

******CHANGE
THERBC ISOT
END

CODE OPTION SUMMARY

   NR          NZ          RMAX        ZMAX
   24          24           .1500       .3000

   BEAM CURRENT            BEAM RADIUS          BEAM ENERGY
     .085000 AMPS             .0700 M             3000.0 EV

   MASS (AMU)              PROFILE              SPREAD ANGLE
      200.59                 GAUS                    .0 DEG.
                                ION MASS =  3.355-025 KG.
                                PEAK CURRENT =  1.035+020 M**(-2) SEC**(-1)
                                ION VELOCITY =   53491.5 M/SEC

   SIGMA                   FLOW                 TEMP
    5.0-019             .140000 AMPS            .060 EV

   ECHAR            VDTR            ETA             RHOMIN          NSTEPS
    10.000            .200            .050          1.00+010           50

   THERMAL BC = 'ISOT' WITH TEMPERATURE     1.00 EV.

   NEUTRALIZER RADIUS =     .0850          2 ITERATIONS.

   PRINTED OUTPUT: LOGICAL UNITS NO. 19 AND  20.

   PLOT DESTINATION = ELEC
   PLOT TITLE =       NASA - S-CUBED ION ENGINE PLASMA CODE

***TIME LEFT =  1077 SECONDS***

******NEWPOT
EMITTER AT NODE    14.
GETRHS -- CURZO,ELJ =  8.54-002  2.46+001
***WARNING*** GETCH --- CH( 5477) = -1.00+000

    ICCG --- RDOTR/RDOTR1 =   1.44-004/  7.77-001      NITER= 31
***WARNING*** GETCH --- CH( 5477) = -1.00+000

    ICCG --- RDOTR/RDOTR1 =   5.35-010/  1.44-004      NITER= 31

***TIME LEFT =  1052 SECONDS***

******PLOT
```

Figure 5.26. Output resulting from lines 49-53 of runstream.

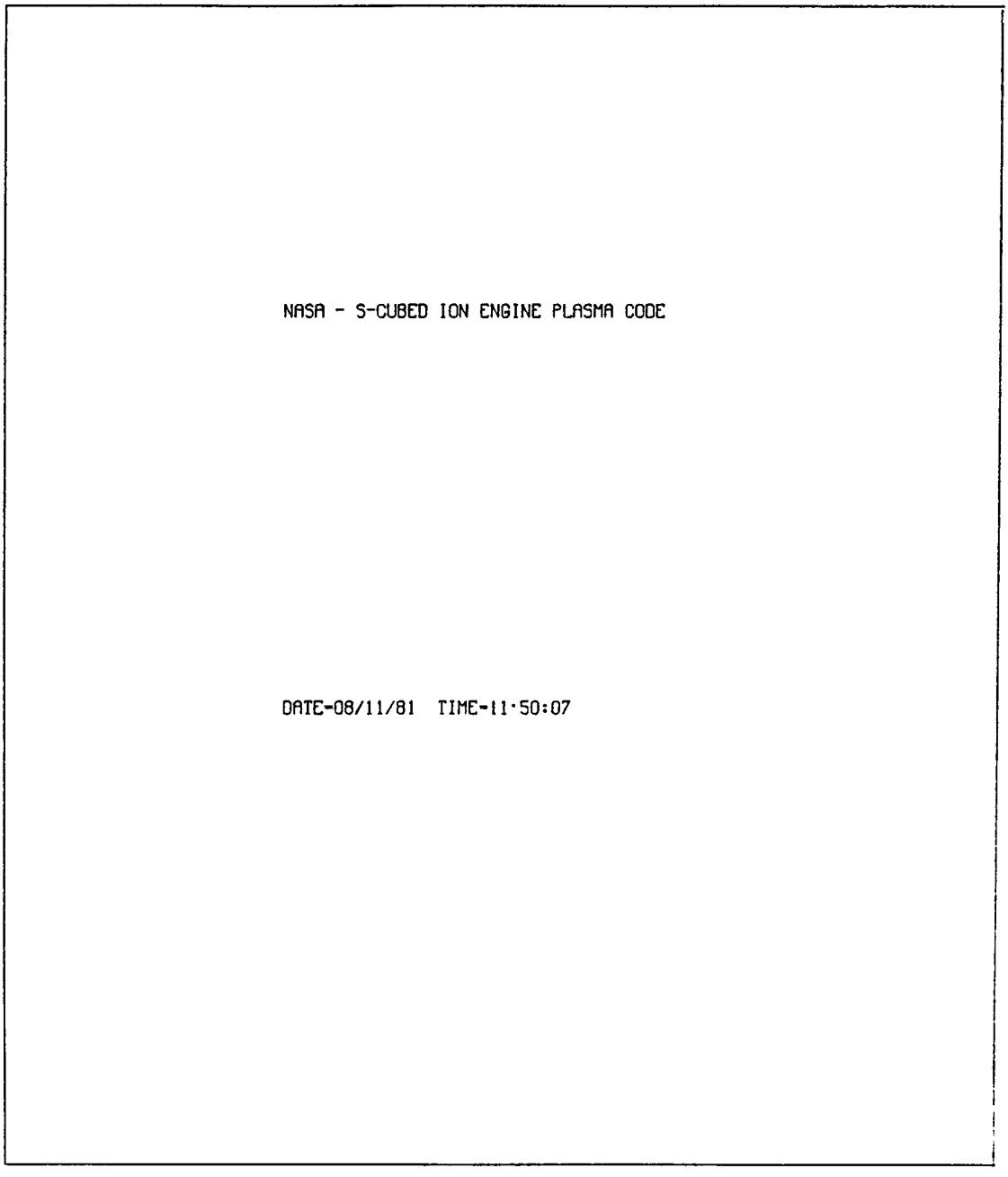

Figure 5.27. Plot title page (line 53).

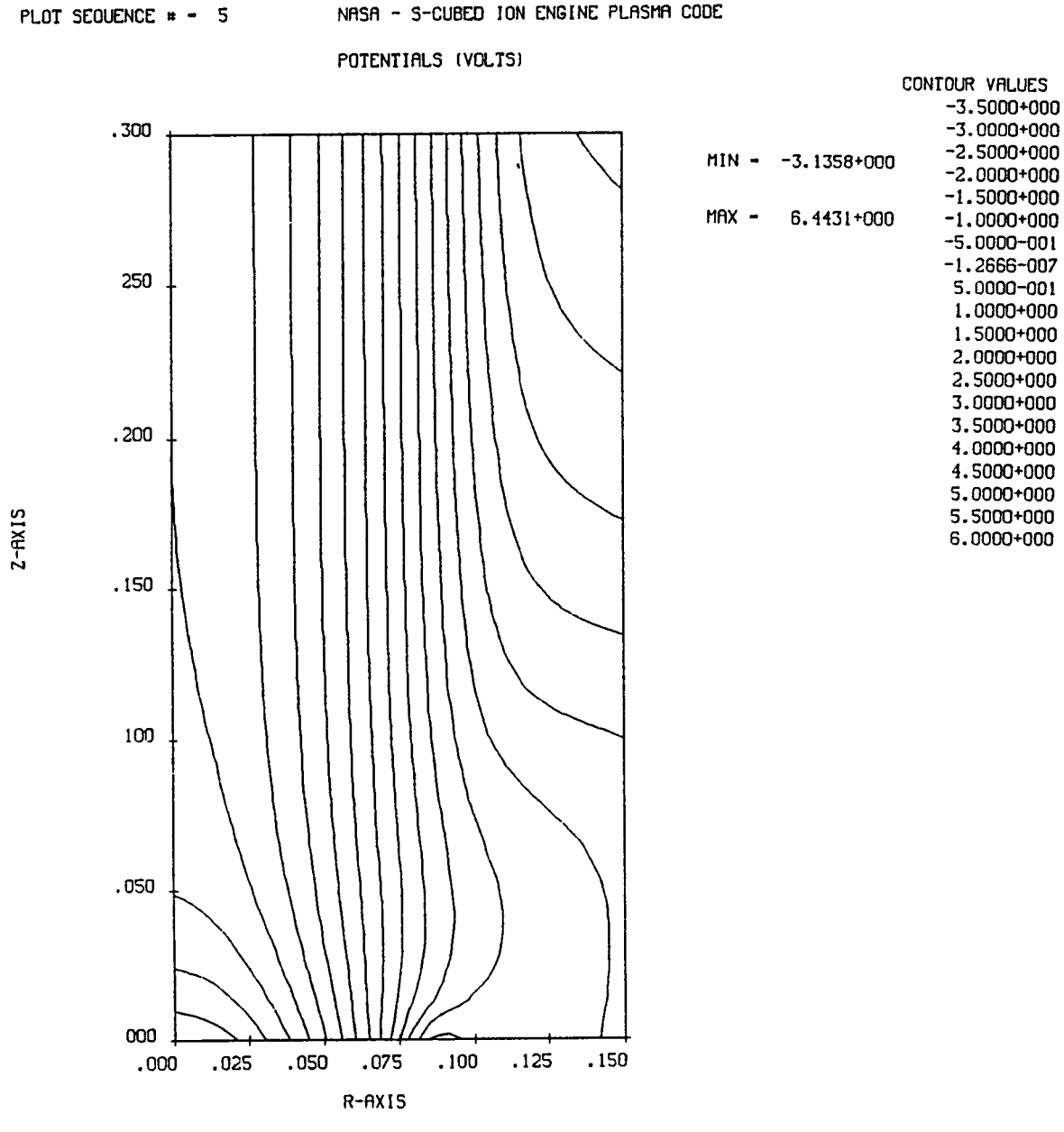

Figure 5.28. Potential contours (line 54).

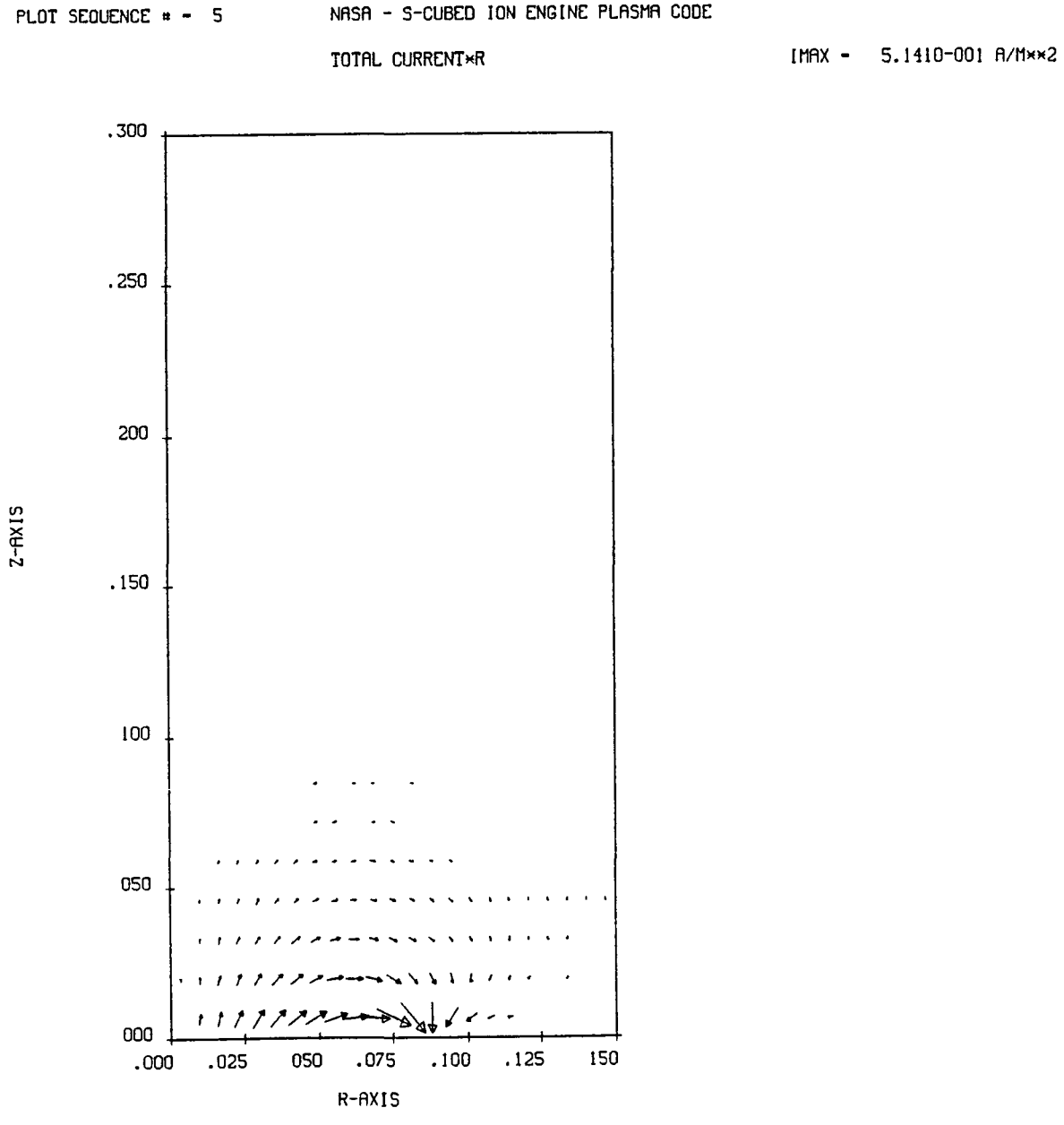

Figure 5.29. Current vector plot (line 55).

```
******CHANGE
THERGC SINK
NITER 4
END

CODE OPTION SUMMARY

   NR          NZ          RMAX        ZMAX
   24          24           .1500       .3000

   BEAM CURRENT            BEAM RADIUS          BEAM ENERGY
     .085000 AMPS             .0700 M             3000.0 EV

   MASS (AMU)              PROFILE              SPREAD ANGLE
      200.59                 GAUS                    .0 DEG.
                                ION MASS =  3.355-025 KG.
                                PEAK CURRENT =  1.035+020 M**(-2) SEC**(-1)
                                ION VELOCITY =   53491.5 M/SEC

   SIGMA                   FLOW                 TEMP
    5.0-019             .140000 AMPS            .060 EV

   ECHAR            VDTR            ETA             RHOMIN          NSTEPS
    10.000           .200             .050          1.00+010          50

   THERMAL BC = 'SINK' WITH TEMPERATURE     1.00 EV.

   NEUTRALIZER RADIUS =     .0850          4 ITERATIONS.

   PRINTED OUTPUT: LOGICAL UNITS NO. 19 AND  20.

   PLOT DESTINATION = ELEC
   PLOT TITLE =         NASA - S-CUBED ION ENGINE PLASMA CODE

***TIME LEFT =  1051 SECONDS***

******NEWPOT
EMITTER AT NODE     14.
GETRHS -- CURZO,ELJ =  8.54-002  2.46+001
***WARNING*** GETCH --- CH( 5477) = -1.00+000
    ICCG --- RDOTR/RDOTR1 =   1.44-004/  7.77-001     NITER= 31
    ICCG --- RDOTR/RDOTR1 =   2.86-014/  4.41-002     NITER= 21
***WARNING*** GETCH --- CH( 5477) = -1.00+000
    ICCG --- RDOTR/RDOTR1 =   1.23-006/  3.66-002     NITER= 31
    ICCG --- RDOTR/RDOTR1 =   1.13-016/  2.36-004     NITER= 21
***WARNING*** GETCH --- CH( 5477) = -1.00+000
    ICCG --- RDOTR/RDOTR1 =   1.21-007/  9.45-005     NITER= 31
    ICCG --- RDOTR/RDOTR1 =   5.08-019/  2.29-006     NITER= 21
***WARNING*** GETCH --- CH( 5477) = -1.00+000
    ICCG --- RDOTR/RDOTR1 =   1.48-010/  1.22-006     NITER= 31
    ICCG --- RDOTR/RDOTR1 =   1.57-020/  1.94-008     NITER= 20



***TIME LEFT =   986 SECONDS***

******PLOT
```

Figure 5.30. Output resulting from lines 57-62 of runstream.

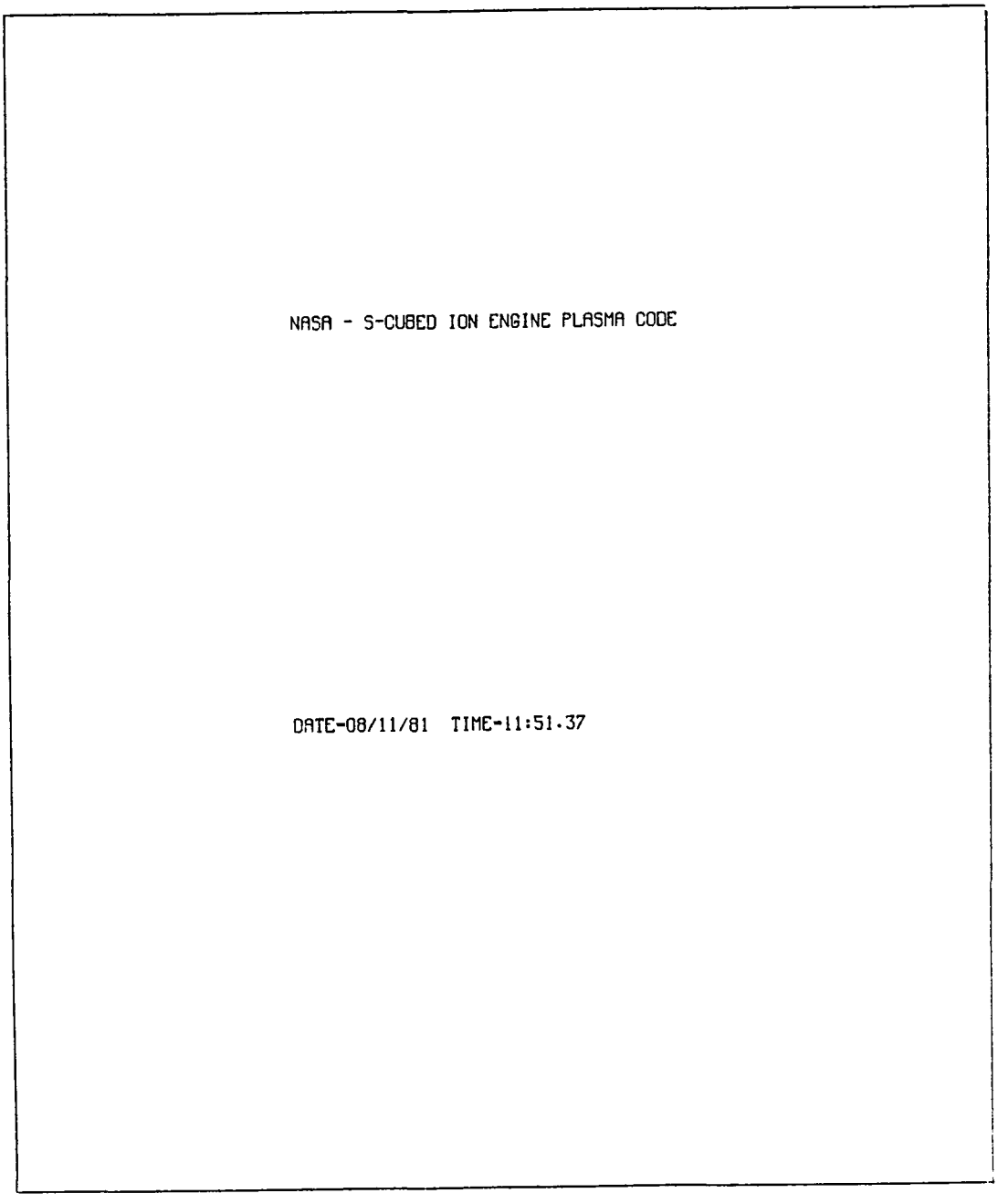

Figure 5.31. Plot title page (line 62).

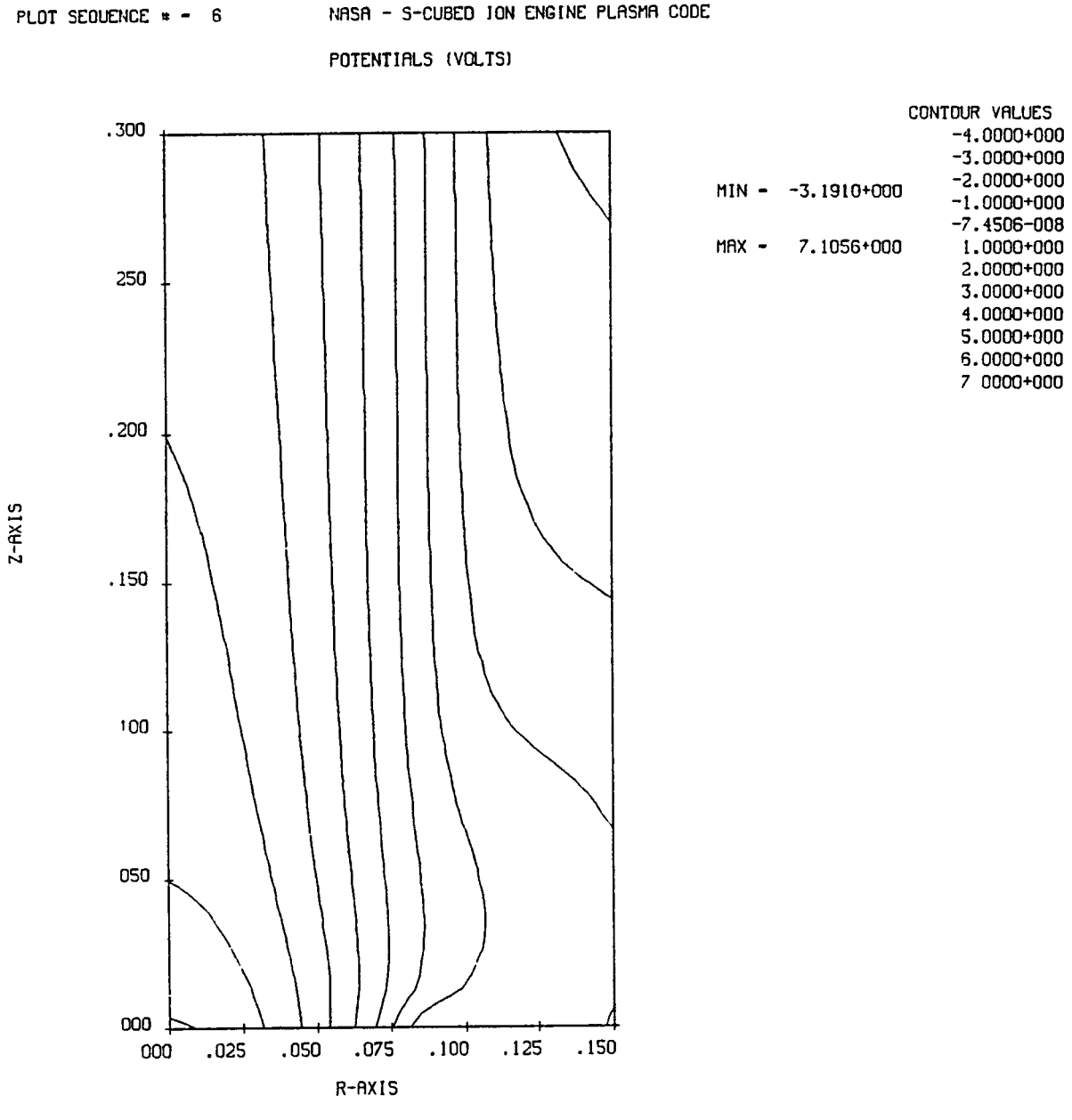

Figure 5.32. Potential contour plot (line 63).

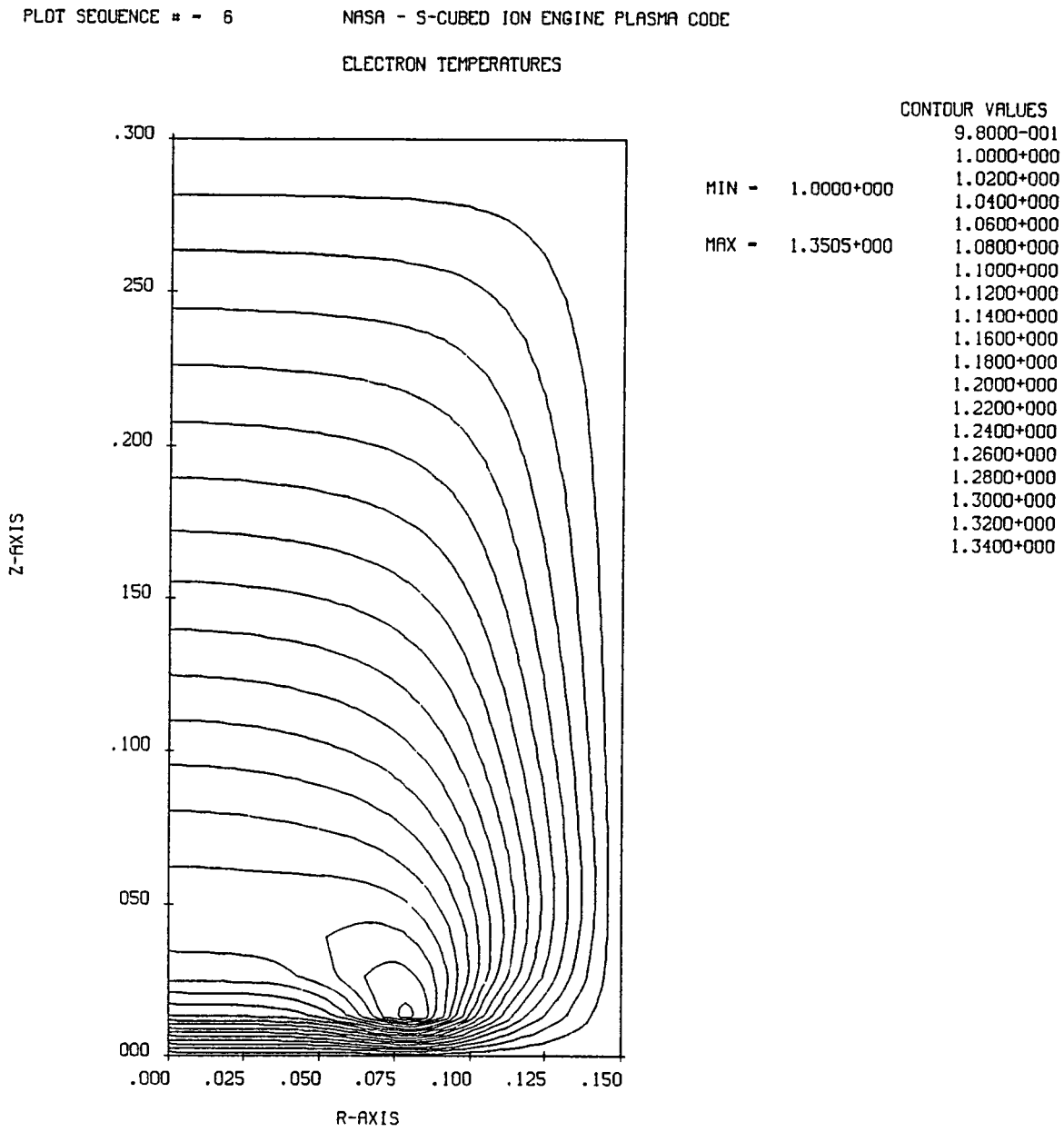

Figure 5.33. Electron temperature contour plot (line 64).

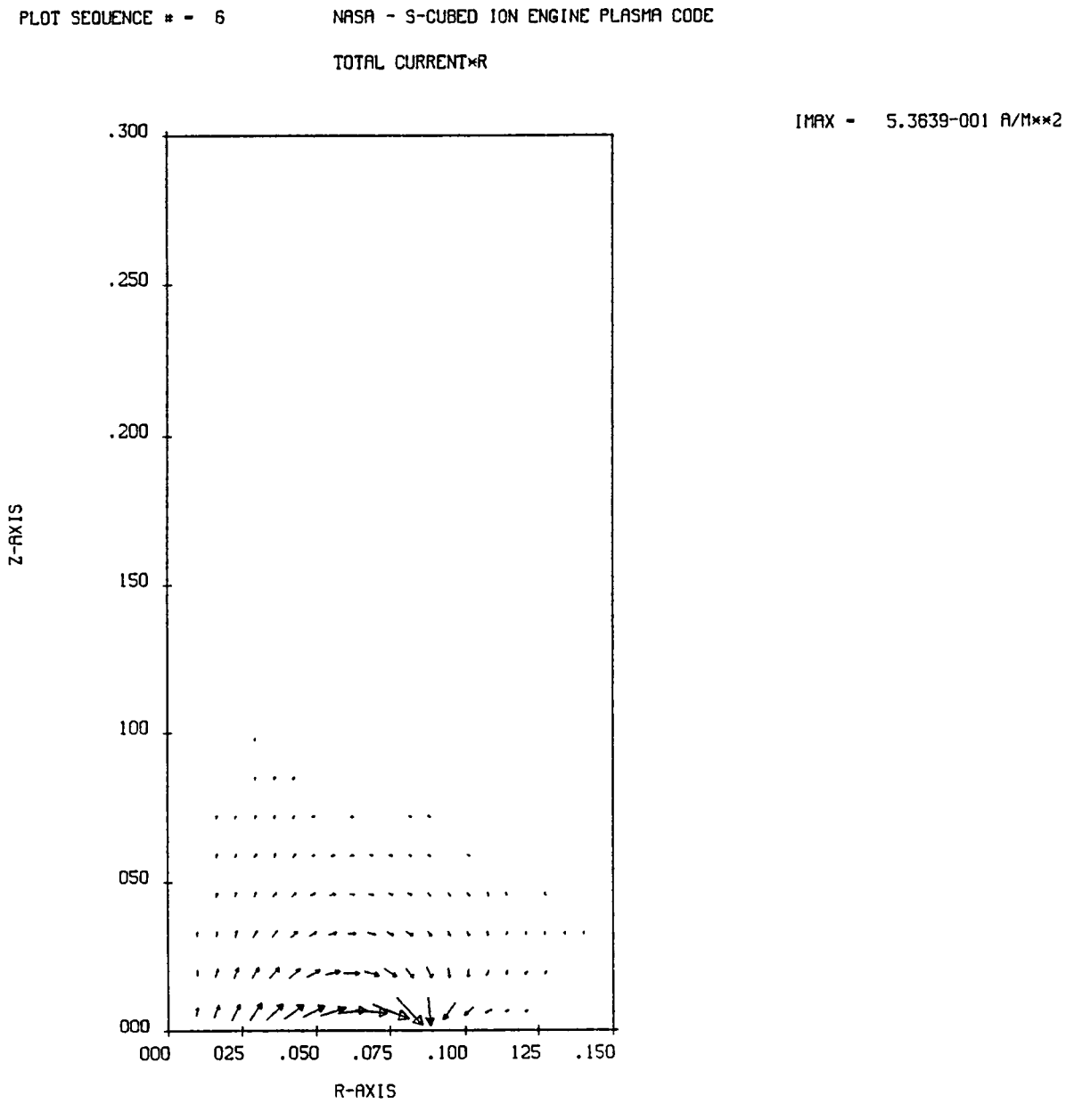

Figure 5.34. Current vector contour plot (line 65).

```
***TIME LEFT =   984 SECONDS***

******END
[EXIT]

[END ION]

@ASG,A NASCAP*PLOTREAD.

@XQT NASCAP*PLOTREAD.
DEVICE OPTION =  3.



                    PLOTTING COMMENCING
                    ...................

..... DISSPLA VERSION 8.2 .....
NO. OF FIRST PLOT  0


END OF DISSPLA 8.2 --    93268 VECTORS GENERATED IN    27 PLOT FRAMES.
-ISSCO-  4186 SORRENTO VALLEY BLVD.,SAN DIEGO CALIF. 92121

DISSPLA IS A CONFIDENTIAL PROPRIETARY PRODUCT OF ISSCO AND ITS USE
   IS SUBJECT TO A NONDISSEMINATION AND NONDISCLOSURE AGREEMENT.

   NBUFS=  325      NCALLS=    7567
[EXIT]

@PMD,EL

@ASG,PU SAVE9.

@ASG,PU SAVE21.

@COPY 9.,SAVE9.
FURPUR 28R1 U1 E35 S74T11 08/11/81 11:53:00
     2 BLOCKS COPIED.

@COPY 21.,SAVE21.
    54 BLOCKS COPIED.
```

Figure 5.35. Output resulting from lines 67-72 of runstream, including execution of graphics interface to DISSPLA plot package.

APPENDIX A

AIAA 81-0141

FLUID MODEL OF NEUTRALIZED ION BEAMS

D. E. Parks, M. J. Mandell and I. Katz

S-CUBED
La Jolla, CA 92038

AIAA 19th Aerospace Sciences Meeting

January 12-15, 1981
St. Louis, MO

FLUID MODEL OF NEUTRALIZED ION BEAMS

D. E. Parks, M. J. Mandell and I. Katz
Systems, Science and Software
La Jolla, California 92038

Abstract

The purpose of the present study is to determine the capability of a fluid model of electron transport to explain observed properties of ion thruster generated plasmas. Calculations reported here show that when the effective collision frequency in such a model is of the order of the electron plasma frequency, the resulting electric potential variations and electron temperatures are in qualitative agreement with values measured in the plasma generated by the SERT II thruster. Both theory and probe measurements made in flight and ground tests indicate substantial departures from the barometric law and strong variations of plasma potential across the beam boundary.

Nomenclature

$\vec{B}$ magnetic field
C collision operator in Boltzmann-Vlasov equation
$\vec{E}$ electric field
$f_a d\vec{r}d\vec{v}$ number of particles of type a in phase space volume element $d\vec{r}\,d\vec{v}$ at $\vec{r},\vec{v}$
$\vec{F}$ total energy flux
$F_a = q_a(\vec{E} + \vec{v}\times\vec{B}/c)$
$\vec{I}$ unit tensor
J net current density
k Boltzmann's constant
m_a mass of particle of species a
m electron mass
n electron density $= \int f(\vec{r},\vec{v},t)d\vec{v}$
$p = 1/3\ m\int f\ v'^2 d\vec{v}$ = scalar electron pressure
$\vec{p}$ $m\int f\ \vec{v}'\vec{v}'d\vec{v} = p\vec{I} + \vec{\tau}$, pressure tensor
$Q = 1/2\ m\int v'^2 C\ d\vec{v}$
q_a charge on particle of species a
q magnitude of electron charge
$\vec{q}$ heat flux, Eq. (7)
$\vec{R}$ position vector of a particle
$R = \int m\vec{v}\ C\ d\vec{v}$
T electron temperature
$\vec{v}$ velocity of a particle
$\vec{v}' = \vec{v} - \vec{V}$
$\vec{V}$ mean or drift velocity $= 1/n \int f(\vec{r},\vec{v},t)d\vec{v}$
λ_c mean free path for pair collisions between electrons
$\theta = kT$
η plasma resistivity
κ thermal conductivity of plasma
ν effective collision frequency
ν_{ei} electron-ion collision frequency
$\vec{\vec{\tau}} = nm\ \overline{\vec{v}\vec{v}} - \langle v'^2\rangle/3\ \vec{\vec{I}}$ = stress tenson
$\tau = \eta^{-1}$
ϕ electric potential
ω_p electron plasma frequency

1. Introduction

The purpose of the present study is to determine the capability of a fluid model of electron transport to explain observed properties of ion thruster generated plasmas. Calculations reported here show that when the effective collision frequency in such a model is of the order of the electron plasma frequency, the resulting electric potential variations and electron temperatures are in qualitative agreement with values measured in the plasma generated by the SERT II thruster. Probe measurements made in SERT II[1] flight and ground test experiments[2] indicate substantial departures from the barometric law[3-7] and show strong variations of plasma potential across the beam boundary.

We propose to explain the plasma properties observed in the aforementioned experiments in terms of anomalous resistance of the plasma to the flow of electron current. The calculations are based on fluid equations expressing conservation of charge, momentum, and energy. We adopt the classical (ignoring thermoelectric effects) form of the equations of electron transport,[8] but permit reduced values of the transport coefficients. Predicted space dependent potentials, electron temperatures and current densities agree qualitatively with experimental results.

While the plasma is not collision dominated, randomization of electron velocities may still occur through enhanced levels of fluctuating fields, such as those initiated by streaming instabilities. Such fields are probably effective in coupling neutralizer electrons into the bulk plasma and in equalizing the mean drift of electrons with ions in the thruster beam. Such mechanisms are often approximated by introducing an effective collision frequency, ν.

Within a meter or so of the ion thruster, the electron densities are in the range

$$10^8 \lesssim n \lesssim 10^{13}\ \text{cm}^{-3}$$

and their velocity distribution is characterized by temperature θ between about one and ten electron volts. The Debye length

$$\lambda_D = 700\sqrt{\frac{\theta}{n}}\ \text{cm}$$

is typically small compared to distances L over which there is a substantial variation of macroscopic plasma properties such as density, potential, and temperatures. On the other hand, the mean free path for pair

collisions λ_c

$$\lambda_c = 10^{12}\, E^{1/2}\, \vartheta^{1/2}/n \text{ cm}, \quad E \gtrsim \vartheta$$

for electrons of energy E (eV) is typically long compared to L, so that as previously asserted the behavior of the plasma is controlled by collective rather than collisional effects. Since $\lambda_D \ll L$, the plasma is quasineutral, departures from neutrality amounting roughly to

$$\delta n/n \sim \left(\frac{\lambda_D}{L}\right)^2 \sim 10^{-4} ,$$

the space around the vehicle is strongly shielded from surface potentials. This is in contrast to the situation that prevails in charging of spacecraft in geosynchronous orbit where effects of space charge are entirely negligible and potentials are determined as solutions of Laplace's equation.

Although collisionless, thruster-generated plasmas exhibit macroscopic behavior similar in many respects to that of a collisional plasma. Such behavior is perhaps not totally unexpected in view of the fact that in both non-equilibrium and equilibrium plasmas electrons are scattered by fluctuating electric fields. A primary difference between the equilibrium and non-equilibrium cases is in the magnitude of the fluctuating fields.

Several investigators have measured properties of thruster generated plasmas.[3-7] In the experiments of Ogawa, et al., on cesium ion beams neutralized by electrons from a hot wire, measurements were made of the density, potential, and electron temperature in the beam plasma. The potential difference between the neutralizer wire and the plasma could be varied by changing the position of the wire, the large potential differences (electron injection voltages) occurring when the wire was completely withdrawn from the beam plasma. An important result of the Ogawa experiments was that over a wide range of conditions electron density n and plasma potential ϕ were well correlated by the barometric law

$$n(\vec{r}) = \text{const} \exp(q\phi(\vec{r})/kT) \qquad (1)$$

The approximate validity of the barometric law was further verified by Kaufman.[7]

Since the barometric law is a thermal equilibrium concept, it can be completely valid only if the plasma is isothermal. The plasma is only approximately isothermal, noticeable deviation occurring as one proceeds from the beam axis beyond the beam edge into the plasma formed by ambient and charge exchange ions. Kaufman observes an electron temperature in the charge exchange plasma only about half that in the beam.[7] Ogawa[5] and Sellen[3] obtained measurable temperature variations in the beam plasma over several tens of centimeters in the downstream direction from the accelerator grid. The largest deviations from the barometric law were observed for large injection potentials ($\gtrsim$10 volts). Probe traces in such cases also indicated departures of the electron spectrum from a Maxwellian shape.

Probe measurements of the plasma potential in the thruster beam were made in SERT II flight and ground test experiments. The measurements show strong variation of plasma potential across the beam boundary about 20 cm downstream from the thruster grids. Such results are difficult to explain on the basis of a barometric law relationship unless the electron temperature or density variation from beam center to beam edge is much higher than might be expected from other measurements made in similar configurations. We anticipate, however, that such is not the case and, instead, that the observed behavior should be explained in terms of the anomolous resistivity of the thruster generated plasma to the flow of electron current. Thus, the primary objective of the following sections of the report is to determine the capability of simple transport models to explain, at least qualitatively, the experimental results.

The next section summarizes the kinetic equation for the electron distribution and the first few moment equations expressing conservation of charge, momentum, and energy. In Section 3 we state the approximations leading to the transport equations which we eventually solve. The method of solution and the results of calculations will be the subject of Sections 4 and 5 respectively. The final section, Section 6, summarizes the conclusions of this study.

2. Exact Equations for Electron Gas

In principle, a kinetic approach based on the Vlasov-Boltzmann equation fully describes the spacecraft generated plasma. The complexity of such an approach, however, makes it impractical as a basis for conducting multidimensional calculations of plasma behavior. Besides, except near sources and collecting surfaces, where the distribution function may change markedly, one should be able to adequately describe the plasma in terms of certain average properties of the distribution, such as temperature, density, and particle and heat fluxes. Below, the exact equations describing the plasma are given in order that the reader may be aware of the effects neglected in arriving at the approximate equations that are subsequently solved.

Quite generally the state of the plasma can be specified by the distribution function $f_a(\underline{r},\underline{v},t)$ that characterize each particle component a, where $f_a(\underline{r},\underline{v},t)d\underline{r}\, d\underline{v}$ represents the number of particles of species a in the six dimensional volume element $d\underline{r}\, d\underline{v}$ about the position $\underline{r},\underline{v}$ in phase space. The kinetic equations which

describe the distribution are

$$\frac{\partial f_a}{\partial t} + \vec{v}\cdot\nabla f_a + \frac{\vec{F}_a}{m_a}\cdot\nabla_v f_a = C_a \qquad (2)$$

For particles of mass m_a and charge q_a in an electric field $\vec{E}$ and a magnetic field $\vec{B}$ the "smoothed" force on a particle is $\vec{F}_a$. The effects of collisions between particles is taken account of by the collision term denoted here by C_a. Here we attempt to describe the plasma in terms of its density n, mean velocity $\vec{V}$, and certain higher velocity moments. For convenience, we have omitted the particle species subscript a. The first three moments of the kinetic equation yield conservation equations for particles, momentum and energy, as summarized below:[8]

Conservation of Particles

$$\frac{\partial n}{\partial t} + \nabla\cdot n\vec{V} = 0 \qquad (3)$$

Conservation of Momentum

$$\frac{\partial}{\partial t}(mn\vec{V}) + \nabla\cdot mn\vec{V}\vec{V} + \nabla\cdot\vec{\vec{P}} - qn\left(\vec{E} + \frac{\vec{V}\times\vec{B}}{c}\right) = \vec{R} \qquad (4)$$

Conservation of Energy

$$\frac{\partial}{\partial t}\left(\frac{nm}{2}\left(V^2 + \left\langle v'^2\right\rangle\right)\right) + \nabla\cdot\vec{F} = qnE\cdot V + \vec{R}\cdot\vec{V} + Q \qquad (5)$$

where

$$\vec{F} = \left[nm\left(\frac{V^2}{2} + \frac{\left\langle v'^2\right\rangle}{2}\right) + p\right]\vec{V} + \vec{\vec{\tau}}\cdot\vec{V} + \vec{q} \qquad (6)$$

is the total energy flux,

$$\vec{q} = nm\left\langle\frac{v'^2}{2}\right\rangle\vec{V} \qquad (7)$$

is the heat flux,

$$Q = \int\frac{mv'^2}{2}\,C\,d\vec{v} \qquad (8)$$

and $\langle\ \rangle$ denotes an average over the distribution f.

So far, the equations are quite general and involve no assumption that the gas is collision dominated or retains a Maxwellian spectrum of velocities. Separate conservation equations may be written not only for different particle species, but also for different groups or particles of the same charge and mass. Primary electrons, for example, with significant streaming energies could be treated as distinct from the main electron population which is taken to have a Maxwellian distribution of velocities. For the present, however, and until experimental or theoretical considerations dictate otherwise, we shall consider electrons as a whole and that their distribution varies slowly in space.

3. Approximations for Electron Gas

Consider that the plasma is in a steady state and that quasi-neutrality pertains throughout the bulk plasma (that is, away from electrodes and collecting surfaces). The electrons and ions each satisfy the particle continuity equation

$$\nabla\cdot n_i\vec{V}_i = 0 \quad (i = +,-) \qquad (9)$$

with $n_+ = n_- = n$. The momentum equation simplifies considerably if the electron drift velocity $\vec{V}$ is small compared to the random velocity $\langle v'^2\rangle^{1/2}$ and if the velocity distribution is nearly isotropic. Then, in the absence of magnetic fields,

$$\nabla p + en\vec{E} = \vec{R} \qquad (10)$$

where $\vec{R}$ represents the collisional drag between ions and electrons. In a classical plasma dominated by collisions, $\vec{R}$ is composed of a part proportional to the relative motion $\vec{u} = \vec{V}_e - \vec{V}_i$ between electrons and ions, leading to plasma resistivity, and to a thermal part proportional to the gradient of electron temperature, which is frequently neglected. In this approximation, equation (4) becomes

$$\nabla p + en\vec{E} = \eta ne\vec{j} \qquad (11)$$

where $\vec{j}$ is the net current density and the plasma resistivity η is related to the electron-ion collision frequency ν_{ei} by

$$\eta^{-1} = \frac{\omega_p^2}{4\pi}\frac{1}{\nu_{ei}} \qquad (12)$$

If the plasma is non-resistive and isothermal, equation (11) yields the barometric law, equation (1). In this sense, equation (11), or more generally the complete electron momentum equation, may be regarded as the generalization of the barometric law.

If the plasma is not collision dominated, randomization of electron velocities may still occur through the enhanced levels of fluctuating fields in the plasma, such as occur for electron two-stream instabilities, or electron-ion instabilities of the ion-acoustic or Bunemann type.[8,9] These mechanisms are probably effective in coupling neutralizer electrons into the bulk plasma and in equalizing electron and ion mean drift velocities. They are often approximated by introducing an effective collision frequency, ν, in place of ν_{ei}.

The determination of electron temperatures in the plasma requires consideration of the energy balance equation, equation (5). Making the same approximations in the equation expressing conservation of energy that were made in the momentum equation, yields

$$\nabla\cdot\vec{F} = qn\vec{E}\cdot\vec{V} + \vec{R}_e\cdot\vec{V}_e + Q_{ei} \qquad (13)$$

with

$$\vec{F} = \frac{5}{2}\, p\vec{V} + \vec{q} \qquad (14)$$

Here $5/2\ p\vec{V}$ is the enthalpy flux of the drifting electrons, $\vec{q}$ the macroscopic heat flux, and $\vec{R}\cdot\vec{V}$ is related to the effective joule heating associated with the relative motion of electrons and ions. The quantity $\vec{R}$ appears also in the electron momemtum equation; for a plasma controlled by collective effects it should be approximated in the energy equation in the same manner as in the momentum equation. The heat flux, $\vec{q}$, contains new features. Classically, $\vec{q}$ contains two terms; one proportional to the relative drift velocity between electrons and ions, and the other proportional to the gradient of electron temperature.(8)

For the initial calculations, we ignore the drift contributions to the energy flux, the electron-ion heating Q_{ei}, and assume that the heat flux is proportional to the temperature gradient. The energy balance equation thus assumes the simple form

$$\nabla\cdot\kappa\nabla\Theta + mn\nu(\vec{v}_e-\vec{v}_i)^2 = 0 \qquad (15)$$

4. Ion Engine Neutralizer Code

The basic physics of an ion engine neutralizer model was presented in the preceding sections. This physical model has been incorporated into a two-dimensional (R-Z) computer code, which is described below. A sample calculation of neutralization in a thruster similar to SERT II is discussed below. Results are given for space dependent electric potentials, electron temperatures, and current densities.

Code Description

The ion thruster model has been incorporated into a two-dimensional (R-Z) computer code following the block diagram shown in Figure 1. For this initial version the ion currents and densities were assumed known. In a later version, it would be possible to allow a multicomponent ion composition to be determined self-consistently with the temperature and potential. The code operates entirely in MKS units.

The code has been run interactively, with all relevant information on disk file. As long as previous information exists on disk, the program may be entered from the two noted entry points as well as the beginning. For developmental purposes, it was found convenient to "hard-wire" many features of a particular problem into the code, while others are prompted for input. A flexible on-line graphics program, which plots information on the disk file, has also been developed.

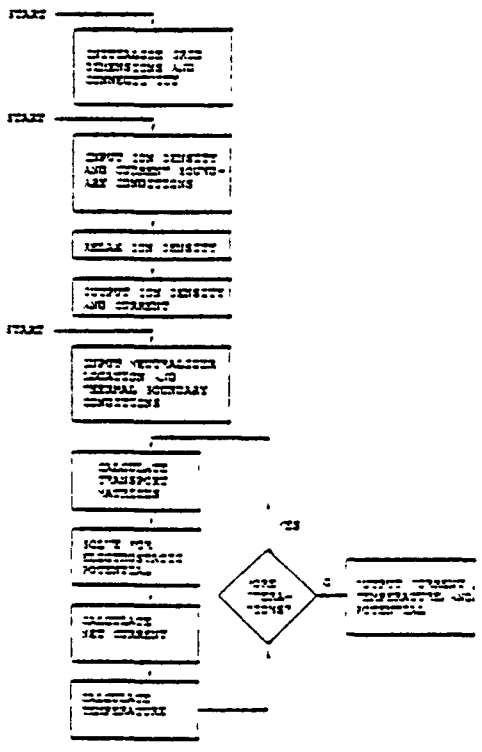

Fig. 1 Block diagram for ion engine neutralization code.

At present, the code assumes ion velocities everywhere and ion currents at the input boundary to be known. The code then calculates plasma densities such that $\nabla\cdot(ny) = 0$ is numerically satisfied. Typically, ion velocities are taken to be either purely axial or to be radial from a point source on the axis exterior to the mesh. As the code requires non-zero plasma density everywhere, a background density of "slow" ions may be added. It should be possible to handle multiple ion species with interconversion fairly easily.

The neutralizer is assumed to be a ring at specified distance from the axis, emitting a current of electrons equal to the ion beam current. The net current in the plasma is given by

$$j = nq(\vec{v}_i - \vec{v}_e) \qquad (16)$$

$$= \sigma\left(-\nabla\phi + \frac{q}{n}\nabla p\right), \qquad (17)$$

where now $p = nkT$ is the electron pressure. [For $\sigma\to\infty$ and $qkT\to$ (constant) we find $\phi = a\ln n$.] The code determines electrostatic potentials by solving $\nabla\cdot j = 0$. (See Appendix A.) It is necessary to iterate between this equation and the temperature equation (equation 15), since the pressure is a function of temperature.

The plasma temperature satisfies the equation

$$\nabla\cdot(-\kappa\nabla\vartheta) = \frac{j^2}{\sigma} \qquad (18)$$

where κ is the thermal conductivity and the right-hand-side represents the ohmic generation of heat. For this preliminary version, convective heat transport has been neglected. On the various boundary regions, either isothermal or insulating boundary conditions may be specified. Since, in practice, we take κ to have a power law dependence on ϑ, $\kappa = n\kappa'\vartheta^{n-1}$, the equation actually solved is

$$-\nabla\cdot\kappa'\nabla(\vartheta^n) = \frac{j^2}{\sigma} \quad . \qquad (19)$$

For convenience, the transport coefficients σ and κ' are calculated by a single isolated subroutine. The conductivity σ may depend on both density and temperature, and κ' on density only. The present version assumes a relaxation rate proportional to the plasma frequency:

$$\sigma = n^{1/2}\,\frac{e^2}{m}\,\frac{1}{8.98\alpha}\ , \qquad (20)$$

where the parameter α is taken to be 0.51. By the classical Weideman-Franz law,

$$\kappa = \frac{3}{2}\,\sigma\left(\frac{k}{q}\right)^2 T \ . \qquad (21)$$

If we measure temperature in eV, k = q, so that $\kappa' = 3/4\ \sigma$.

5. Computational Results

A calculation was performed for neutralization of a 0.23 ampere, purely axial beam of 3 keV mercury ions in a constant density background plasma. The beam had a radius of ~7 cm, and a ring neutralizer was placed at a 17 cm radius. The given plasma density (Figure 2) had a peak of 16.1×10^{14} m^{-3}, and an ambient density of 1.0×10^{14} m^{-3}. These conditions approximate those occurring in the plasma produced by the SERT II thruster. The temperature profile (Figure 3) was calculated with insulating boundary conditions at the thruster. The maximum temperature occurs at the beam entrance, where the heat generation is greatest. The peak temperature was 5 eV, compared with a 1 eV assumed background. The electrostatic potentials are shown in Figures 4 and 5. Strong potential variations across the beam edge and a potential dip near the neutralizer are calculated features in qualitative agreement with experimental results (Figure 5) [11]. While the strong edge fields conform approximately to the barometric law at the local temperature, they deviate substantially from the results that would be obtained with $\nu \ll \omega_p$ or by using the barometric law as the point of departure (that is, a zero resistivity, isothermal calculation). Current-vector plots (Figures 6 and 7) indicate that the beam is neutralized by electrons entering the beam from the side. The ion current is 50 percent neutralized at ~15 cm downstream from the thruster.

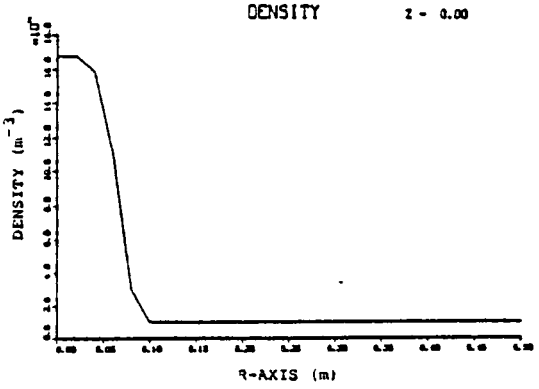

Fig. 2 Plasma density for SERT II ion thruster model.

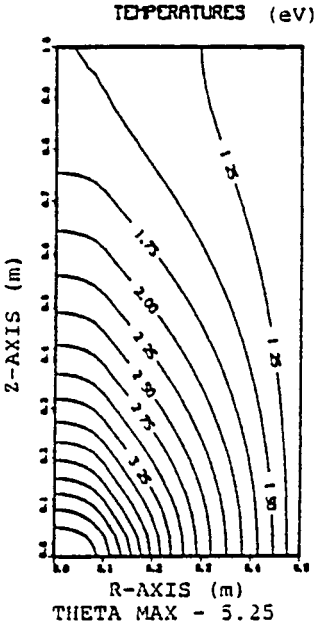

Fig. 3 Temperature profile for SERT II ion thruster model.

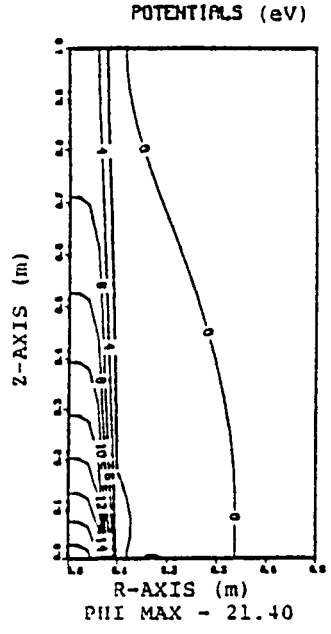

Fig. 4 Electrostatic potentials for SERT II ion thruster model.

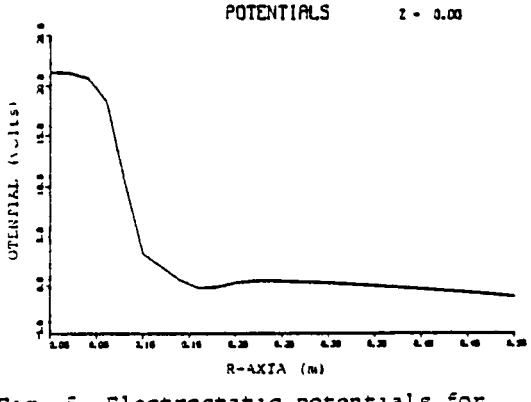

Fig. 5 Electrostatic potentials for SERT II ion thruster model.

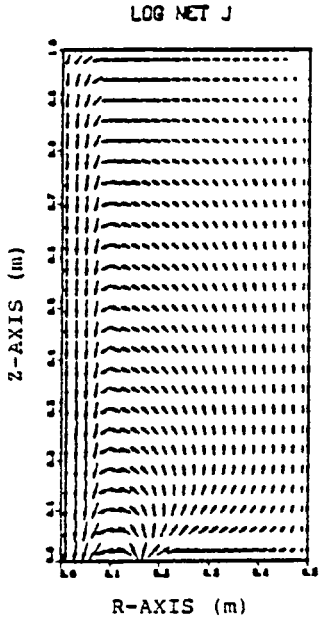

Fig. 6 Current vectors for SERT II ion thruster model. The length of each arrow is weakly dependent on current.

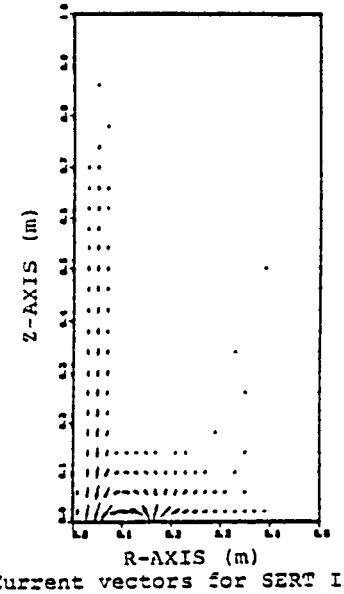

Fig. 7 Current vectors for SERT II ion thruster model. The length of each arrow is proportional to radius times current density.

6. Summary and Conclusions

The consequences of the assumption that the electron gas near an ion thruster behaves as a resistive fluid have been examined. Theoretical results obtained here are in qualitative agreement with experimental observations. Such agreement indicates that the properties of thruster

generated plasmas can be described by fluid equations having a classical form but with an effective collision frequency near ω_p, much in excess of the classical value for pair (electron-ion) collisions.

Further work should be performed to test qualitative and quantitative predictive capabilities of fluid models of thruster plasmas, and to better understand the relationship between ersatz fluid models of the type invoked here and the underlying plasma physical mechanisms embodied in the collisionless Vlasov equation.

Appendix A. Mathematical Considerations on the Variational Formulation of Poisson's Equation

In our theory of ion engine neutralization, it is necessary to solve equations of the form

$$\nabla\cdot[\sigma(\underline{r})\nabla\phi] = S(\underline{r}) \tag{A.1}$$

subject to fixed-value boundary conditions at some nodes and normal-gradient boundary conditions at others. We need to show that equation (A.1) is exactly the equation equivalent to the variational formulation, and that the normal-gradient boundary conditions are equivalent to a surface charge.

Theorem 1

Minimization of

$$\int d^3\underline{r}\left\{\frac{\sigma(\underline{r})}{2}|\nabla\phi|^2 + \phi(\underline{r})S(\underline{r})\right\} \tag{A.2}$$

is equivalent to equation (A.1).

Proof

Minimization of $\int d^3\underline{r}\,L(\phi,\nabla\phi,\underline{r})$ requires

$$\nabla\cdot\frac{\partial L(\phi,\nabla\phi,\underline{r})}{\partial(\nabla\phi)} - \frac{\partial L(\phi,\nabla\phi,\underline{r})}{\partial\phi} = 0 \tag{A.3}$$

Taking L as the integrand of (A.2), equation (A.3) yields exactly equation (A.1).

Theorem 2

In the finite-element formulation for the minimization of (A.2), normal-gradient boundary conditions are equivalent to surface charge.

Proof

In the finite-element formulation, minimization of (A.2) leads to the equations

$$\frac{\partial}{\partial\phi_i}\left\{\frac{1}{2}\sum_{jk}\phi_j W_{jk}\phi_k + \sum_i \phi_i S_i\right\} = 0 \tag{A.4}$$

where

$$W_{jk} = \int_\Omega d^3\underline{r}\;\sigma(\underline{r})[\nabla N_j(\underline{r})]\cdot[\nabla N_k(\underline{r})] \tag{A.5}$$

$$S_i = \int_\Omega d^3r\; N_i(\underline{r})\; S(\underline{r}) \;, \tag{A.6}$$

$N_i(\underline{r})$ are nodal interpolation functions and ϕ_i are node values for the unknown field.

Since $\underline{\underline{W}}$ is symmetric, these equations are

$$\sum_j W_{ij}\phi_j + S_i = 0 \tag{A.7}$$

Using (A.5) we find

$$\sum_j W_{ij}\phi_j = \int_\Omega d^3\underline{r}[\nabla N_i(\underline{r})]\cdot[\sigma(\underline{r})\nabla\bar{\phi}(\underline{r})] \tag{A.8}$$

where

$$\bar{\phi}(\underline{r}) = \sum_i N_i(\underline{r})\phi_i$$

The integrand of (A.8) can be rewritten as

$$\nabla\cdot[\sigma(\underline{r})N_i(\underline{r})\nabla\bar{\phi}(\underline{r})] - N_i(\underline{r})\nabla\cdot[\sigma(\underline{r})\nabla\bar{\phi}(\underline{r})] \tag{A.9}$$

Writing $\underline{D}(\underline{r}) = \sigma(\underline{r})\nabla\bar{\phi}(\underline{r})$, and using the divergence theorem, equation (A.7) becomes

$$\int_S d^2\underline{r}\; N_i(\underline{r})\;\underline{D}(\underline{r})\cdot\hat{n} - \int_\Omega d^3\underline{r}\; N_i(\underline{r})\;\nabla\cdot\underline{D}(\underline{r}) + S_i = 0 \tag{A.10}$$

where the first integral runs over the surface of volume Ω. By analogy with electrostatics, the second and third terms are the "volume charge" associated with node i, while the first, involving the surface-normal-gradient of the potential, is non-zero only on surface nodes and may be compensated by a corresponding surface-charge density.

Corollary

Consider the equation

$$\nabla\cdot\underline{J} = 0 \tag{A.11a}$$

where

$$\underline{J} = \sigma(\nabla\phi - g(\underline{r})\nabla f) \;, \tag{A.11b}$$

and $f(\underline{r})$, $g(\underline{r})$ are known functions. If the inhomogeneous term is evaluated using equation (A.8), equation (A.11), with no further qualifications, will give zero-normal-current boundary conditions when solved by the finite-element method.

Furthermore, non-zero normal current boundary conditions, $\hat{n} J_B(r)$, can be invoked by adding an inhomogeneous term to the surface node equations.

Proof

Substituting (A.11) into (A.10), the finite element equations are

$$\int_S d^2\underset{\sim}{r}\, N_i(\underset{\sim}{r})\, \underset{\sim}{J}(\underset{\sim}{r})\cdot\hat{n} - \int d^3\underset{\sim}{r}\,\underset{\sim}{\nabla}\cdot\underset{\sim}{J}(\underset{\sim}{r})\, N_i(\underset{\sim}{r}) = 0 \tag{A.12}$$

As the second term is to vanish (within the finite-element approximation), it follows that the first term is equal to the right-hand-side. Thus, replacing the right-hand-side with

$$\int_S d^2\underset{\sim}{r}\, N_i(\underset{\sim}{r})\, J_B(\underset{\sim}{r}) \tag{A.13}$$

will produce the specified boundary conditions.

References

1. Kerslake, W. R., D. C. Byers and J. F. Staggs, "SERT II: Mission and Experiments," J. Spacecraft 7, 1, p. 4, 1970.

2. Byers, David C. and John F. Staggs, "SERT: Thruster System Ground Testing," J. Spacecraft 7, 1, p. 7, 1970.

3. Sellen, J. M., Jr., W. Bernstein and R. F. Kemp, "Generation and Diagnosis of Synthesized Plasma Streams," Rev. Sci. Instr. 36, p. 316, 1965.

4. Bernstein, W. and J. M. Sellen, Jr., "Oscillations in Synthetic Plasma Beams," Phys. Fluids 6, p. 1032, 1963.

5. Ogawa, H. S., R. K. Cole and J. M. Sellen, Jr., "Factors in the Electrostatic Equilibration Between a Plasma Thrust Beam and the Ambient Space Plasma," AIAA Paper No. 70-1142, AIAA 8th Electric Propulsion Conference, 1970.

6. Ogawa, H. S., R. K. Cole and J. M. Sellen, Jr., "Measurements of Equilibration Potential Between a Plasma Thrust Beam and a Dilute Space Plasma," AIAA Paper No. 69-263, AIAA 7th Electric Propulsion Conference, 1969.

7 Kaufman, Harold R., "Interaction of a Solar Array with an Ion Thruster Due to the Charge-Exchange Plasma," NASA Report CR-135099, 1976.

8. Braginskii, S. I., Reviews of Plasma Physics, Vol. 1, Ed. M. A. Leontovich, Consultants Bureau, New York, p. 205, 1965.

9. Krall, Nicholas A. and Alvin W. Trivelpiece, Principles of Plasma Physics, McGraw-Hill, New York, 1973.

10. Bunemann, O., "Dissipation of Currents in Ionized Media," Phys. Rev. 115, p. 503, 1959.

11. Kerslake, W. R., private communication, NASA-Lewis Research Center, Cleveland, OH, November, 1979.

APPENDIX B

AIAA 81-0740

PARASITIC CURRENT LOSSES DUE TO SOLAR ELECTRIC PROPULSION GENERATED PLASMAS

I. Katz, D. E. Parks, M. J. Mandell and G. W. Schnuelle

S-CUBED
La Jolla, CA 92038

AIAA/JSASS/DGLR 15th INTERNATIONAL ELECTRIC PROPULSION CONFERENCE

April 21-23, 1981
Las Vegas, NV

Published in Journal of Spacecraft and Rockets, 19, p. 129, 1982.

PARASITIC CURRENT LOSSES DUE TO SOLAR ELECTRIC PROPULSION GENERATED PLASMAS

I. Katz,* D. E. Parks,** M. J. Mandell,† G. W. Schnuelle†
Systems, Science and Software
La Jolla, California 92038

Abstract

Solar electric propulsion is a leading candidate for many upcoming space missions. Under many circumstances plasma produced by charge-exchange reactions within the ion beam dominates the ambient environment near the spacecraft. The calculations presented here contain a predictive hydrodynamic model for the charge-exchange plasma expansion, and a fully three-dimensional model for the structure of the plasma sheath around the solar array wing. Results of calculations for several configurations and voltage levels indicate that with kilovolt biases power losses of ~10 percent or more are likely, even with only one engine in operation, and that ameliorative measures should focus on the inboard portion of the solar arrays.

Nomenclature

$\vec{E}$ = electric field
f_r = radial mass flux
f_z = axial mass flux
$\vec{F}_{ij}$ = acceleration on $\vec{V}_{ij}$
k = Boltzman's constant
m = ion mass
n = electron density
n_A = ambient plasma density
q = magnitude of electron charge
r = radial coordinate
$r_i^{(v)}$ = radial location of velocity vector $\vec{V}_{ij}$
$r_i^{(\rho)}$ = radial location of ion density ρ_{ij}
S_k = k^{th} surface boundary of Ω_{ij}
T = electron temperature
$\vec{V}$ = ion velocity
Z = axial coordinate
$z_j^{(v)}$ = axial location of velocity vector $\vec{V}_{ij}$
$z_j^{(\rho)}$ = radial location of ion density ρ_{ij}
α = angle from the thruster beam direction
Δr = radial mesh spacing
Δz = axial mesh spacing
θ = kT
ρ = ion density
ϕ = electric potential
Ω_{ij} = volume of cell associated with $\vec{V}_{ij}$

1. Introduction

Solar electric propulsion is a leading candidate for lifting large structures from shuttle orbit to geostationary altitude. Previous studies [1,2] demonstrated that plasma produced by charge-exchange reactions within the ion beam may dominate the ambient environment near the spacecraft. Currents flowing through this plasma between the engine neutralizers and the solar arrays are a drain on the power systems. If the losses become too large, they may have a substantial mission impact.

Simple calculations have been performed to estimate parasitic currents flowing through the charge-exchange plasma. [1,2] While the potential seriousness of the interaction was identified, the ad hoc nature of the previous work made clear the need for a more accurate treatment of the expansion of the charge-exchange plasma and the resultant solar array power losses. The calculations presented here are an improvement over previous work in that they contain a predictive model for the charge-exchange plasma expansion, and a fully three-dimensional model for the structure of the plasma sheath around the solar array wing.

The generation mechanism of the charge-exchange plasma is clearly understood. [3] However, until recently there were no predictive models of the expansion dynamics of these slow moving ions. This work, as well as that of Robinson, Kaufman and Winder, [4] describe the ions as streaming under the electric field created by barometric law behavior of the plasma electrons. The model described here treats the ions numerically as a cold fluid while Reference 4 calculates representative ion trajectories by particle pushing. Both calculations are presently done assuming axial symmetry.

The collection of ions and electrons by solar arrays has been the subject of much recent interest. Experiments have been performed on large array-like objects in the vacuum tank at NASA/JSC. [5] A three-dimensional computer code, which simulates plasma interactions in Low Earth Orbit (LEO) was developed by the authors and provided qualitative and quantatitive agreement with experiment. [6] This program, NASCAP/LEO, in a somewhat modified form is used in this study to describe the charge-exchange plasma-solar array interactions.

In this paper we present a new model for the expansion of the charge-exchange plasma from an ion thruster. We then use this predicted charge-exchange plasma as the environment surrounding solar arrays in the LEO plasma interaction model. From this we obtain improved estimates of power losses for a variety of solar array configurations.

*Program Manager, **Senior Research Scientist, †Research Scientist

2. Theory

For this study we have considered a single 30 cm diameter mercury thruster producing 2 A of beam current and 25 mA of charge-exchange current. [3] The charge-exchange ions are emitted radially, with energies of 5-10 eV, within a downstream distance equal to one diameter of the beam. This gives a density of $\sim 2.5 \times 10^{14}$ m^{-3} at the beam edge, which exceeds the Low Earth Orbit (LEO) plasma density of 10^{10}-10^{12} m^{-3}. Thus the charge-exchange plasma will dominate the ambient to a distance of several meters from the thruster in LEO, and over the entire spacecraft for substantially more tenuous environments.

The conditions in this plasma are long collision lengths ($\sim 10^{3}$ m) and short Debye lengths ($\sim 10^{-3}$ m). In this regime we assume that the electron gas adjusts itself to maintain isothermal, quasi-neutral conditions. This implies a barometric law potential,

$$\phi = \theta \ell n(n/n_A) \qquad (1)$$

where θ is the electron temperature (eV), n the local plasma density, and n_A the ambient plasma density. The barometric law is not an essential feature of the model. In the future we expect to remove the isothermal restriction and utilize fluid-like equations to describe the electrons. [7] The barometric law potential causes expansion of the ion cloud as it emerges from the beam edge. Far downstream the electrostatic force become small, so that the ion density takes the form $f(\alpha)/r^2$, where α is the polar angle relative to the beam and r the distance from the engine.

The ion gas is modeled hydrodynamically, i.e., we assume the ion density and velocity to be a well-defined function of position, and the ion thermal motion to be unimportant. This representation is chosen for ease of generalization, as opposed to using particle pushing techniques which require extensive computer time for three-dimensional applications. The motion then satisfies the equations of continuity of mass and momentum:

$$\frac{\partial \rho}{\partial t} = -\vec{\nabla} \cdot (\rho \vec{v}) \qquad (2)$$

$$\frac{\partial}{\partial t} (\rho v_\alpha) = -\vec{\nabla} \cdot (v_\alpha \rho \vec{v}) + \frac{\rho q E_\alpha}{m} \qquad (3)$$

where subscript α denotes a Cartesian component, and $\vec{E}$ is the electric field. The challenge is to develop numerical methods capable of finding the steady-state solution to equations (1-3) in the R-Z (cylindrical) geometry appropriate to the problem.

3. Numerical Methods

In order to suppress spurious numerical oscillations we solved equations (2) and (3) using upwind differencing on a staggered mesh. [8] The computational mesh is shown in Figure 1. The thruster beam starts on the z = 0 plane and is pointed along the positive z axis. Charge-exchange ions are produced downstream within the thruster beam, and the charge-exchange ions are expelled from the main beam radially by electric fields within the beam. The physical space is located within the solid boundary; mesh points outside the physical space are computationally convenient and serve to maintain boundary conditions. Velocities are defined at the points indicated by crosses, which form an evenly spaced r-z mesh:

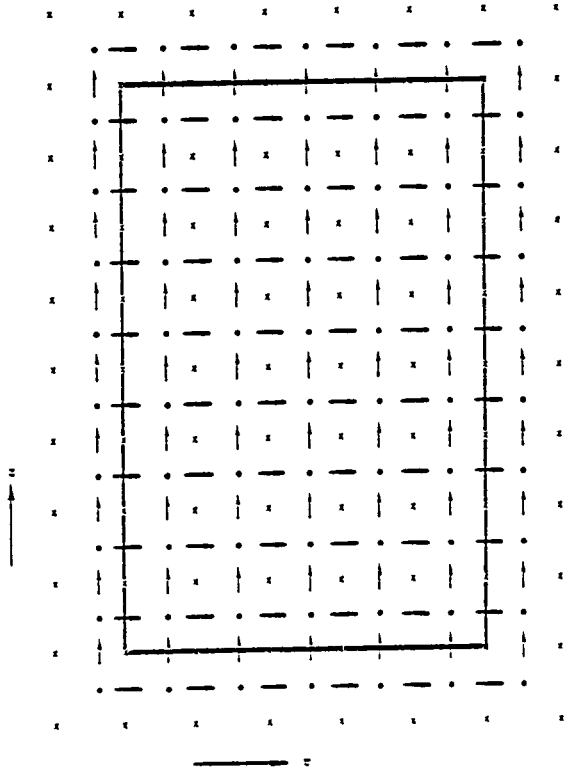

Fig. 1 Computational space, showing points for definition of velocity (×), density (•), and mass flux (—►).

$$r_i^{(v)} = r_o + i\,\Delta r \qquad (4a)$$

$$z_j^{(v)} = z_o + j\,\Delta z \qquad (4b)$$

Densities are defined at the centroids of the quadrilaterals formed by the crosses:

$$r_i^{(\rho)2} = \frac{1}{2}\left(r_i^{(v)2} + r_{i+1}^{(v)2}\right) \qquad (5a)$$

$$z_j^{(\rho)} = \frac{1}{2}\left(z_j^{(v)} + z_{j+1}^{(v)}\right) \qquad (5b)$$

Mass fluxes, $\underset{\sim}{f}$, are defined at the arrows in a fully "upwind" sense:

$$v_r\left(r_i^{(v)}, z_j^{(\rho)}\right) = \frac{1}{2}\left[v_r\left(r_i^{(v)}, z_j^{(v)}\right) + v_r\left(r_i^{(v)}, z_{j+1}^{(r)}\right)\right] \tag{6a}$$

$$(\Delta r) v_z\left(r_i^{(\rho)}, z_j^{(v)}\right) = \left(r_{i+1}^{(v)} - r_i^{(\rho)}\right) v_z\left(r_i^{(v)}, z_j^{(r)}\right) + \left(r_i^{(\rho)} - r_i^{(v)}\right) v_z\left(r_{i+1}^{(v)}, z_j^{(v)}\right) \tag{6b}$$

$$f_r\left(r_i^{(v)}, z_j^{(\rho)}\right) = \left(r_k^{(\rho)} \Big/ r_i^{(v)}\right) \rho\left(r_k^{(\rho)}, z_j^{(\rho)}\right) v_r\left(r_i^{(v)}, z_j^{(\rho)}\right)$$

$$k = \begin{cases} i-1 & \text{if } v_r \geq 0 \\ i & \text{if } v_r < 0 \end{cases} \tag{6c}$$

$$f_z\left(r_i^{(\rho)} m z_j^{(v)}\right) = \rho\left(r_i^{(\rho)}, z_\ell^{(\rho)}\right) v_z\left(r_i^{(\rho)}, z_j^{(v)}\right)$$

$$\ell = \begin{cases} j-1 & \text{if } v_z \geq 0 \\ j & \text{if } v_z < 0 \end{cases} \tag{6d}$$

With the above definitions, it is straightforward to timestep the integral form of equation (2), using as control volumes the rectangles formed by the four crosses (velocity definition points) surrounding a density definition point.

Equation (3) is then used to construct $d\vec{v}/dt$. We use a finite difference method to evaluate the divergence term as follows:

a. Define mass fluxes flowing between the crosses in Figure 1, i.e., normal to the arrows. This is done by taking weighted averages of nearby already defined fluxes:

$$4r_i^{(\rho)} f_r\left(r_i^{(\rho)}, z_j^{(v)}\right) = \sum_{k=1}^{i+1} \sum_{\ell=j-1}^{j} r_k^{(v)} f_r\left(r_k^{(v)}, z_\ell^{(\rho)}\right) \tag{7}$$

$$4r_i^{(v)} f_z\left(r_i^{(v)}, z_j^{(\rho)}\right) = \sum_{k=i-1}^{i} \sum_{\ell=j}^{j+1} r_k^{(\rho)} f_z\left(r_k^{(\rho)}, z_\ell^{(v)}\right) \tag{8}$$

b. Define densities associated with velocity definition points:

$$4r_i^{(v)} \rho\left(r_i^{(v)}, z_j^{(v)}\right) = \sum_{k=i-1}^{i} \sum_{\ell=j-1}^{j} r_k^{(\rho)} \rho\left(r_k^{(\rho)}, z_\ell^{(\rho)}\right) \tag{9}$$

These densities are needed at both their previous and current (just updated) values.

c. Define velocities at the arrows:

$$\left(r_{i+1}^{(v)} - r_i^{(v)}\right) \underset{\sim}{v}\left(r_i^{(\rho)}, z_j^{(v)}\right) = \left(r_i^{(\rho)} - r_i^{(v)}\right) \underset{\sim}{v}\left(r_{i+1}^{(v)}, z_j^{(v)}\right) + \left(r_{i+1}^{(v)} - r_i^{(\rho)}\right) \underset{\sim}{v}\left(r_i^{(v)}, z_j^{(v)}\right)$$

$$\left(z_{j+1}^{(v)} - z_j^{(v)}\right) \underset{\sim}{v}\left(r_i^{(v)}, z_j^{(\rho)}\right) = \left(z_j^{(\rho)} - z_j^{(v)}\right) \underset{\sim}{v}\left(r_i^{(v)}, z_{j+1}^{(\rho)}\right) + \left(z_{j+1}^{(v)} - z_j^{(\rho)}\right) \underset{\sim}{v}\left(r_i^{(v)}, z_j^{(\rho)}\right)$$

d. Determine the change in velocity by

$$\Omega_{ij} \frac{d}{dt}\left[\rho\left(r_i^{(v)}, z_j^{(v)}\right) \underset{\sim}{v}\left(r_i^{(v)}, z_j^{(v)}\right)\right] = -\sum_k S_k\left(\hat{n}_k \cdot \underset{\sim}{f}_k\right) \underset{\sim}{v}_k + \Omega_{ij} \underset{\sim}{F}_{ij}$$

where Ω_{ij} is the volume

$$r_{i-1}^{(\rho)} < r < r_i^{(\rho)};\ z_{i-1}^{(\rho)} < z < z_i^{(\rho)},$$

S_k are the surfaces bounding that volume, and $\underset{\sim}{F}_{ij}$ is the force at $\left(r_i^{(v)}, z_j^{(v)}\right)$. Specifically, using

$$\Omega_{ij} = \pi\left(r_i^{(\rho)2} - r_{i-1}^{(\rho)2}\right)\left(z_i^{(\rho)} - z_{i-1}^{(\rho)}\right),$$

we obtain the following expression for the divergence of the momentum flux integrated over the volume:

$$-\sum_k S_k\, \hat{n}_k \cdot \underset{\sim}{f}_k\, \underset{\sim}{v}_k =$$

$$2\pi\left(z_i^{(\rho)}-z_{i-1}^{(\rho)}\right)\left[r_{i-1}^{(\rho)}\ f_r\left(r_{i-1}^{(\rho)},z_i^{(v)}\right)\right.$$
$$\underset{\sim}{v}\left(r_{i-1}^{(\rho)},z_i^{(v)}\right)$$
$$\left.-\ r_i^{(\rho)}\ f_r\left(r_i^{(\rho)},z_i^{(v)}\right)\ \underset{\sim}{v}\left(r_{i-1}^{(\rho)},z_i^{(v)}\right)\right]$$
$$+\ \pi\left(r_i^{(\rho)2}-r_{i-1}^{(\rho)2}\right)\left[f_z\left(r_i^{(v)},z_{i-1}^{(\rho)}\right)\ \underset{\sim}{v}\left(r_i^{(v)},z_{i-1}^{(\rho)}\right)\right.$$
$$\left.-\ f_z\left(r_i^{(v)},z_i^{(\rho)}\right)\ \underset{\sim}{v}\left(r_i^{(v)},z_i^{(\rho)}\right)\right]\ .$$

The velocities are advanced using

$$\underset{\sim}{v}_{ij}(t)=\rho_{ij}(t-dt)\ \underset{\sim}{v}_{ij}(t-dt)/\rho_{ij}(t)$$
$$+\ (q/m)\ \underset{\sim}{E}\left(r_i^{(v)},z_j^{(v)}\right)dt$$
$$-\ \frac{dt}{\Omega_{ij}\rho_{ij}(t)}\sum_k\ S_k\left(\hat{n}_k\cdot\underset{\sim}{f}_k\ \underset{\sim}{v}_k\right)\ .$$

These formulae are accurate to first order in dt and second order in $(\Delta r,\Delta z)$.

e. Additionally, provision is made for optional velocity smoothing at each time-step.

The problem is run until there is no variation of velocities in time. This empirical steady state is generally achieved in a few times the time it takes for a fluid particle to traverse the mesh.

4. Results

We have applied the above model to calculate the expansion of an ion charge-exchange plume with initial conditions similar to a case measured by Hughes Research Laboratory.[3] The initial conditions were:

Emission energy (radial) = 10 eV.
Initial radius $r_1^{(v)}$ = .15 m.
Current density $q\ o\left(r_1^{(v)},z\right)v_r\left(r_2^{(v)},z\right)$

$$=\begin{cases}0 & z<0\\ .123\ \exp(-z/.22) & z>0\end{cases}$$

(total current = 25 mA)
Electron temperature θ = 1 eV.
Mass (Hg ion) = 3.34×10^{-25} kg.
Ambient density $n_A = 10^{12}\ m^{-3}$.

It follows that

$$v_r\left(r_1^{(v)},z\right)=3095\ \text{m/sec}$$

$$\rho\left(r_1^{(v)},0\right)=2.48\times10^{14}\ m^{-3}$$

$$\phi_{max}=\theta\rho\ell n\left[\rho\left(r_1^{(v)},0\right)/n_A\right]=5.5\ \text{V}.$$

The calculation was done in three phases:

a. .15 m < r < 1.15 m; Δr = 0.05 m
-1.0 m < z < 1.0 m; Δz = 0.10 m

b. 1.0 m < r < 5.0 m; Δr = 0.2 m
-2.0 m < z < 2.0 m; Δz = 0.2 m

c. 2.0 m < r < 12 m; Δr = 0.5 m
-4.0 m < z < 4 m; Δz = 0.4 m

Initial conditions for the second and third phases were obtained by interpolating data from the previous phase and renormalizing to retain the correct total current. At each phase, the calculation was carried out until steady-state densities and velocities were reached.

The results are shown in Figures 2 and 3. It is seen that the initially asymmetric expansion (Figure 2) becomes roughly symmetric by a radius of ~1 m from the beam. This is seen in Figure 3a, in which spherical (r^2+z^2) scaling maintains constant arrow length, and in Figure 3b, which indicates radial contours of equal (r^2+z^2) times the density. The density (m^{-3}) beyond 1 m from the engine is reasonably approximated by

$$\rho\approx10^{13}\ (\sin\alpha)^{12}/(r^2+z^2)$$

where α is the angle from the beam direction. A closer inspection of Figure 3b indicates that the plume extends further upstream than downstream. This is attributable to "pressure blowoff" at the upstream plume edge near the engine where the density gradient is high.

The plasma parameters determined from the above model are used as input to a fully three-dimensional computer program designed to predict current collection by high voltages in low temperature, short Debye length plasmas.[6,9] This model uses an analytic, nonlinear space charge formulation, correct in both Debye screening and thin sheath limits, to determine the electrostatic potential and the boundary of the plasma sheath. The model allows the plasma temperature and density to vary in space. Figure 4 gives a sample of electrostatic potential contours near a solar array wing, illustrating the asymmetry caused by the charge-exchange plasma being predominantly on one side of the wing. By tracking electrons inward from the sheath boundary, good parasitic current estimates are obtained. Iterating on the two stages of the calculation allows non-local effects to be included. Additionally, a high resolution capability is available to compute the current distribution over a complex pattern of solar cells.

Table 1 gives sample results for an 8 m × 30 m, 25 kw solar array for several

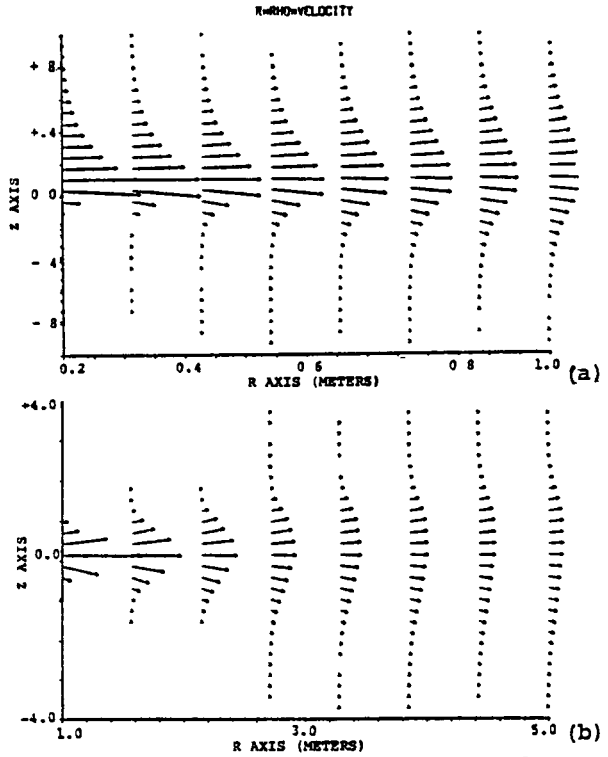

Fig. 2 Cylindrically scaled current density plots for ion plume flow (a) near the beam, and (b) in the "spherical expansion" region.

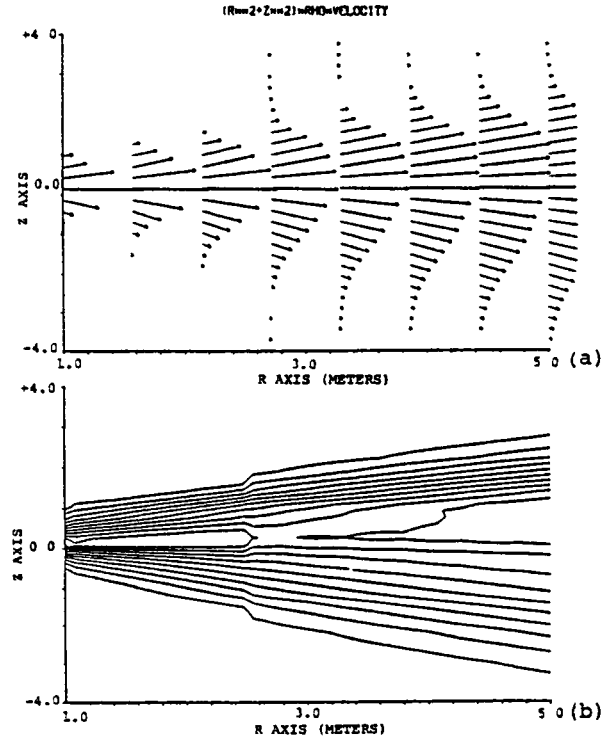

Fig. 3 Spherically scaled plots of (a) current density and (b) particle density contours.

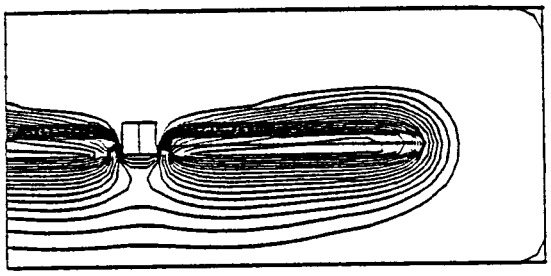

Fig. 4 Potential contours about a 2 kV solar array in the presence of the charge-exchange plume. Note that the potential is more shielded above the wing (where the charge-exchange plasma is located) than below. The contour differences are 100 volts.

orientations and configurations. In these calculations, the spacecraft body was held at plasma ground and the solar array was divided into three equal sections, each of which was positively biased. Parasitic currents to both sides of each 10 m section of the wing were separately monitored. Several trends are apparent: (1) The inboard section of the wing draws most of the current, even though it is at a low voltage. This is because of the r^{-2} expansion of the charge-exchange plasma. (2) The current to the outboard section is similar to the center section current, due to the large end effect in the tenuous plasma. (3) When the beam is in the plane of the panel, an increased loss is caused by the array's intersecting the charge-exchange pancake. It is apparent from these results that with kilovolt biases power losses of ~10 percent or more are likely, even with only one engine in operation, and that ameliorative measures should focus on the inboard portion of the solar arrays.

5. Discussion

As large, high powered solar electric propulsion vehicles come closer to reality, it becomes more important to place realistic bounds on the plasma array interactions. Previous studies [1,2] had assumed simple models of the charge-exchange expansion. The expansion model is so important in estimating power losses that the authors' previous work [2] parameterized the results in terms of an undetermined expansion angle. The calculations presented here are a vast improvement, inasmuch as the expansion of the charge exchange plasma is determined on a reasonable theoretical basis and the plasma collection is fully three-dimensional.

However, certain other aspects of the model presented here are just as primitive as in the earlier studies. In particular the isothermal barometric law description of the electrons, the lack of self-consistency between expansion and sheath models, and the absence of any turbulent

Table 1 Power losses for 8 m × 30 m solar array for one thruster and various configurations

Configuration	Voltage Inboard	Voltage Center	Voltage Outboard	Current (one side) Inboard	Current (one side) Center	Current (one side) Outboard	Power Loss (per wing)
a,d	1000	2000	3000	1.4	0.6	0.6	4.4
b,d	2000	2000	2000	4.7	0.6	0.5	12.0
b,d	1000	2000	3000	3.7	0.6	0.5	6.4
a,c	1000	2000	3000	1.1	0.3	0.4	5.9
a,c	100	1000	2000	0.8	0.3	0.4	2.3
a,d	200	200	200	1.4	0.3	0.2	0.38
a,d	400	400	400	1.5	0.3	0.3	0.85

a - Beam in plane of panel
b - Beam normal to plane of panel
c - Both sides biased
d - Back of panel grounded

All voltages in volts, currents in amps, and power losses in kilowatts.

heating mechanism during electron collection place severe restrictions on the accuracy of these results. For mission analysis, there also remains unanswered the question of charge-exchange plasma generation and expansion in a multiple thruster configuration. These are some of the technical questions which must be addressed if we are to provide an accurate assessment of parasitic current losses due to ion propulsion generated plasmas.

References

1. Kaufman, H. R., "Interaction of a Solar Array with an Ion Thruster Due to the Charge-Exchange Plasma," NASA CR-135099, 1976.

2. Parks, D. E. and I. Katz, "Spacecraft-Generated Plasma Interactions with High-Voltage Solar Array," J. Spacecraft and Rockets, 16, 259, 1979.

3. Poeschel, R. L., E. I. Hawthorne, et al., "Extended Performance Solar Electric Propulsion Thrust System Study," NASA CR135281, 1977.

4. Robinson, R. S., H. R. Kaufman and D. R. Winder, "Simulation of Charge-Exchange Plasma Propagation Near an Ion Thruster Propelled Spacecraft," AIAA-81-0744, AIAA/JSASS/DGLR 15th International Electric Propulsion Conference, Las Vegas, NV, April 21-23, 1981.

5. McCoy, J. E. and A. Konradi, "Sheath Effects Observed on a 10 meter High Voltage Panel in Simulated Low Earth Orbit Plasma," Spacecraft Charging Technology-1978, 315, NASA Conference Publication 2071, AFGL-TR-79-0082, 1979.

6. Katz, I., M. J. Mandell, G. W. Schnuelle, D. E. Parks and P. G. Steen, "Plasma Collection by High Voltage Spacecraft at Low Earth Orbit," J. of Spacecraft and Rockets, Vol. 18, No. 1, p. 79, January-February 1981.

7. Parks, D. E., M. J. Mandell and I. Katz, "Fluid Model of Neutralized Ion Beams," AIAA-81-0141, AIAA 19th Aerospace Sciences Meeting, St. Louis, MO, January 12-15, 1981.

8. Richtmyer, R. D. and K. W. Morton, Difference Methods for Initial-Value Problems, Interscience Publishers, New York, Second Edition.

9. Mandell, M. J., I. Katz, P. G. Steen and G. W. Schnuelle, "The Effect of Solar Array Voltage Patterns on Plasma Power Losses," IEEE Trans. Nuc. Sci., Vol. NS-27, No. 6, p. 1797, December 1980.

Acknowledgments

This work supported by NASA/Lewis Research Center, Cleveland, OH under Contract NAS3-21762.

APPENDIX C

NEUTRAL DENSITY FREE EXPANSION MODEL

Problem: A Maxwellian spectrum of velocities is emitted uniformly from a disk of radius a located on the plane $z = 0$. Find the density of particles throughout space.

Geometry:

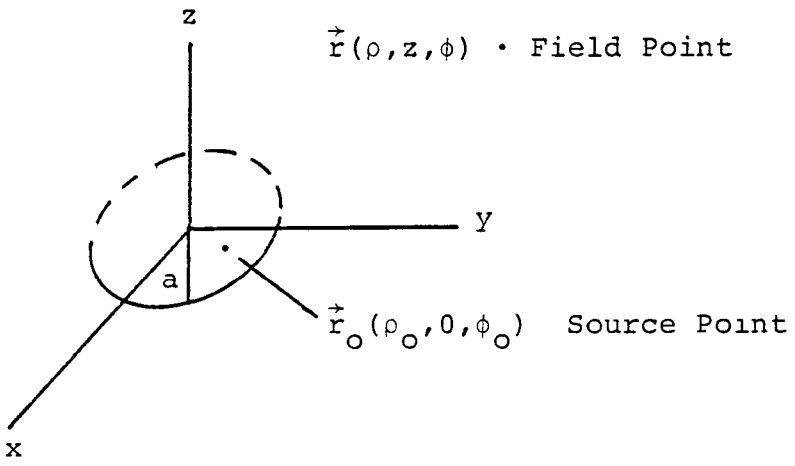

Analysis: On a trajectory

$$f(\vec{\rho},z,\vec{V}_{\perp},v_z) = f_o(\vec{\rho}_o,o,\vec{V}_{\perp},v_z)$$

where f is the distribution function at $\vec{r}$,

$$f_o = 2n_o(\pi V_T^2)^{-3/2} \exp\left[-\frac{V_\perp^2 + V_z^2}{V_T^2}\right] \qquad \rho \leq a,\ v_z > 0$$

$$= 0 \qquad \rho > a \text{ or } v_z < 0$$

n_o = density $\qquad z = 0,\ \rho < a$

$V_T^2 = 2\ kT/m$

Since $\vec{r}$ and $\vec{r}_o$ are connected by a trajectory

$$\vec{\rho} - \vec{\rho}_o = \vec{V}_\perp\, z/v_z$$

$$d^2\vec{V}_\perp dv_z = \frac{v_z^2}{z^2}\, d^2\vec{\rho}_o\, dv_z$$

$$n = 2n_o(\pi V_T^2)^{-3/2} \int d^2\vec{\rho}_o \int \frac{v_z^2}{z^2} \exp\left\{-\left[\frac{(\rho-\vec{\rho}_o)^2}{z^2} + 1\right]\frac{v_z^2}{V_T^2}\right\}\, dv_z$$

$$= 2n_o(\pi V_T^2)^{-3/2}\, z \int d^2\vec{\rho}_o \int \exp\left\{-\left[(\vec{\rho}-\vec{\rho}_o)^2 + z^2\right]x^2\right\}\, x^2 dx$$

$$= 2n_o(\pi V_T^2)^{-3/2}\, z \int d^2\vec{\rho}_o\, \frac{\sqrt{\pi}}{4}\left[\frac{(\vec{\rho}-\vec{\rho}_o)^2 + z^2}{V_T^2}\right]^{-3/2}$$

$$= \frac{n_o}{2\pi}\, z \int_0^a \int_0^{2\pi} \rho_o d\rho_o d\phi \left[\rho^2 + \rho_o^2 + z^2 - 2\rho\rho_o \cos\phi\right]^{-3/2}$$

$$= \frac{n_o}{2\pi}\left(-\frac{\partial}{\partial z}\right) \int_0^a \int_0^{2\pi} \rho_o d\rho_o d\phi \left[\rho^2 + \rho_o^2 + z^2 - 2\rho\rho_o \cos\phi\right]^{-1/2}$$

Observations:

1. For $\rho < a$, the integral is singular for $z \to 0$; $n(\rho,0) = n_o$ for $\rho < 0$, $n(\rho,0) = 0$ $\rho > a$.

2. The density field is formally equivalent to the E_z field of a disk with a uniform distribution of surface charges.

3. Asymptotically, $(\rho^2 + z^2 = \eta^2 >> a^2)$

   $n \sim z/r^3$

Integration: The integral over ρ_o can be performed analytically

$$n = \frac{n_o}{2\pi} z \int_0^{2\pi} d\phi (z^2+\rho^2\sin^2\phi)^{-1} \left[r - \frac{r^2-a\rho\cos\phi}{(r^2+a^2-2a\rho\cos\phi)^{1/2}} \right]$$

where

$$r = (\rho^2 + z^2)^{1/2}$$

DISTRIBUTION LIST

National Aeronautics and Space Administration
Washington, D. C. 20546

Attn:	W. R. Hudson/Code RP	1 copy
	D. P. Williams, III/Code RS-5	1 copy

National Aeronautics and Space Administration
Ames Research Center
Moffett Field, CA 94035

Attn:	H. Lum, Jr./M.S. 244-7	1 copy

National Aeronautics and Space Administration
Goddard Space Flight Center
Greenbelt, MD 20771

Attn:	R. O. Bartlett/Code 408.0	1 copy
	A. Kampinsky/Code 727.0	1 copy
	E. G. Stassinopoulos/Code 601.0	1 copy
	R. S. Bever/Code 405.0	1 copy

Jet Propulsion Laboratory
4800 Oak Grove Drive
Pasadena, CA 91103

Attn:	Ray Goldstein	1 copy
	H. Garrett	1 copy
	E. V. Pawlik	1 copy
	Paul Robinson	1 copy

National Aeronautics and Space Administration
Lyndon B. Johnson Space Center
Houston, TX 77058

Attn:	J. E. McCoy/Code SN3	1 copy
	A. Konradi/Code SN3	1 copy

National Aeronautics and Space Administration
Langley Research Center
Hampton, VA 23665

Attn:	J. W. Goslee/M.C. 364	2 copies

National Aeronautics and Space Administration
Lewis Research Center
21000 Brookpark Road
Cleveland, OH 44135

Attn:	Head, Mechanics, Fuels and Physics Section/ M.S. 501-11	1 copy
	Technology Utilization Office/M.S. 7-3	1 copy
	Report Control Office/M.S. 5-5	1 copy
	Office of Reliability and Quality Assurance/ M.S. 500-211	1 copy
	AFSC Liaison Office/M.S. 501-3	2 copies
	Library/M.S. 60-3	2 copies
	J. C. Roche/M.S. 77-4	24 copies
	Patent Counsel/M.S. 500-318	1 copy

DISTRIBUTION LIST (Continued)

National Aeronautics and Space Administration
George C. Marshall Space Flight Center
Marshall Space Flight Center, AL 35812
Attn: C. R. Chappell/ES 51 — 1 copy
J. H. Harlow/PF 13 — 1 copy
M. R. Carruth/PF 13 — 1 copy
R. N. Seitz/EF 31 — 1 copy

National Aeronautics and Space Administration
Scientific and Technical Information Facility
P. O. Box 8757
Baltimore/Washington International Airport
Maryland 21240
Attn: Accessioning Department — 10 copies

Air Force Geophysics Laboratory
Hanscom Air Force Base, MA 01731
Attn: PH/C. P. Pike — 1 copy
PHG/A. G. Rubin — 1 copy

Air Force Materials Laboratory
Wright-Patterson Air Force Base, OH 45433
Attn: MBE/W. Lehn — 1 copy

Air Force Office of Scientific Research
Bolling Air Force Base
Washington, D. C. 20332
Attn: H. R. Radoski/NP — 1 copy

Air Force Weapons Laboratory
Kirtland Air Force Base, NM 87117
Attn: Capt. W. G. Kuller — 1 copy
Capt. D. Hanifen — 1 copy

Headquarters Space Division (AFSC)
Los Angeles AF Station
P. O. Box 92960
Worldway Postal Center
Los Angeles, CA 90009
Attn: YLVS/Lt. R. Weidenheimer — 1 copy

Defense Nuclear Agency Headquarters
Washington, D. C. 20305
Attn: RAEV/Maj. H. Joonsar — 1 copy

Department of Electrical Engineering
Pennsylvania State University
121 Electrical Engineering
East Building
University Park, PA 16801
Attn: J. Robinson — 1 copy

DISTRIBUTION LIST (Continued)

Department of Physics
University of California at San Diego
P. O. Box 109
La Jolla, CA 92037
Attn: E. C. Whipple — 1 copy

Aerojet Electrosystems Company
1100 West Hollyvale Street
Azusa, CA 91720
Attn: C. Fischer/Dept. 6751 — 1 copy

Aerospace Corporation
P. O. Box 92957
Los Angeles, CA 90009
Attn: J. R. Stevens — 1 copy
R. M. Broussard — 1 copy
J. F. Fennell — 1 copy

Beers Associates, Inc.
P. O. Box 2549
Reston, VA 22090
Attn: Dr. Brian Beers — 1 copy

Boeing Aerospace Company
P. O. Box 3999
Seattle, WA 98124
Attn: H. Liemohn/M.S. 8C-23 — 1 copy
D. Tingey/M.S. 8C-23 — 1 copy

Communications Satellite Corporation
Comsat Laboratories
Clarksburg, MD 20734
Attn: A. Meulenberg, Jr. — 1 copy

European Space Agency
ESTEC
Zwartweg, Noordwijk
Netherlands
Attn: John Reddy, P.B. TTM, 1719 8 2883 — 1 copy

Ford Aerospace and Communications Corporation
Western Development Laboratories Division
3939 Fabian Way
Palo Alto, CA 94303
Attn: D. M. Newell/M.S. G-80 — 1 copy
J. Pherson/M.S. N-01 — 1 copy

General Dynamics Convair
Kearny Mesa Plant
P. O. Box 80847
San Diego, CA 92138
Attn: J. I. Valerio/Mail Zone 42-6210 — 1 copy

DISTRIBUTION LIST (Continued)

General Electric Company
Valley Forge Space Center
P. O. Box 8555
Philadelphia, PA 19101
Attn: V. Belanger/U-2439 — 1 copy
A. Eagles — 1 copy

Grumman Aerospace
Bethpage, NY 11714
Attn: M. Stauber — 1 copy

Hughes Aircraft Company
P. O. Box 92919
Los Angeles, CA 90009
Attn: E. Smith/M.S. A620 — 1 copy
A. H. Narevsky — 1 copy

Hughes Research Laboratories
3011 Malibu Canyon Road
Malibu, CA 90265
Attn: Dr. Jay Hyman — 1 copy

IRT Corporation
P. O. Box 80817
San Diego, CA 92138
Attn: J. Wilkenfeld — 1 copy

JAYCOR
P. O. Box 85154
San Diego, CA 92138
Attn: E. P. Wenaas — 1 copy

Kaman Science
1500 Garden of the Gods Road
Colorado Springs, CO 80907
Attn: F. Rich — 1 copy

Lee W. Parker, Inc.
252 Lexington Road
Concord, MA 01742
Attn: L. Parker — 1 copy

Lockheed Palo Alto Research Laboratory
3251 Hanover Street
Palo Alto, CA 94303
Attn: J. B. Reagan/Bldg. 205, Dept. 52-12 — 1 copy
D. P. Cauffman — 1 copy

Martin Marietta Corporation
P. O. Box 179
Denver, CO 80201
Attn: D. E. Hobbs/M.S. D8350 — 1 copy
K. Killian/M.S. D8350 — 1 copy

Massachusetts Institute of Technology
Lincoln Laboratory
P. O. Box 73
Lexington, MA 02173
Attn: F. G. Walther — 1 copy

McDonnell Douglas Astronautics Company
5301 Bolsa Avenue
Huntington Beach, CA 92647
Attn: W. P. Olson — 1 copy

Mission Research Corporation
5434 Ruffin Road
San Diego, CA 92123
Attn: V. van Lint — 1 copy

RCA Astroelectronics Division
P. O. Box 800
Princeton, NJ 08540
Attn: H. Strickberger/M.S. 91 — 1 copy
W. Franklin — 1 copy

Science Applications, Inc.
101 Continental Building
Suite 310
El Segundo, CA 90245
Attn: D. McPherson — 1 copy

Science Applications, Inc.
2860 South Circle Drive
Colorado Springs, CO 80906
Attn: E. E. O'Donnell — 1 copy

Simulation Physics, Inc.
41 B Street
Burlington, MA 01803
Attn: R. G. Little — 1 copy

SRI International
333 Ravenswood Avenue
Menlo Park, CA 90425
Attn: J. Nanevicz — 1 copy

TRW Systems
One Space Park
Redondo Beach, CA 90278
Attn: G. T. Inouye/Bldg. R-5, Rm. 2011 — 1 copy

Lockheed Missile and Space Company
P. O. Box 504
Sunnyvale, CA 94086
Attn: G. Pack — 1 copy

End of Document